

9. SITE 911¹

Shipboard Scientific Party²

HOLE 911A

Date occupied: 22 August 1993
Date departed: 22 August 1993
Time on hole: 4 days, 1 hr, 55 min
Position: 80°28.466'N, 8°13.640'E
Bottom felt (drill pipe measurement from rig floor, m): 912.4
Distance between rig floor and sea level (m): 10.84
Water depth (drill pipe measurement from sea level, m): 901.6
Total depth (from rig floor, m): 1418.2
Penetration (m): 505.8
Number of cores (including cores with no recovery): 53
Total length of cored section (m): 505.8
Total core recovered (m): 464.51
Core recovery (%): 91.8
Oldest sediment cored:
Depth (mbsf): 505.8
Nature: silty clay
Earliest age: Pliocene

HOLE 911B

Date occupied: 26 August 1993
Date departed: 26 August 1993
Time on hole: 7 hr
Position: 80°28.476'N, 8°13.636'E
Bottom felt (drill pipe measurement from rig floor, m): 912.1
Distance between rig floor and sea level (m): 11.14
Water depth (drill pipe measurement from sea level, m): 901.0
Total depth (from rig floor, m): 1024.2
Penetration (m): 112.1
Number of cores (including cores with no recovery): 15
Total length of cored section (m): 112.1
Total core recovered (m): 112.9
Core recovery (%): 100.7
Oldest sediment cored:
Depth (mbsf): 112.1
Nature: silty clay
Earliest age: Quaternary

HOLE 911C

Date occupied: 26 August 1993
Date departed: 27 August 1993
Time on hole: 12 hr, 15 min
Position: 80°28.485'N, 8°13.637'E
Bottom felt (drill pipe measurement from rig floor, m): 913.2
Distance between rig floor and sea level (m): 11.14
Water depth (drill pipe measurement from sea level, m): 902.0
Total depth (from rig floor, m): 1041.1
Penetration (m): 127.9
Number of cores (including cores with no recovery): 15
Total length of cored section (m): 127.9
Total core recovered (m): 126.07
Core recovery (%): 99
Oldest sediment cored:
Depth (mbsf): 127.9
Nature: silty clays
Earliest age: Quaternary

Principal results: Site 911 is located on the shallow southern part of the Yermak Plateau, at a moderate distance Northeast of Site 910. The site was intended to drill a thick blanketing sequence of Neogene and Quaternary sediments, the upper part of which was to be studied for the glacial history of the Arctic Ocean and the influx of Atlantic surface water into the Arctic. Site 911 also was intended to be a shallow member of a bathymetric transect aimed at studying depth gradients in sediment accumulation. Three holes were drilled, the first to a maximum depth of 505.8 mbsf.

The sediments recovered at Site 911 (Holes 911A, 911B, and 911C) consist primarily of unlithified, homogeneous, very dark gray clayey silts and silty clays of Quaternary and Pliocene age. Silty mud and clayey mud appear as minor lithologies in layers that commonly have a very dark gray or very dark olive gray color. In general, biogenic particles are rare. Slight to intensive bioturbation is present throughout the entire sequence. A single lithologic unit has been defined that can be divided into 2 subunits, primarily based on variations in dropstone abundances.

Lithologic Subunit IA (0–380.4 mbsf), Quaternary to Pliocene. Subunit IA is distinguished by an increase in dropstone abundance to peak values of about six per core, having siltstones, sandstones, and shales as dominant lithologies, and coal fragments, plutonic rocks, and limestones as minor lithologies.

Lithologic Subunit IB (380.4–505.8 mbsf), Pliocene. Subunit IB is defined by a smaller content of dropstones than in Subunit IA. Between Cores 151-911A-41X and -49X, only one or no dropstone has been found. Below this level, significant numbers of dropstones have been found only in Core 151-911A-52X. The dropstones are also smaller in diameter (average 1.3 cm) and consist mostly of plutonic rocks and sand-/siltstones.

The cores from the three holes recovered a Quaternary and Pliocene sequence of ice-rafted sediments with scattered occurrences of calcareous microfossils. Glacial sediments contain rare to common Quaternary and Pliocene benthic and planktonic foraminifers and calcareous nannofossils. The boundary between the Pliocene and Quaternary is recognized only in the deepest hole, 911A, between the base of the acme of small-sized cal-

¹Myhre, A.M., Thiede, J., Firth, J.V., et al., 1995. *Proc. ODP, Init. Repts.*, 151: College Station, TX (Ocean Drilling Program).

²Shipboard Scientific Party is as given in the list of participants preceding the Table of Contents.

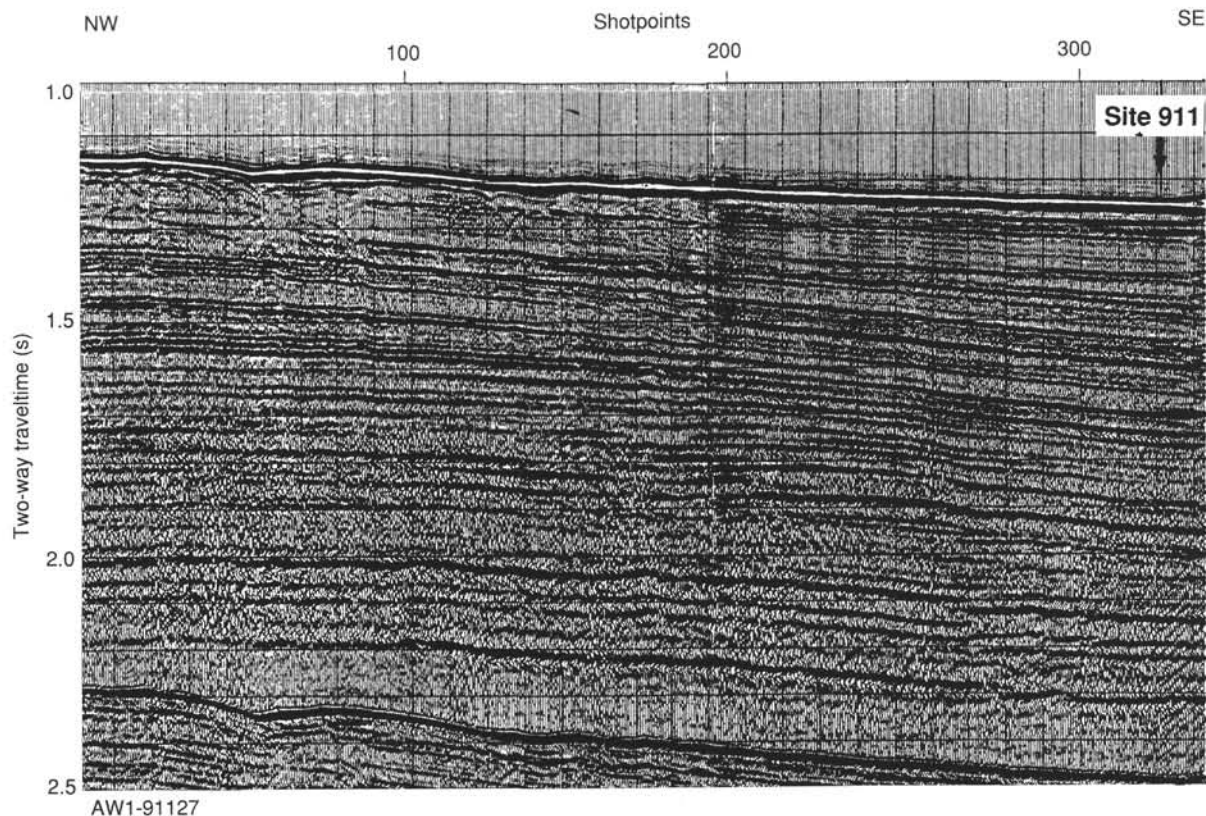


Figure 1. Seismic line AWI-91127. Site 911 is located at shotpoint 324.

careous nannofossil *Gephyrocapsa* (uppermost Pliocene) in Core 151-911A-28X (265.1 mbsf) and the first occurrence of *G. caribbeanica* (Quaternary) in Core 151-911A-23X (216.8 mbsf). Planktonic foraminifer data support this stratigraphic interpretation. Siliceous microfossils are absent with the exception of rare recrystallized and reworked specimens. Reworked planktonic and benthic foraminifers, probably ice-rafted, occur in the lower part of Hole 911A. Sedimentation rates at Site 911 ranged from 170 m/m.y. in the Pliocene and pre-Jaramillo, and were reduced to about 100 m/m.y. during the last million years. The high Quaternary and Pliocene sedimentation rates are similar to those at the other sites at the Yermak Plateau.

Three Schlumberger tool strings were run at Hole 911A: the quad combination (sonic, induction, lithodensity, natural gamma-ray), the Formation MicroScanner, and the geochemical logging tool. The interval logged (107–476 mbsf) covers lithologic Subunits IA and IB. No major lithologic variations are found downhole, a feature reflected in the downhole natural gamma-ray activity log, which has cyclicity but no major trends. Several of the recorded logs exhibit a cyclic nature, most prominently the resistivity logs. Preliminary spectral analyses defined spectral power in the 40-k.y. and 100-k.y. bands, reflecting Milankovitch frequencies.

Physical property measurements have been performed on materials from Hole 911A and Hole 911B only. Both holes exhibited evidence of the presence of relatively high amounts of gas and of drilling disturbances (biscuiting) in the deep parts of the sequences, so that the information was limited. The concentration of headspace methane is high throughout the sedimentary section, ranging from 8000 to 80,000 ppm. Based on the physical property measurements, five geotechnical units can be defined, mainly reflecting the downcore variability of bulk densities. Sediments in the top 50 m show some evidence for overcompaction, similar to but of less magnitude than those at Site 910.

BACKGROUND AND OBJECTIVES

Site 911 (proposed site YERM-3) (Fig. 17 of “Introduction” chapter, this volume) is situated on the southeastern part of the marginal Yermak Plateau, Northwest of the Svalbard archipelago. The site is roughly 35 km East-Northeast of Site 910 in about 900-m water depth. Whereas Site 910 is located on the summit of the plateau that curves gently in a North-northeastward direction (Fig. 7 of “Introduction” chapter, this volume), Site 911 is situated on the upper slope toward the Nansen Basin. A thick sequence of sediments drapes basement, which is not observed on the multichannel seismic line AWI-91127 (Fig. 1). Based on refraction measurements in the area (Sundvor et al., 1982b), basement is buried by 1500 to 2000 m of sediments. It is located in an area where the seismic section shows sequences of high-frequency, continuous reflectors with high amplitudes changing between intervals of continuous reflectors but with low amplitude. The sedimentary sequence is gently dipping to the Southeast and appears to increase in thickness toward the Southeast as well. We refer to the “Site 910” chapter (this volume) for general geological background information on this region.

Scientific Objectives

The site was planned as one of the more shallow end members of a transect across the Yermak Plateau, in addition to being one of the northeasternmost tie points in a North-South transect into the Norwegian-Greenland Sea. The site was proposed to study Neogene variations in climate and oceanography with special emphasis on the Neogene Arctic glacial history and the Neogene variations in Atlantic Ocean water influx to the Arctic Ocean. The objectives are similar to those proposed for Site 910.

Table 1. Coring summary, Site 911.

Core	Date (Aug. 1993)	Time (UTC)	Depth (mbsf)	Length cored (m)	Length recovered (m)	Recovery (%)	Core	Date (Aug. 1993)	Time (UTC)	Depth (mbsf)	Length cored (m)	Length recovered (m)	Recovery (%)
151-911A-							46X	24	1625	428.6-438.2	9.6	7.78	81.0
1H	22	1040	0.0-9.5	9.5	9.48	99.8	47X	24	1820	438.2-447.8	9.6	10.39	108.2
2H	22	1110	9.5-19.0	9.5	9.46	99.6	48X	24	1955	447.8-457.5	9.7	10.33	106.5
3H	22	1130	19.0-28.5	9.5	9.62	101.0	49X	24	2140	457.5-467.2	9.7	7.83	80.7
4H	22	1220	28.5-38.0	9.5	9.47	99.7	50X	24	2330	467.2-476.8	9.6	9.77	102.0
5H	22	1245	38.0-47.5	9.5	8.40	88.4	51X	25	0140	476.8-486.5	9.7	9.96	102.0
6H	22	1320	47.5-57.0	9.5	9.98	105.0	52X	25	0345	486.5-496.2	9.7	10.34	106.6
7H	22	1425	57.0-65.2	8.2	7.76	94.6	53X	25	0600	496.2-505.8	9.6	10.03	104.5
8H	22	1450	65.2-74.7	9.5	10.16	106.9							
9H	22	1515	74.7-84.2	9.5	10.91	114.8							
10H	22	1600	84.2-93.7	9.5	9.96	105.0					505.8	464.51	91.8
11H	22	1630	93.7-101.9	8.2	8.14	99.2	151-911B-						
12H	22	1700	101.9-111.4	9.5	9.99	105.0	1H	26	1335	0.0-3.8	3.8	3.78	99.5
13H	22	1730	111.4-120.9	9.5	10.10	106.3	2H	26	1355	3.8-13.3	9.5	9.74	102.0
14H	22	1800	120.9-130.4	9.5	9.69	102.0	3H	26	1415	13.3-22.8	9.5	9.67	102.0
15H	22	1835	130.4-139.9	9.5	8.78	92.4	4H	26	1435	22.8-32.3	9.5	9.82	103.0
16X	22	1920	139.9-149.4	9.5	7.82	82.3	5H	26	1450	32.3-41.8	9.5	9.65	101.0
17X	22	2005	149.4-159.0	9.6	6.23	64.9	6H	26	1510	41.8-44.8	3.0	2.97	99.0
18X	22	2100	159.0-168.6	9.6	7.72	80.4	7H	26	1535	44.8-49.8	5.0	4.96	99.2
19X	22	2150	168.6-178.3	9.7	7.63	78.6	8H	26	1600	49.8-59.3	9.5	9.38	98.7
20X	22	2225	178.3-187.9	9.6	8.68	90.4	9H	26	1620	59.3-68.0	8.7	8.78	101.0
21X	22	2340	187.9-197.5	9.6	9.11	94.9	10H	26	1640	68.0-75.7	7.7	7.65	99.3
22X	23	0050	197.5-207.2	9.7	8.17	84.2	11H	26	1700	75.7-84.7	9.0	9.30	103.0
23X	23	0155	207.2-216.8	9.6	8.77	91.3	12H	26	1720	84.7-94.2	9.5	9.23	97.1
24X	23	0300	216.8-226.4	9.6	11.25	117.2	13H	26	1745	94.2-101.0	6.8	6.83	100.0
25X	23	0405	226.4-236.1	9.7	4.53	46.7	14H	26	1810	101.0-107.0	6.0	6.04	100.0
26X	23	0515	236.1-245.8	9.7	8.82	90.9	15H	26	1835	107.0-112.1	5.1	5.10	100.0
27X	23	0610	245.8-255.5	9.7	6.56	67.6							
28X	23	0725	255.5-265.1	9.6	9.74	101.0					112.1	112.90	100.7
29X	23	0855	265.1-274.7	9.6	9.50	98.9	151-911C-						
30X	23	1025	274.7-284.3	9.6	8.20	85.4	1H	26	2010	0.0-5.7	5.7	5.70	100.0
31X	23	1145	284.3-294.0	9.7	9.93	102.0	2H	26	2045	5.7-15.2	9.5	6.55	68.9
32X	23	1330	294.0-303.6	9.6	8.59	89.5	3H	26	2110	15.2-24.7	9.5	9.07	95.5
33X	23	1510	303.6-313.3	9.7	6.48	66.8	4H	26	2135	24.7-34.2	9.5	8.91	93.8
34X	23	1650	313.3-322.9	9.6	8.85	92.2	5H	26	2200	34.2-41.7	7.5	7.55	100.0
35X	23	1830	322.9-332.6	9.7	7.88	81.2	6H	26	2220	41.7-51.2	9.5	9.18	96.6
36X	23	2000	332.6-342.2	9.6	7.28	75.8	7H	26	2240	51.2-60.7	9.5	8.95	94.2
37X	23	2150	342.2-351.9	9.7	7.75	83.3	8H	26	2305	60.7-69.5	8.8	9.28	105.0
38X	23	2355	351.9-361.4	9.5	10.39	109.3	9H	26	2325	69.5-77.6	8.1	8.09	99.9
39X	24	0145	361.4-370.9	9.5	8.09	85.1	10H	26	2340	77.6-84.1	6.5	6.59	101.0
40X	24	0320	370.9-380.4	9.5	8.48	89.2	11H	27	0005	84.1-89.9	5.8	5.85	101.0
41X	24	0500	380.4-390.0	9.6	9.05	94.3	12H	27	0055	89.9-99.4	9.5	10.24	107.8
42X	24	0730	390.0-399.6	9.6	10.45	108.8	13H	27	0220	99.4-108.9	9.5	10.12	106.5
43X	24	1000	399.6-409.3	9.7	6.02	62.0	14H	27	0340	108.9-118.4	9.5	9.45	99.5
44X	24	1220	409.3-418.9	9.6	4.87	50.7	15H	27	0415	118.4-127.9	9.5	10.54	110.9
45X	24	1430	418.9-428.6	9.7	9.34	96.3							
											127.9	126.07	98.6

OPERATIONS

Transit to Site 911

The 18-nmi transit to Site 911 required 1.75 hr for an average speed of 10.6 kt. The seismic survey started at 0200 hr, 22 August, and covered 12 nmi in 2.25 hr at 5.3 kt. A Datasonics 354B beacon was dropped at 0520 hr, the seismic gear retrieved, and the ship returned to location.

Hole 911A

An advanced hydraulic piston corer/extended core barrel (APC/XCB) bottom-hole assembly (BHA) was run. The precision depth recorder (PDR) indicated a water depth of 918.4 mbrf. Core 151-911A-1H established the water depth as 901.6 mbsf. Cores 151-911A-1H through -15H were taken from 0.0 to 139.9 mbsf (Table 1), with 139.9 m cored and 141.9 m recovered (101.4% recovery). APC coring was terminated after Core 15H, because it was the eleventh core with a partial stroke in very stiff clays. Cores were not oriented because of the high latitude. The Adara temperature shoe was run on Cores 4H, 7H, and 10H. The formation was extremely stiff, compacted, gray silty clay with occasional ice-rafted debris (IRD).

Cores 151-911A-16X through -53X were taken with the XCB from 139.9 to 505.8 mbsf, with 365.9 m cored and 322.61 m recovered (88.2% recovery). Headspace gas increased to 600,000 ppm at

50 mbsf. C_1/C_2 ratios of about 2000 to 4000 indicate the gas was biogenic. Gas breakout in the core liners caused considerable core disturbance, and holes had to be drilled in the liners to relieve the gas. Some slight H_2S odor was detected at 400 mbsf.

The hole was prepared for logging by circulating the hole clean at total depth (TD), and making a conditioning trip to 78.9 mbsf. A bridge was reamed out at 392 mbsf, and 28 m of fill was cleaned out to 505.8 mbsf TD. The bit was positioned at 78.9 mbsf for logging. We were eager to log down to the bottom of the hole; therefore, the side entry sub (CSES) was put in the string and required 2.5 hr to rig up.

The logs were run as follows:

Log No. 1: Induction/Sonic (DIT/HLDT/SDT/NGT). Log to 476 mbsf (28 m fill) in 5.5 hr.

Log No. 2: FMS/NGT. Found bottom at 1255 mbrf and log up. Run in with CSES to 434.0 mbsf. The FMS would not clear the bit until it was circulated free. The FMS was run to 452.6 mbsf and logged up with the CSES in 2.75 hr.

Log No. 3: Geochemical. Log to 445.6 mbsf without the CSES in 5.75 hr.

Soft clays apparently were closing in the hole. The CSES required 1.5 hr to rig down and was used to run the FMS log 110 m deeper. The hole was displaced with heavy mud, and the bit cleared the seafloor at 1234 hr, 26 August, ending Hole 911A.

Hole 911B

The ship was moved 20 m North, and Hole 911B was spudded at 1320 hr, 26 August, to provide high-resolution sampling. Core 151-911B-1H established the water depth as 901.0 mbsl. Cores 151-911B-1H through -15H were taken from 0.0 to 112.1 mbsf, with 112.1 m cored and 112.89 m recovered (100.7% recovery). APC-coring was terminated after Cores 151-911B-7H through -15H were partial strokes with the advance-by-recovery method used. Cores were not oriented, and heat-flow measurements were not taken. Coring parameters and formation remained the same as in Hole 911A. The bit cleared the seafloor at 1930 hr, 26 August, ending Hole 911B.

Hole 911C

The ship was moved 20 m North, and Hole 911C was spudded at 2000 hr, 26 August, to provide high-resolution sampling. Core 151-911C-1H established the water depth as 902.0 mbsl. Cores 151-911C-1H through -15H were taken from 0.0 to 127.9 mbsf, with 127.9 m cored and 126.07 m recovered (98.6% recovery). APC-coring was terminated after Cores 151-911C-8H through -15H were partial strokes with the advance-by-recovery method used. Cores were not oriented, and heat-flow measurements were not taken. Coring parameters and formation remained the same as in Hole 911A. The bit cleared the rotary table at 0747 hr, 27 August, ending Hole 911C.

Ice Observations

The *Fennica* was sent to YERM-1 to report on the ice conditions. The ice was 3–4 m thick in 20-m × 20-m blocks about 2 nmi from the location; however, the ice moved within 0.6 nmi when the current shifted to the North. The location was in a bay in the ice, and the conclusion was that the *Fennica* could not protect the location; therefore, a decision was made to go to YERM 2A to allow the ice at YERM 1 to clear up some more.

LITHOSTRATIGRAPHY

Introduction

The sediments recovered at Site 911 (Holes 911A, 911B, and 911C) are primarily unlithified, homogeneous, very dark gray clayey silts and silty clays of Quaternary and Pliocene age. Silty mud and clayey mud appear as minor lithologies in layers that commonly have a very dark gray or very dark olive gray color. These layers have an average thickness of ~10 to 15 cm and show mostly gradational contacts (Fig. 2). Sharp color changes of gray, olive gray, dark olive gray, and black are typical for the uppermost three cores of this site and may reflect early diagenetic processes, because texture and composition only change insignificantly (Fig. 3). In general, biogenic particles are rare, and reach amounts of ≤1% on average. Slight to heavy bioturbation is present throughout the entire sequence (Fig. 4). Dropstones of various sizes, amounts, and lithologies were found in nearly all cores.

The lithostratigraphic description (Table 2) is predominantly based on Hole 911A (0–505.8 mbsf), as Hole 911B (0–112.1 mbsf) and Hole 911C (0–127.9 mbsf) recovered much shorter intervals. Sediment texture and composition (Figs. 5 through 8) indicate sharp minor variations in grain size as well as in the siliciclastic particle composition throughout this site, but display no clear transition or boundary that would define different units. Consequently, a single lithologic unit was identified and was divided into two subunits (Table 2), primarily based on variations of dropstone abundance (Fig. 7).

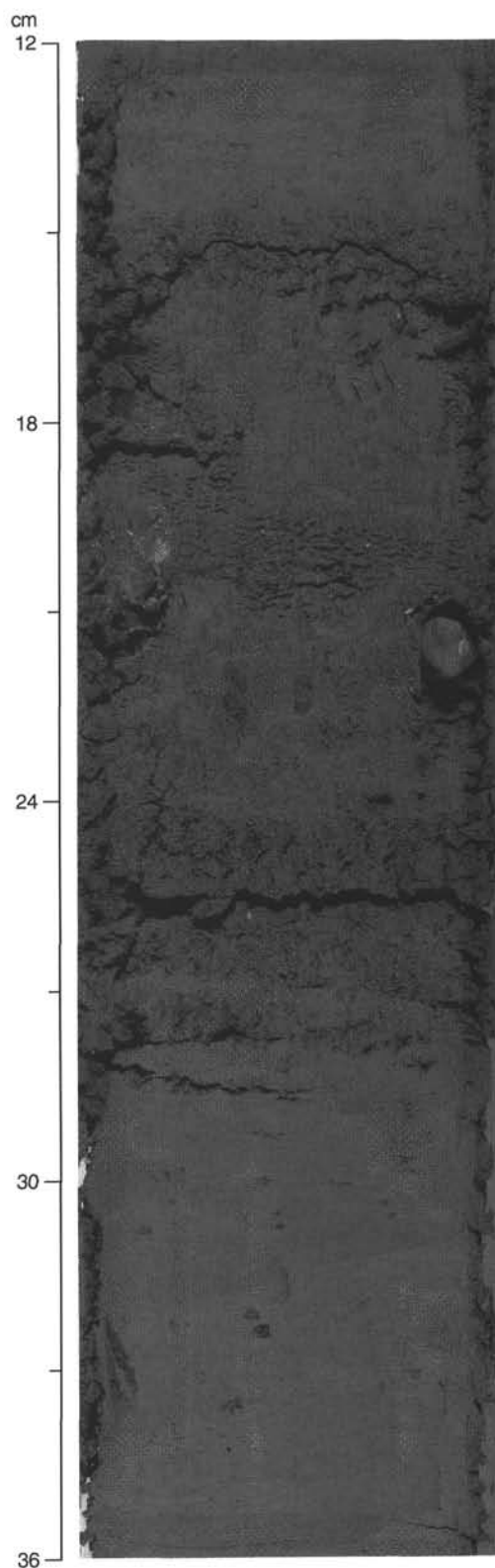


Figure 2. Very dark gray or very dark olive gray silty clay and clayey mud appear as minor lithologies. These layers display mostly gradational contacts and vary in thickness (average 10–15 cm). Dropstones are abundant (151-911A-18X-3, 22 cm, is an example).

Description of Lithologic Subunits

Subunit IA

Cores 151-911A-1H through -40X (0–380.4 mbsf), 151-911B-1H through -15H (0–112.1 mbsf), 151-911C-1H through -15H (0–127.9 mbsf)
 Thickness: 380.4 m
 Age: Quaternary/Pliocene

Lithologic Subunit IA is distinguished by an increase in dropstone abundance to a peak value of six per core (in Core 151-911A-40X). Siltstones, sandstones, and shales are the dominant types, and coal fragments, plutonic rock, quartzite, and limestones are the minor types. The dropstones >1.0 cm in diameter average 1.5 to 2.0 cm measured along the major axis.

The sediment texture (Fig. 8) of Subunit IA displays high-amplitude fluctuations of the sand-, silt-, and clay-size amounts. The average values for clay-sized (~58%), silt-sized (~35%), sand-sized (~7%) content are rather constant, defining the major lithologies of very dark gray, dark gray, olive gray, and very dark olive gray silty clay and clayey silt. Light to heavy bioturbation is present throughout Subunit IA. Black Fe-sulfide filled burrows are the dominant feature, whereas white silt-/sand-filled burrows are less common. The black Fe-sulfide type commonly obscures the original sediment color and may be a major contributor to the very dark gray color.

The variation of siliciclastic components (Fig. 5) reflects similar high-amplitude fluctuations and displays average amounts for quartz (18%), feldspar (8%), and mica (trace). Inorganic calcite particles of mainly fine silt size (Fig. 6) are present with distinct high abundance peaks up to 80%, but occur commonly as background concentrations of ~5%. In addition to the siliciclastic fraction, trace amounts of biogenic components, such as calcareous nannofossils, foraminifers, and sponge spicules, were observed in 10 smear slides.

Subunit IB

Cores 151-911A-41X through -53X (380.4–505.8 mbsf)
 Thickness: 125.4 m
 Age: Pliocene

Lithologic Subunit IB is defined by a decrease of dropstones (Fig. 7, Table 3). Between Cores 151-911A-41X and -49X only one or no dropstone are present per core. Below this level, significant amounts of dropstones have been found only in Core 151-911A-52X. Plutonics and sand-/siltstones are the dominant dropstone types in this unit. These dropstones have a smaller average size (1.3 cm).

The sediment texture of Subunit IB indicates high-amplitude fluctuations of the sand-, silt-, and clay-size percentages. The average values for clay (~55%), silt (~39%), and sand (~6%) are nearly similar to those of Subunit IA and within the error range for this type of analysis. The major lithologies of very dark gray, dark gray, and very dark olive gray silty clay and clayey silt seem to be homogeneous. Moderate to heavy bioturbation is present in Subunit IB. Black Fe-sulfide filled burrows are dominant, whereas the abundance of white silt-/sand-filled burrows decreases from that of Subunit IA.

The variation of siliciclastic components (Fig. 5) reflects high-amplitude fluctuations and shows average values for quartz (18%), feldspar (8%), and mica (trace). Biogenic components were not observed during the smear slide studies. Inorganic calcite particles are more commonly present as background (~5%) and in distinct peaks reaching values up to 80% (Fig. 6).

Interpretation

Site 911 sediments imply a glacial-marine depositional environment near and/or under the ice edge/sea ice cover, which was prima-

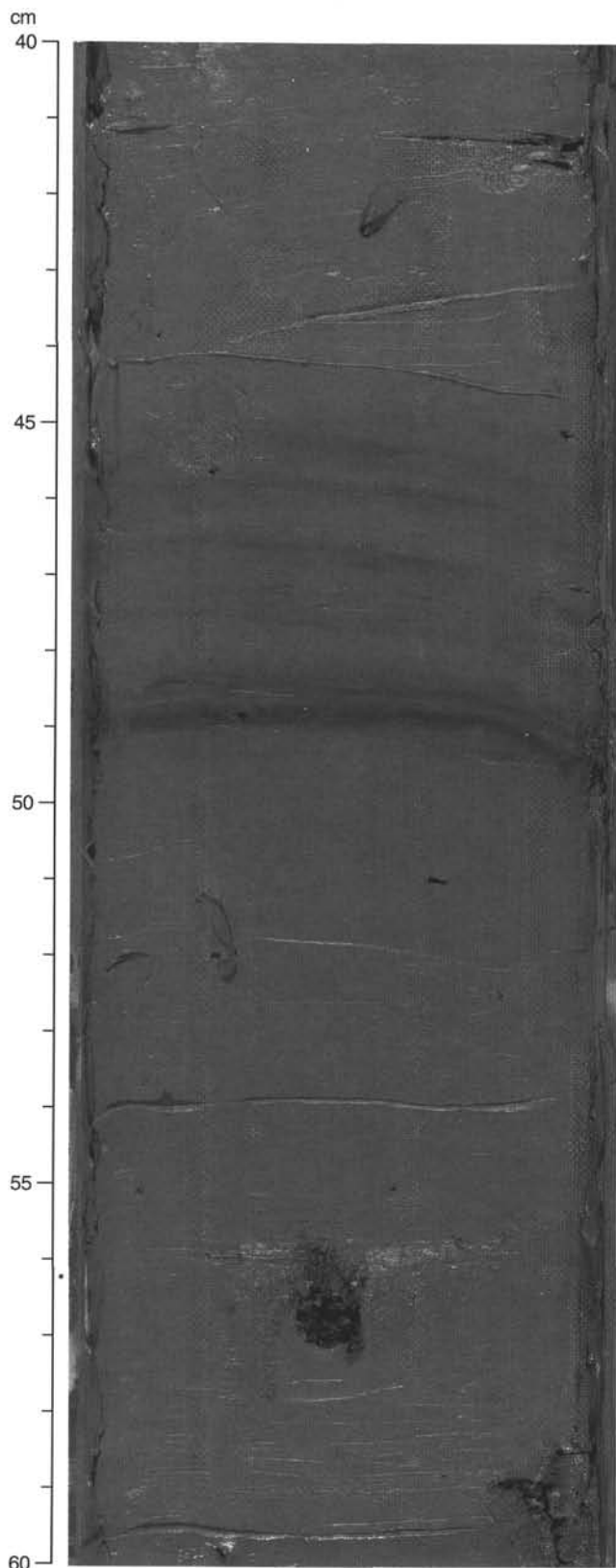


Figure 3. Sharp color changes of gray, olive gray, dark olive gray, and black may reflect early diagenetic processes, because texture and composition change insignificantly. These color changes are common for the uppermost three cores (Interval 151-911A-1H-3, 40–60 cm).

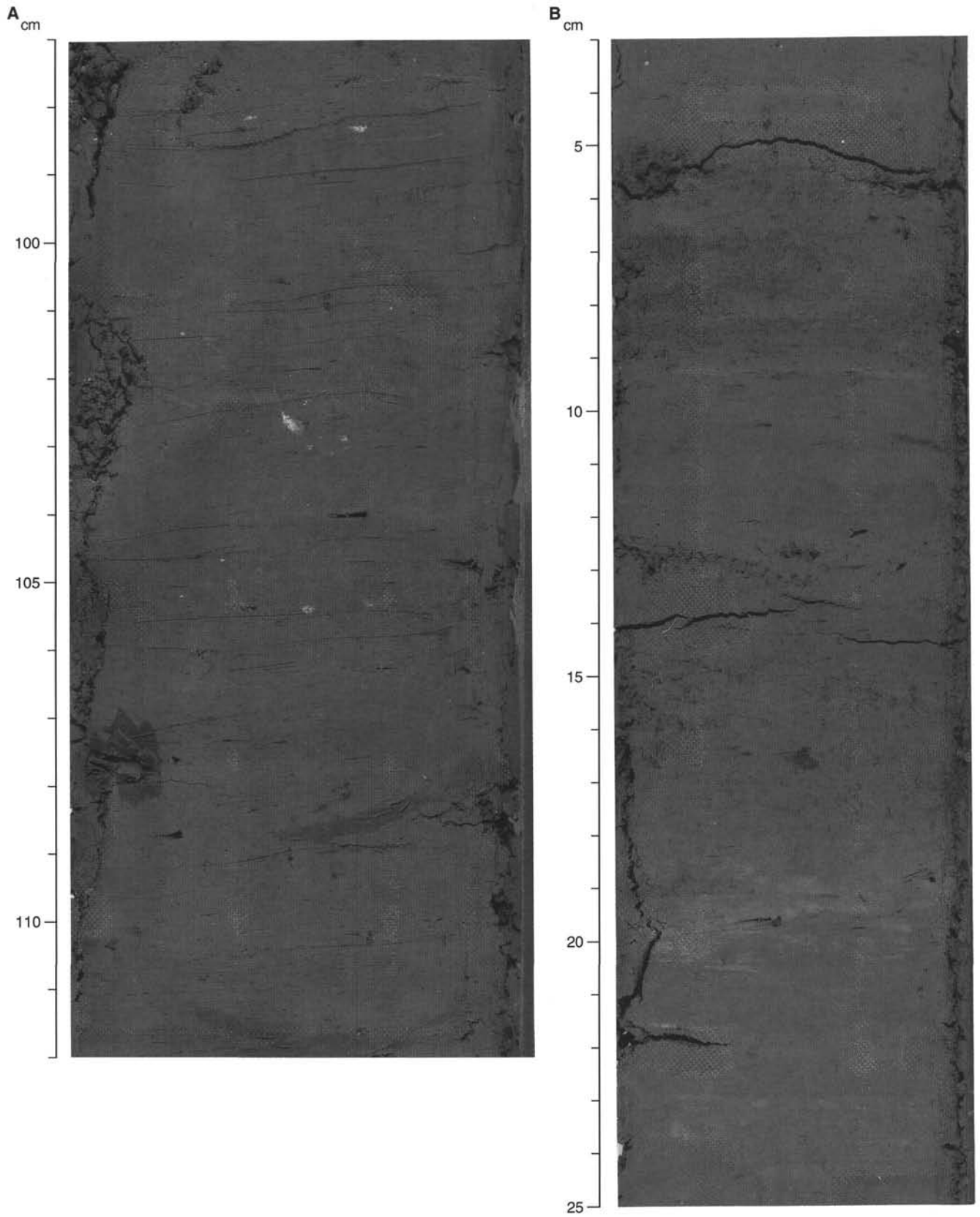


Figure 4. Different degrees of bioturbation. **A.** Section 151-911A-41X-4, 97–112 cm, shows moderate bioturbation. Burrows are commonly filled with white silt. **B.** Interval 151-911A-18X-5, 18–20 cm, displays a mottled contact caused by heavy bioturbation.

Table 2. Summary of lithologic subunits, Site 911.

Subunit	Dominant lithology	Interval, mbsf (thickness, m)	Age	Occurrence (hole-core-section)
IA	Homogeneous silty clay and clayey silt, with dropstone abundances reaching 6 per core	0–380.4 (380.4)	Quaternary/Pliocene	911A-1H-1 to 911A-40X-CC 911B-1H-1 to 911B-15H-CC 911C-1H-1 to 911C-15H-CC
IB	Homogeneous silty clay and clayey silt, with dropstone abundances reaching <6 per core	380.4–505.8 (125.4)	Pliocene	911A-41X-1 to 911A-53X-CC

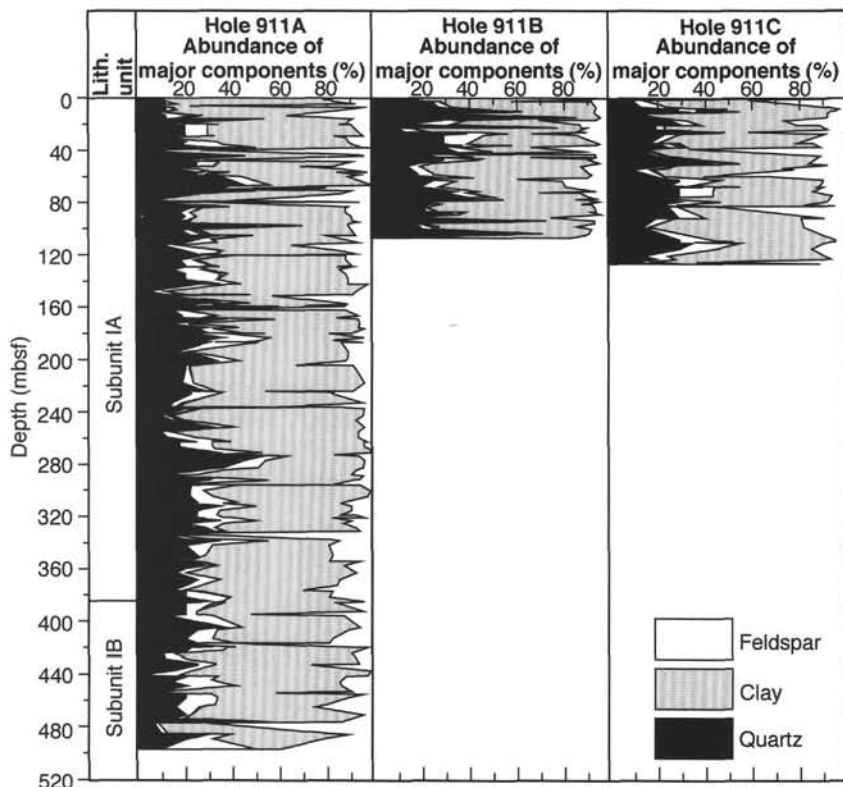


Figure 5. Lithologic subunits, estimates from smear slide data for variations of major siliciclastic components (quartz, feldspar, clay) vs. depth for Holes 911A, 911B, and 911C.

rily controlled by the oceanographic and climatic setting. The dominant lithology of silty clay and clayey silt documents high-amplitude variations in grain size as well as composition of the primarily siliciclastic bulk sediment.

Pliocene to Quaternary sediments of Subunits IA and IB are characterized by a range in dropstone occurrence. Subunit IB contains relatively fewer dropstones ≥ 1.0 cm and none ≥ 2.0 cm, whereas Subunit IA contains substantially more dropstones of all sizes. Biogenic particles are rare. Variations in the dropstone type (plutonic in Subunit IB, sand-/siltstone in Subunit IA) may indicate that the source areas of dropstone material have changed. The irregular presence of silt-sized inorganic carbonate particles (Fig. 6) is poorly understood, as the origin of these particles is uncertain.

A clear cyclic contrast of interglacial/glacial deposits as documented at the Vøring Plateau, Legs 38 and 104 (Talwani, Udintsev, et al., 1976; Henrich et al., 1989b; Thiede et al., 1989; Wolf and Thiede, 1991), cannot be observed. One reason for the lack of interglacial deposits may be that Site 911 is located at a position that today is ice-free only during the summer season, when the West Spitsbergen Current (WSC) reaches this region for two to three months. During the remainder of the year the sedimentation is controlled by the waning and waxing of the ice cover. It seems that a significant amount of siliciclastic particles is transported either by sea ice or by icebergs. Possible source regions for icebergs are glaciers on Svalbard or northern Greenland. Sea ice loaded with shelf sediments is

common throughout the entire Arctic Ocean (Wollenburg, 1993). The transpolar drift over the Yermak Plateau South to the Fram Strait may have contributed to an important amount of sediment by seasonal melting of sea ice and icebergs even during interglacial times. Sedimentation rates of up to 10 cm/k.y. (cf. "Biostratigraphy" and "Paleomagnetism" sections, this chapter) indicate that the above described sedimentation mechanism is a likely one, because a seasonal siliciclastic particle supply is able to provide the required quantity for deposition.

BIOSTRATIGRAPHY

Introduction

Site 911 was selected to study trends in Neogene sediment accumulation on the Yermak Plateau and to further investigate the glacial history of the Arctic Gateway. A Quaternary and Pliocene sequence of ice-rafted sediments with scattered occurrences of calcareous microfossils was recovered. Figure 9 summarizes calcareous microfossil results. Siliceous microfossils are absent, with the exception of rare recrystallized radiolarians from 5.7 mbsf in Hole 911C (Sample 151-911C-1H-CC) to 476.8 mbsf in Hole 911A (Sample 151-911A-50X-CC) and reworked diatoms and silicoflagellates in Sample 151-911A-18X-5, 75–76 cm (165.4 mbsf). Reworking is more prevalent at Site 911 than at other sites previously investigated on Leg 151. Re-

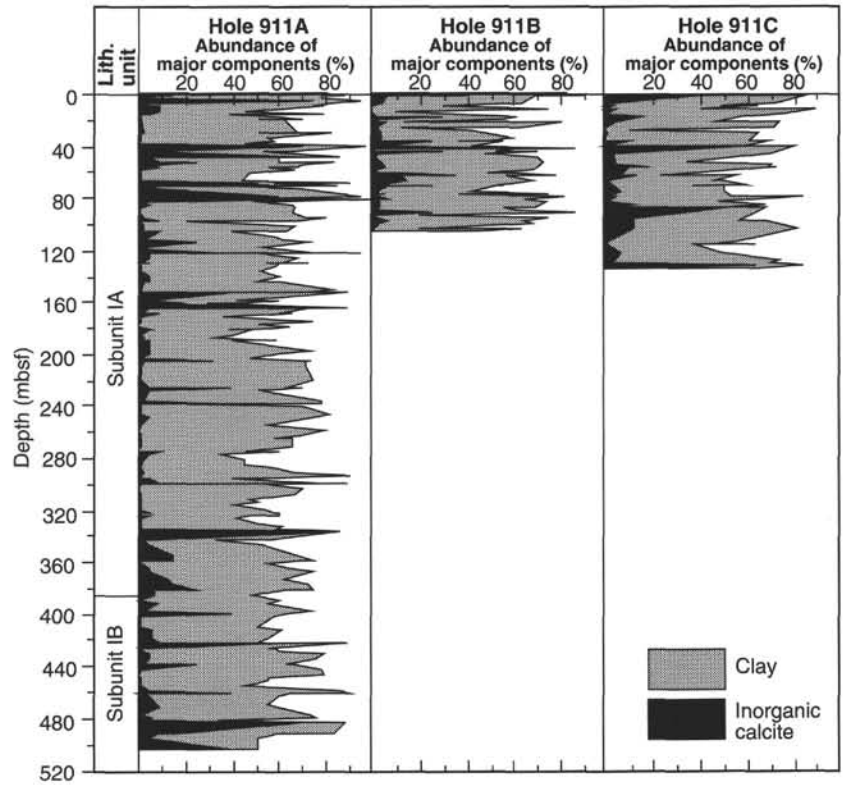


Figure 6. Estimates from smear slide data for variations in clay and inorganic carbonate particle vs. depth for Holes 911A, 911B, and 911C.

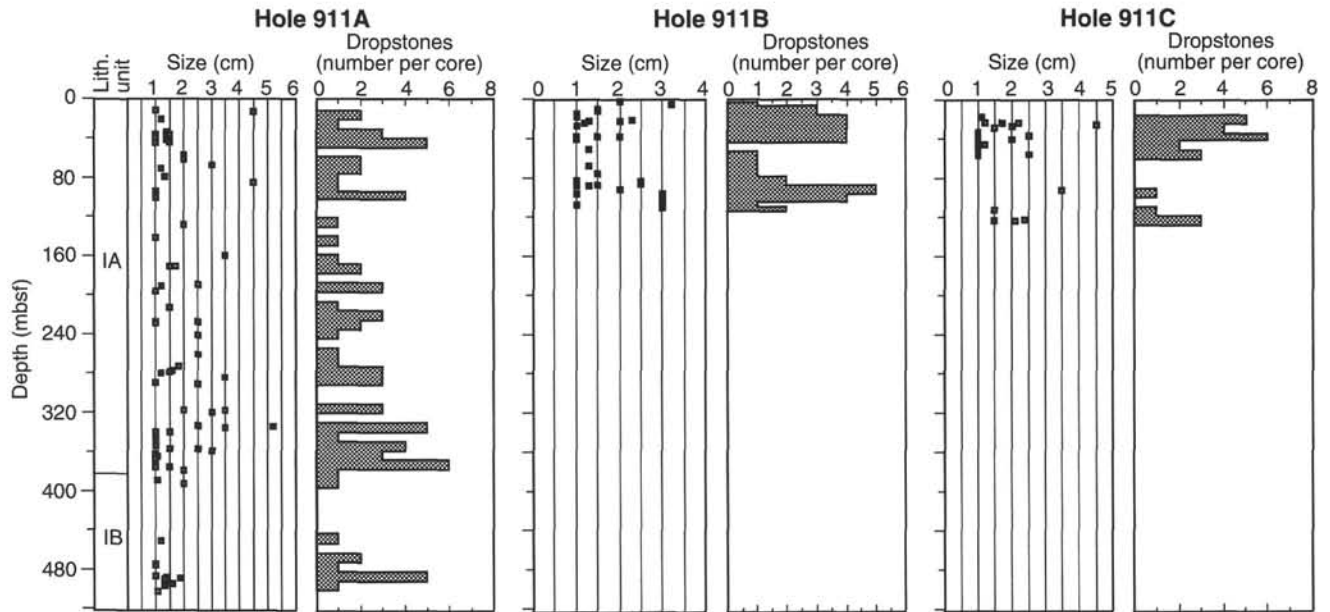


Figure 7. Dropstone size and abundance vs. depth for Holes 911A, 911B, and 911C.

worked benthic foraminifers, probably ice-rafted, occur in the lower part of Hole 911A; very poorly preserved reworked Cretaceous radiolarians are present in Sample 151-911A-47X-CC (447.8 mbsf).

Diatoms

All samples from Site 911 are barren of diatoms, with the exception of rare, reworked diatoms in Sample 151-911A-18X-5, 75–76 cm, 165.4 mbsf. The reworked diatoms are derived from predominantly lower Miocene deposits, but include older forms as well.

Silicoflagellates

All samples from Site 911 are barren of silicoflagellates, with the exception of rare lower Miocene and older reworked silicoflagellates in Sample 151-911A-18X-5, 75–76 cm.

Radiolarians

Radiolarians are absent from Site 911 with the exception of rare, recrystallized spongodiscids and spumellarians, which are too poorly preserved for identification or stratigraphic utility. These forms are

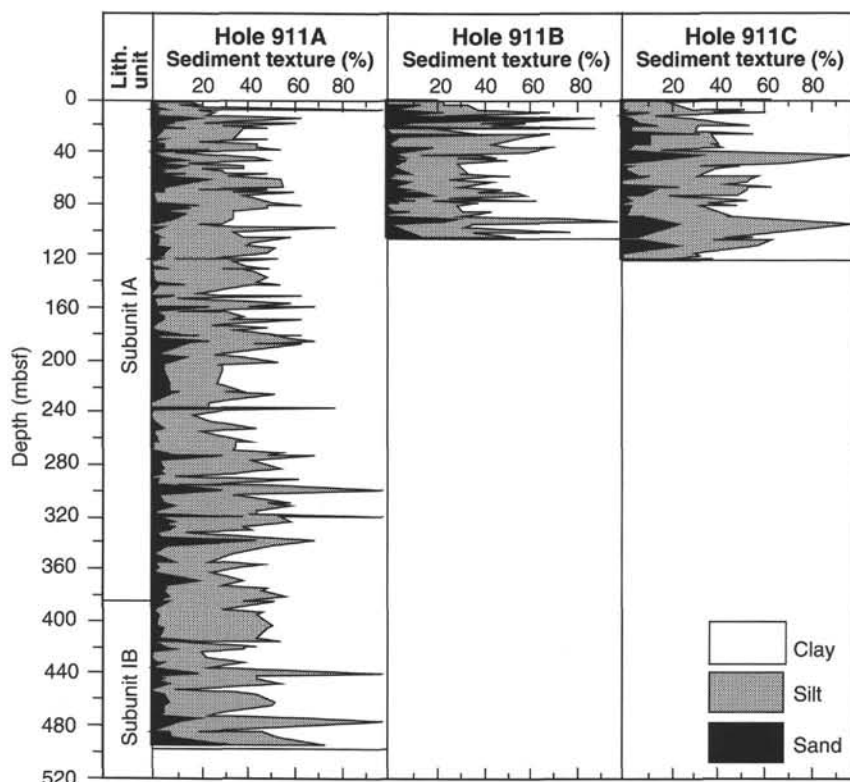


Figure 8. Lithologic subunits, estimates from smear slide data for variations of sediment texture (sand-, silt-, clay-size) vs. depth for Holes 911A, 911B, and 911C.

present in scattered intervals throughout Holes 911B and 911C and from 187.9 to 476.8 mbsf in Hole 911A. Inasmuch as identification of these forms is impossible, their true age is unknown. Two specimens of Cretaceous radiolarians have been found in Pliocene sediments in Sample 151-911A-47X-CC from 447.8 mbsf.

Calcareous Nannofossils

Core-catcher samples from Holes 911A, 911B, and 911C were studied for calcareous nannofossils. Nannofossil abundances are few to common, and preservation is moderate to good in the upper part of the sequence (Samples 151-911A-1H-CC through -23X-CC). Marker species of Martini's zonation (1971) and Quaternary markers described by Takayama and Sato (1987) and Sato et al. (1991) are present.

Samples 151-911A-1H-CC through -4H-CC contain *Gephyrocapsa caribbeanica* and *Gephyrocapsa oceanica*, which indicate the NN19 to NN21 zones of the Quaternary. *Pseudoemiliana lacunosa* and *Emiliana huxleyi*, which define the top of NN19 and base of NN21, respectively, are absent. However, because the abundance of calcareous nannofossils is low, detailed correlation with NN19, NN20, and NN21 zones is not possible.

P. lacunosa occurs in Samples 151-911A-6H-CC through -23X-CC with *G. caribbeanica* and *G. oceanica*. These samples are assigned to the middle to lower Quaternary NN19 Zone. In this interval, the marker species of Sato et al. (1991), a large form of *Gephyrocapsa* spp. (larger than 6 μm), is present in Samples 151-911A-14H-CC through -19X-CC. Furthermore, Sample 151-911A-19X-CC contains *Helicosphaera sellii* with the large form of *Gephyrocapsa*. On this basis, the datums 8, 9, 10, and 11 of Sato et al. (1991) are traced to the intervals between Samples 151-911A-12H-CC/14H-CC, -15H-CC/19X-CC, -19X-CC/23X-CC, and below -23X-CC, respectively. This also indicates that Samples 151-911A-14H-CC through -23X-CC are correlated to the interval between the Cobb Mountain

Event and the Olduvai Event in Matuyama Reversed Epoch of the magnetostratigraphy. Sample 151-911A-23X-CC is correlated with the lower Quaternary, slightly above the Olduvai Event.

The interval from Sample 151-911A-23X-CC through -45X-CC is barren of calcareous nannofossils except for Sample 151-911A-28X-CC, which contains *Coccolithus pelagicus*, *Crenalithus doronicoides*, *Dictyococcites productus*, *P. lacunosa*, and small size *Gephyrocapsa* without *G. caribbeanica* and *G. oceanica*. On the basis of these calcareous nannofossil species, this sample is correlated to the uppermost Pliocene near NN18/NN19 boundary in or just below the Olduvai Event of the magnetostratigraphy. Therefore, the Pliocene/Quaternary boundary is situated between Samples 151-911A-23X-CC and -28X-CC.

Sample 151-911A-46X-CC is characterized by an abundance of *C. doronicoides*, *D. productus*, and *P. lacunosa*. On the basis of this assemblage, which lacks *Gephyrocapsa*, Sample 151-911A-46X-CC is assigned to the NN15 to NN18 zones, upper lower Pliocene to upper Pliocene. Nannofossils are rare to absent from Sample 151-911A-47X-CC to the bottom of Hole 911A (Sample 151-911A-53X-CC).

Samples 151-911B-1H-CC through -14H-CC and all core-catcher samples from Hole 911C are characterized by the occurrences of *G. caribbeanica* and *Gephyrocapsa* sp. (small). Calcareous nannofossil assemblages in both of these sequences are assigned to the Quaternary.

Planktonic Foraminifers

The drilled sequences of Holes 911A, 911B, and 911C contain assemblages of Quaternary and Pliocene planktonic foraminifers including *Neoglobobadrina atlantica* sin. and both dextral and sinistral forms of *N. pachyderma*. All core-catcher samples from the three holes and five additional samples from Hole 911A were processed. Only 40% of the samples contain planktonic foraminifers, most of which are well preserved. Planktonic foraminifers are abun-

Table 3. Occurrences of dropstones at Site 911.

Core, section, interval top (cm)	Depth (mbsf)	Size (cm)	Lithology	Core, section, interval top (cm)	Depth (mbsf)	Size (cm)	Lithology
151-911A-				51X-7, 21	486.01	1.0	Sandstone
2H-3, 15	12.65	1.0	Coal	52X-1, 42	486.92	1.4	Plutonic
2H-3, 71	13.21	4.5	Dark plutonic	52X-2, 55	487.80	1.9	Plutonic
3H-2, 62	21.12	1.2	Sandstone	52X-3, 51	489.26	1.3	Plutonic
4H-5, 30	34.80	1.4	Sandstone	52X-6, 39	493.23	1.6	Plutonic
4H-6, 30	36.30	1.0	Sandstone	52X-8, 28	496.07	1.3	Igneous
4H-6, 48	36.48	1.5	Sandstone	53X-5, 38	501.56	1.1	Quartz
5H-2, 78	40.28	1.0	Sandstone				
5H-4, 10	42.60	1.4	Shale	151-911B-			
5H-5, 44	44.44	1.5	Shale	1H-1, 125	1.25	2.0	Meta. mudstone
5H-5, 116	45.16	1.0	Shale	2H-2, 93	6.23	3.2	Siltstone
5H-6, 37	45.87	1.0	Shale	2H-5, 129	11.09	1.5	Siltstone
7H-1, 87	57.87	2.0	Sandstone	2H-6, 44	11.74	1.5	Siltstone
7H-4, 87	62.37	2.0	Siltstone	3H-1, 42	13.72	1.5	Coal
8H-2, 63	67.33	3.0	Quartz	3H-2, 81	15.61	1.0	?
8H-4, 138	71.08	1.2	Sandstone	3H-4, 85	18.65	1.0	Coal
9H-4, 121	79.51	1.3	Siltstone	3H-CC, 8	22.70	2.3	Olivine basalt
10H-2, 0	85.70	4.5	Siltstone	4H-1, 50	23.30	1.3	Quartzite
11H-1, 33	94.03	1.0	Coal	4H-1, 65	23.45	2.0	Shale
11H-3, 88	97.58	1.0	Siltstone	4H-2, 140	25.70	1.2	Dark crystalline
11H-3, 90	97.60	1.0	Siltstone	4H-4, 5	27.80	1.0	Shale
11H-5, 138	101.08	1.0	Siltstone	5H-5, 49	38.70	1.0	Sandstone
14H-7, 5	128.70	2.0	Siltstone	5H-5, 89	39.10	1.5	Siltstone
16X-2, 5	141.45	1.0	Silty shale	5H-5, 107	39.28	2.0	Sandstone
18X-1, 75	159.75	3.5	Limestone	5H-6, 76	40.56	1.0	?
19X-2, 109	171.19	1.5	Shale	8H-1, 77	50.57	1.3	Sandy shale
19X-2, 116	171.26	1.7	Sandstone	9H-CC, 24	67.97	1.3	Sandstone
21X-2, 22	189.62	2.5	Sandstone	10H-5, 117	75.17	1.5	Schist
21X-3, 9	190.99	1.2	Sandstone	11H-5, 51	82.21	1.0	Siltstone
21X-6, 56	195.96	1.0	Sandstone	11H-6, 6	83.06	2.5	Schist
23X-4, 124	212.94	1.5	Quartzite	12H-1, 35	85.05	2.5	Quartz diorite
24X-9, 54	227.23	1.0	Siltstone	12H-1, 135	86.05	1.5	Siltstone
24X-CC, 28	227.60	2.5	Siltstone	12H-2, 107	87.27	1.3	Quartzite
24X-CC, 52	227.84	1.0	Siltstone	12H-2, 107	87.27	1.0	Pyroclastic
25X-1, 140	227.80	1.0	Shale	12H-2, 107	87.27	1.0	Siltstone
25X-2, 58	228.48	1.0	Limestone	12H-2, 111	87.31	1.0	Siltstone
26X-4, 24	240.84	2.5	Siltstone	12H-5, 72	91.42	2.0	Schist
28X-4, 26	260.26	2.5	Sandstone	13H-1, 72	94.92	3.0	Igneous
29X-6, 67	272.80	1.8	Shale	13H-1, 135	95.55	1.0	Siltstone
30X-2, 126	277.46	1.6	Anthracite	13H-2, 70	96.40	3.0	Sandstone
30X-3, 7	277.77	1.5	Pyrite	13H-5, 34	100.54	3.0	Siltstone
30X-3, 142	279.12	1.2	?	14H-4, 104	106.54	1.0	Siltstone
31X-1, 0	284.30	3.5	Limestone	14H-4, 5	105.55	1.0	Siltstone
31X-4, 63	289.43	1.0	Shale	15H-1, 77	107.77	3.0	CaCO ₃ rich siltstone
31X-5, 23	290.53	2.5	Sandstone	15H-2, 132	109.82	3.0	Sandstone
34X-3, 92	317.22	3.5	Sandstone				
34X-3, 92	317.22	2.0	Sandstone	151-911C-			
34X-4, 131	319.11	3.0	Siltstone	3H-2, 88	17.58	1.1	Sandstone
36X-1, 29	332.89	2.5	Sandstone	3H-6, 28	22.98	1.7	Plutonic
36X-2, 3	334.11	5.2	Quartzite	3H-6, 40	23.10	2.2	?
36X-2, 30	334.38	3.5	Quartzite	3H-6, 47	23.17	1.2	Coal
36X-5, 41	338.90	1.5	Siltstone	3H-6, 110	23.80	1.2	Sandstone
36X-5, 52	339.01	1.0	Basalt	3H-6, 110	23.80	1.0	Quartz
37X-2, 28	344.28	1.0	Siltstone	4H-1, 125	25.95	4.5	Siltstone
38X-2, 21	353.02	1.0	Siltstone	4H-2, 8	26.28	2.0	Coal
38X-3, 128	355.59	1.5	Siltstone	4H-3, 61	28.31	1.5	Metamorphic
38X-4, 30	356.11	2.5	Sulfide	4H-6, 70	32.90	1.0	Sandstone
38X-5, 89	358.13	3.0	Schist	5H-2, 62	36.32	2.5	Siltstone
39X-1, 50	361.90	1.0	Siltstone	5H-2, 101	36.71	1.0	Siltstone
39X-2, 114	363.99	1.1	Quartzite	5H-4, 30	39.00	1.0	Siltstone
39X-3, 131	365.60	1.0	Siltstone	5H-4, 81	39.51	2.0	Igneous
40X-1, 46	371.36	1.0	Siltstone	5H-4, 115	39.85	1.0	Siltstone
40X-2, 114	373.54	1.0	Siltstone	5H-5, 62	40.82	1.0	Siltstone
40X-2, 138	373.78	1.0	Siltstone	6H-3, 27	44.97	1.2	Siltstone
40X-3, 44	374.29	1.0	Siltstone	6H-3, 124	45.94	1.0	Quartzite
40X-3, 59	374.44	1.5	Siltstone	7H-1, 137	52.57	1.0	Coal
40X-6, 87	378.42	2.0	Sandstone	7H-3, 137	55.57	2.5	Siltstone
41X-6, 14	388.04	1.1	Siltstone	7H-4, 100	56.70	1.0	Coal
42X-2, 69	391.71	2.0	Sandstone	12H-2, 114	92.54	3.5	Basalt
48X-2, 132	450.19	1.2	Sandstone	14H-3, 4	111.94	1.5	Sandstone
50X-5, 65	473.85	1.0	Siltstone	15H-3, 110	122.50	2.4	Sandstone
50X-5, 112	474.32	1.0	Siltstone	15H-3, 116	122.56	2.1	Sandstone
				15H-3, 135	122.75	1.5	Sandstone

dant in the upper sequences of the Quaternary sediments and are rare within the Pliocene sequences.

The *N. pachyderma* sin. Zone of the Quaternary extends from the top of the sequence in Hole 911A to Sample 151-911A-22X-CC. The *N. atlantica* sin. Zone of the Pliocene occurs from Sample 151-911A-37X-6, 26–28 cm, through Sample 151-911-51X-CC. Shore-based studies are necessary to better define the Quaternary/Pliocene boundary at this site.

Benthic Foraminifers

Benthic foraminifers were analyzed from nearly all core catchers in Holes 911A and 911C. These benthic foraminifers can be divided into two zones. The upper zone consists of Quaternary species including *Melonis zaandamae*, *Cassidulina teretis*, and *Epistominella* spp. Below Sample 151-911A-29X-CC (274.7 mbsf), preservation and abundance decline. The lower part of Hole 911A contains rare

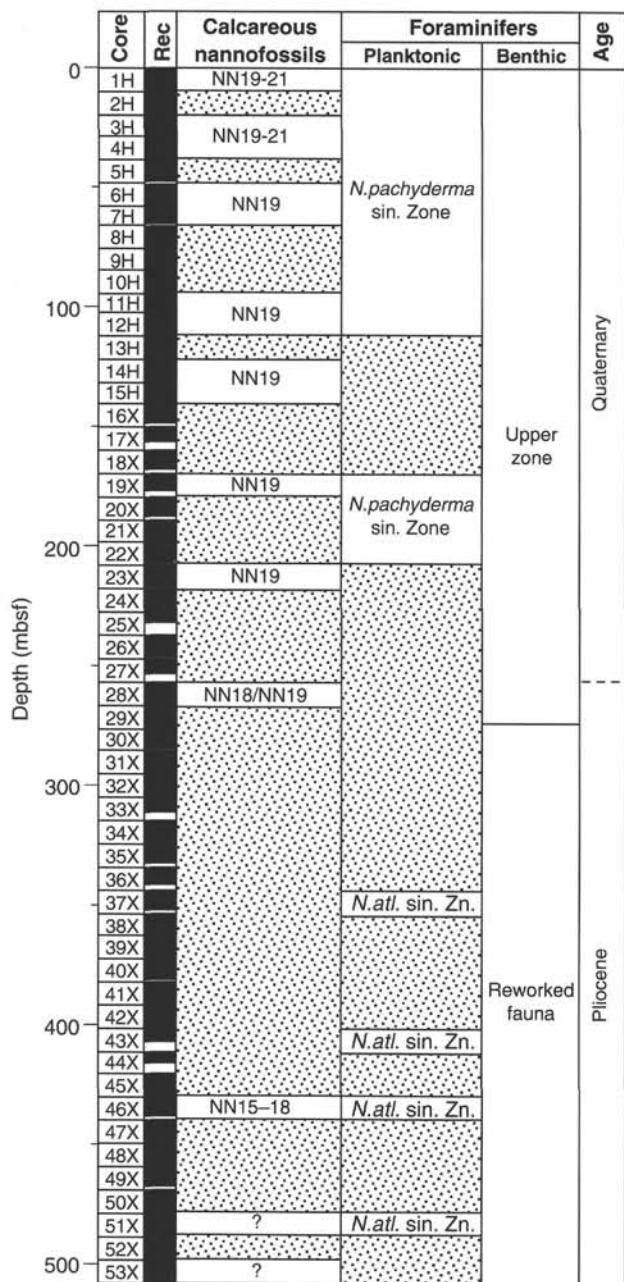


Figure 9. Summary figure of calcareous nannofossil, planktonic, and benthic foraminifer biostratigraphies from Hole 911A.

specimens of *C. teretis*, *M. zaandamae*, and others. These specimens have numerous broken chambers and a frosted surficial texture. The foraminifers in the lower zone are considered to be reworked, and presumably ice-rafted.

Biostratigraphic Synthesis

Glacial sediments recovered at Site 911 contain rare to common Quaternary and Pliocene benthic and planktonic foraminifers and calcareous nannofossils. The boundary between the Pliocene and Quaternary is recognized only in the deepest hole, Hole 911A, between the base of the acme of small-size *Gephyrocapsa* (uppermost Pliocene) in Core 151-911A-28X (265.1 mbsf) and the first occur-

rence of *G. caribbeanica* (Quaternary) in Core 151-911A-23X (216.8 mbsf). Further shore-based studies should refine the position of this boundary within the sequence. Benthic foraminifers within this interval are reworked, although Quaternary species, including *M. zaandamae*, *C. teretis*, and *Epistominella* spp., are present in the upper 265 m of Hole 911A.

Calcareous nannofossils concur in general with the planktonic foraminifers. Quaternary nannofossils of the NN19 to NN21 zones (e.g., *G. caribbeanica* and *G. oceanica*) are present in Cores 151-911A-1H through -4H. Cores 151-911A-6H through -23X are assigned exclusively to the NN19 Zone based on the co-occurrence of *P. lacunosa*, *G. caribbeanica*, and *G. oceanica*. The presence of a large form of *Gephyrocapsa* sp. recognized by Sato et al. (1991) as a marker for the interval between the Cobb Mountain Event and above the Olduvai Event occurs from Samples 151-911A-14H-CC through -19X-CC. Sample 151-911A-28X-CC is characterized by the occurrence of *P. lacunosa* and small-size *Gephyrocapsa* without *G. caribbeanica* and *G. oceanica*. This assemblage indicates the uppermost Pliocene, in or just below the Olduvai Event (between datum 12 and 14 of Sato et al., 1991). The Pliocene/Quaternary boundary is situated between Samples 151-911A-23X-CC and -28X-CC. Biostratigraphic results from calcareous nannofossils and planktonic foraminifers, although limited by low abundances and diversity, are in agreement with magnetostratigraphic results at Site 911.

Samples from 151-911A-29X through -45X are barren of nannofossils. Uppermost lower Pliocene to upper Pliocene calcareous nannofossils, including *C. doronicoides*, *D. productus*, and *P. lacunosa*, are in Core 151-911A-46X, which is assigned to the NN15-18 zones. Species occurring below this interval to the bottom of the hole are not age-diagnostic.

Reworking of microfossils is extensive within the stratigraphic sequence at Site 911. Ice-rafted radiolarians, diatoms, silicoflagellates, and foraminifers are present. Reworking is particularly notable in the benthic foraminiferal assemblages of the lower Quaternary and Pliocene.

PALEOMAGNETICS

Shipboard paleomagnetic studies performed at Site 911 followed the general methods described in the "Explanatory Notes" chapter (this volume). Paleomagnetic studies provided significant temporal constraints for the sedimentary column with the identification of major chronozones and several short subchronozones. Mineralogical analyses were undertaken at this site to determine the nature of these ferrimagnetic iron sulfide concretions and the role they played in the magnetic and other physical properties.

General Magnetic Character of the Site 911 Sediments

As in Site 910, secondary magnetizations acquired by diagenetic iron sulfides play a large role in the natural remanent magnetization measured in Site 911 cores. The magnetic remanence after a 30-mT demagnetization, as well as the magnetic susceptibility measured on the multi-sensor track (MST) system, shows generally low values, except in very thin intervals in which the two quantities peak 10 or 100 times above background (Fig. 10). As was noted in the Site 910 paleomagnetism report, visual inspection of the core shows that these extreme magnetic properties are associated with iron sulfide concretions, mostly distributed below a depth of 320 mbsf in Hole 911A (Fig. 11). One of these concretions (Sample 151-911A-41X-2, 37 cm) exhibited a fairly high natural remanent magnetization (NRM) value of $2.7 \times 10^{-5} \text{ Am}^2 \text{ kg}^{-1}$, suggesting that in some cases the main part of the paleomagnetic signal could result from such concretions. Shipboard X-ray diffraction analyses undertaken on this and other similar concretions show that the dominant mineral is greigite (Fe_3S_4), with possible minor amounts of pyrrhotite (Fe_7S_8). These

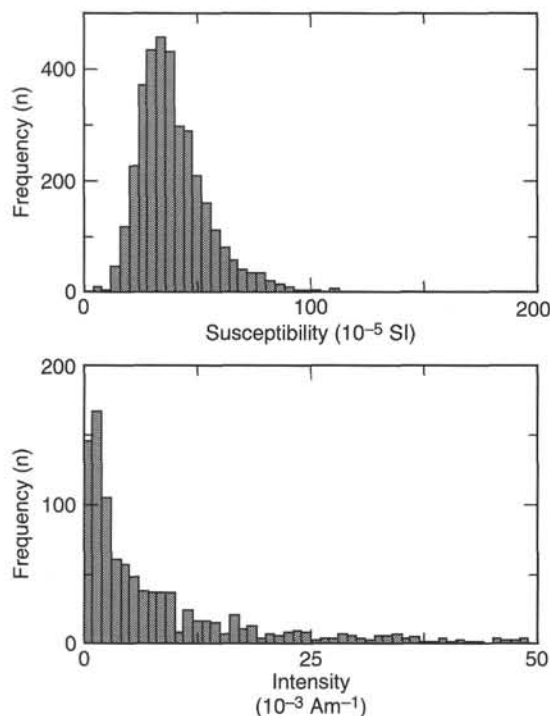


Figure 10. The distributions of magnetic susceptibility values and NRM intensity after 30-mT AF demagnetization in Hole 911B.

concretions have very high electrical conductivities, and are often discerned on Formation MicroScanner images (see "Downhole Measurements" section, this chapter).

Magnetic susceptibility values show a unimodal distribution about a median value at about 4×10^{-4} SI units, with the very spikey iron sulfide signal represented as a slender tail toward higher values (Fig. 11). NRM intensity after 30-mT demagnetization treatment shows a similar distribution, with a median value of intensity at about $2 \times 10^{-3} \text{ Am}^{-1}$.

AF Demagnetization Behavior

Alternating field (AF) demagnetization of discrete samples up to 30 mT was partially accomplished in the 2G pass-through system, with the treatment schedule extended to include 40- and 60-mT steps in the GSD-1 demagnetizer. The samples from Hole 911A exhibited high coercivities (Fig. 12), with median destructive fields on the order of 50 mT in some cases. Figure 12A demonstrates the AF demagnetization of a sample from a reversed polarity interval (77.05 mbsf) with fairly high coercivity. In this sample the NRM vector only slightly changes below the 40-mT demagnetization step, growing in intensity as a steep downward magnetization is removed. In this case, the steep downward magnetization is of relatively small magnitude compared with the characteristic magnetization; thus it perturbs only slightly the resultant NRM at the 30-mT level and would not cause a significant problem for the interpretation of the pass-through record, which is limited to a 30-mT degauss level. However, in cases where the magnitude of the characteristic magnetization was equal or less than the present-day overprint, the pass-through record would be difficult or impossible to interpret. An additional complication that arises at high demagnetizing fields is the acquisition of anhysteretic remanent magnetization (ARM) components. An example of the uncertainty that this effect might generate is evident in Figure 12B, in which the very steeply downward NRM appears to decay to the origin, but possibly continues on through the origin and into the upper

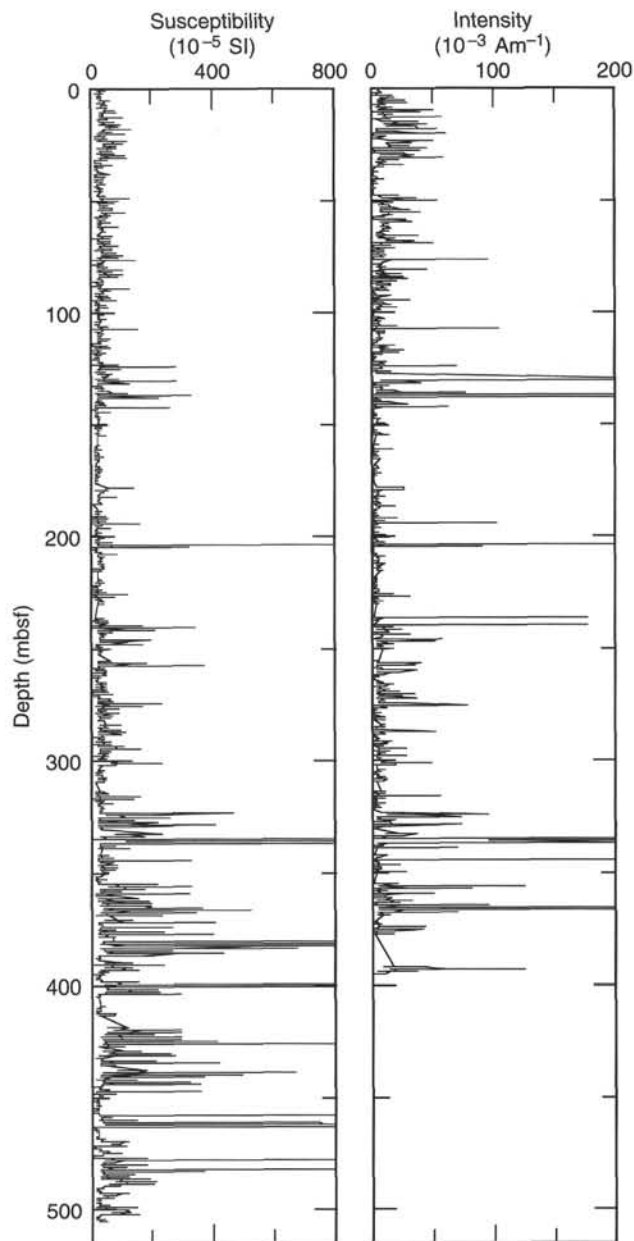


Figure 11. The variation of magnetic susceptibility and NRM intensity after 30-mT demagnetization treatment in Hole 911A.

hemisphere. The presence of a high-coercivity magnetization makes it important to run similar high-demagnetization field experiments on the other discrete samples to verify the pass-through record.

Magnetic Polarity Stratigraphy

Pass-through measurements of NRM after a 30-mT demagnetization were performed on Hole 911A archive core halves from just below the sediment water interface down to 394 mbsf, and on Hole 911B archive halves from just below the seafloor to a depth of 112 mbsf. The magnetic polarity stratigraphy was interpreted from the inclination of the NRM after the 30-mT treatment. As Figure 13 indicates, the magnetization is highly bimodal with twin peaks near the expected normal and reversed geomagnetic field inclinations at the site $\pm 85^\circ$. The normal and reversed polarity distributions are remark-

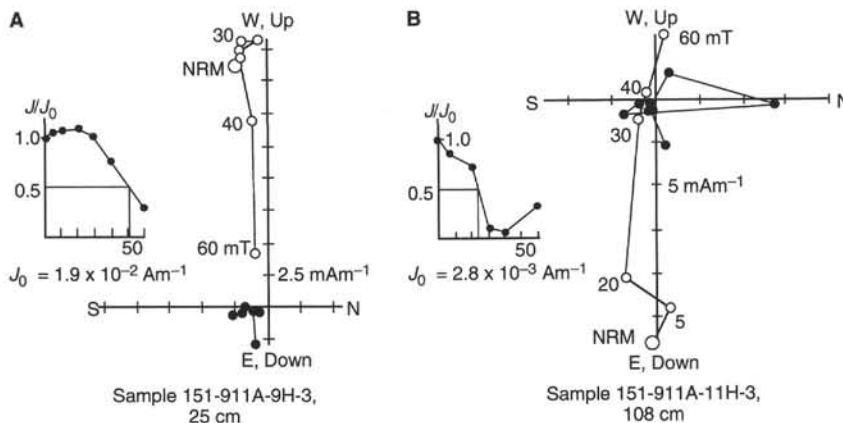


Figure 12. AF demagnetization diagrams for two discrete samples from Hole 911A. Black circles = projection onto the horizontal plane; white circles = projection onto the vertical plane parallel to the split face of the core.

ably symmetric, and the observation that their means do not differ indicates that a present-day overprint does not consistently contaminate the determination of the characteristic magnetization. However, the large proportion of intermediate inclinations suggests that ARM acquisition or other spurious components of magnetization are probably disturbing a significant proportion of the inclination determinations.

A comparison of the inclination vs. depth for Holes 911A and 911B indicates a high degree of correlation between the two records and supports the notion that the paleomagnetic records from the two holes are faithful recorders of the geomagnetic field. However, important discrepancies between the two data sets point out the usefulness of double cored intervals (Fig. 14). The most important discrepancy is the inclination recorded from 50 mbsf to about 70 mbsf, which is characterized by consistent positive inclinations in Hole 911A and contrasts with the intermediate and negative inclinations in the Hole 911B record. Visual inspection of Cores 151-911B-8H, -9H, and -10H indicated that these cores suffered a considerable amount of deformation during the APC process; in some of the cores, the bedding was deformed into conical surfaces with an amplitude of 20–30 cm and much flowage. In Hole 911A the sediment was recovered with much less deformation, and thus the Hole 911A record is considered superior to that of Hole 911B.

In addition to problems with coring deformation, the paleomagnetic record from this site is troubled with errors in depth registration associated with the development of gas voids during drilling and recovery of the core. Based on comparisons of the MST susceptibility records from these two cores, the errors in depth registration amount

to some 8 m or so at a depth of 80 m (ODP depth assignments from Hole 911B associate shallower depths with the same susceptibility features from Hole 911A; see “Physical Properties” section, this chapter). This is clearly demonstrated in the paleomagnetic record by the observation that the normal to reversed transition that occurs in Hole 911A at 90 mbsf is observed at 82 mbsf in Hole 911B. In this

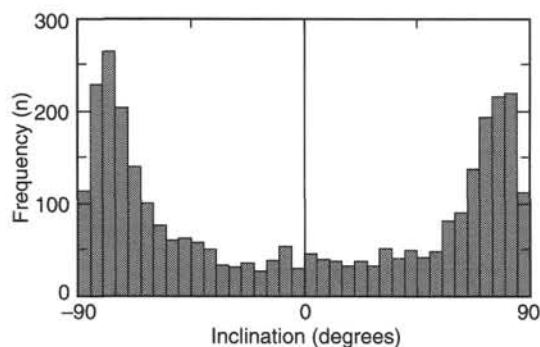


Figure 13. Distribution of inclination values after 30-mT demagnetization treatment in Hole 911A.

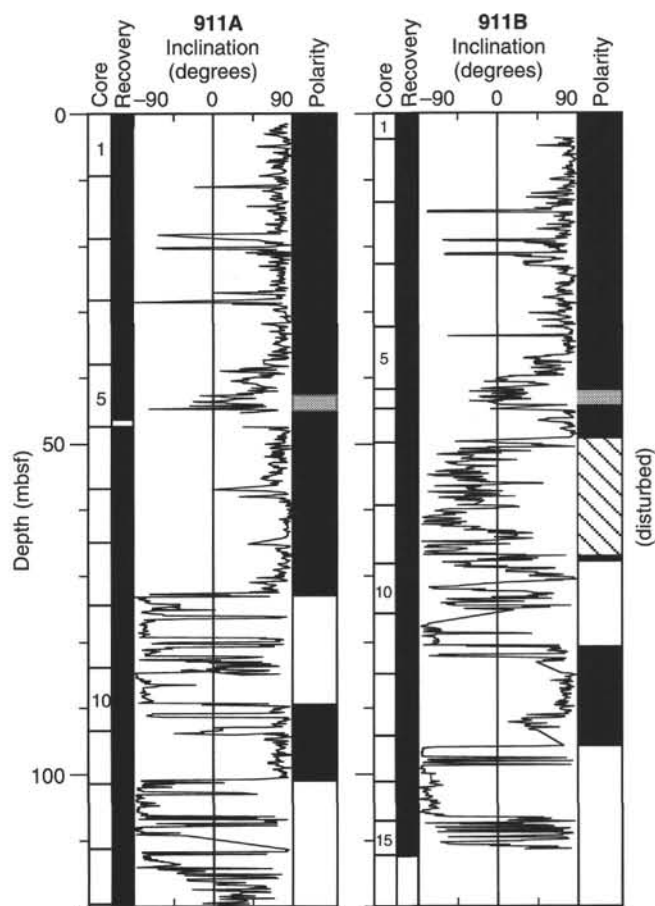


Figure 14. Comparison of the inclination records of the upper 120 mbsf and 111 mbsf of Holes 911A and 911B, respectively. There is little correlation between Hole 911A and Hole 911B directions between 50 and 67 mbsf because of disturbed Cores 151-911B-8H and -9H.

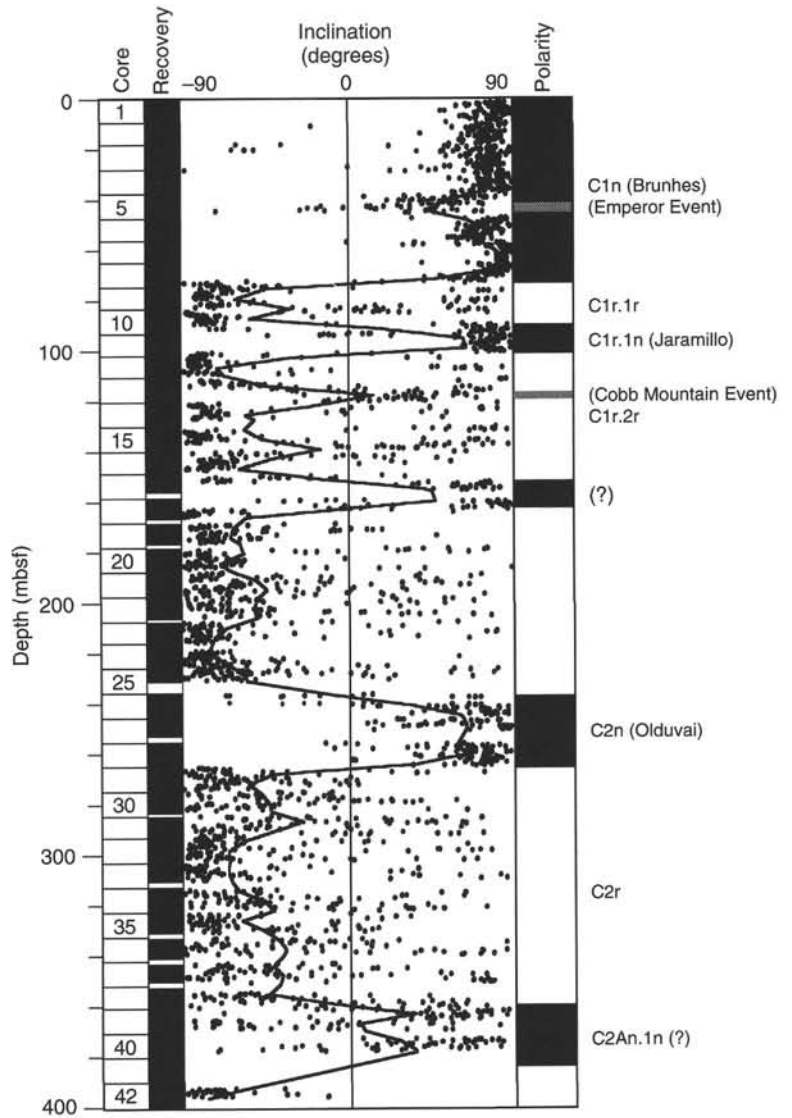


Figure 15. The paleomagnetic record from Hole 911A. The left two columns show the cored intervals, with the length of the recovered core shown in black. The center column is the inclination of the NRM after a 30-mT AF demagnetization treatment. On the right is the interpreted polarity; black = normal polarity; cross-hatching = indeterminate polarity.

report we have used the shipboard depth assigned in Hole 911A for our analysis; as better depth assignments become available, it would be appropriate to propagate the new depths into our analysis. The most reliable depth registration would most likely come from down-hole logging.

In Figure 15 we propose an interpretation of the inclination record in terms of normal and reversed polarity zones. The frequency of intermediate direction measurements makes it difficult to draw magnetozone boundaries on the basis of individual data points. Instead, we have calculated a smoothed curve (running mean) through the data points that captures the salient features of the inclination record and have picked the magnetozone boundaries at the stratigraphic level where the smoothed inclination crosses 0°. At two levels (45 and 120 mbsf) the inclination record seems to cross 0° for a short interval but never completely establishes an interval of the opposite polarity. These we have denoted with gray zones in the polarity interpretation column. The sediment in this section is primarily of reversed polarity with four relatively thin normal intervals. Missed recovery and extremely deformed core sections create some gaps in the section, but the record is fairly well defined by the available data.

Correlation with Geomagnetic Polarity Time Scale and Biostratigraphy

Although part of the NRM is probably carried by iron sulfides, it is possible some of these minerals, such as greigite, formed very early in the diagenetic history of the sediment. Thus, despite the fact that the NRM of the sediments is likely a composite chemical remanent magnetization (CRM) and detrital remanent magnetization (DRM), it is likely that the NRM faithfully records the geomagnetic field from shortly after the time of deposition, and that the polarity stratigraphy provides a chronostratigraphic framework. We have correlated the polarity stratigraphy from Hole 911A to the geomagnetic polarity time scale (GPTS) as shown in Figure 15. In this hole we have identified the Brunhes, Matuyama, and Gauss chronozones, as well as the Jaramillo and Olduvai subchronozones. We have tentatively identified the Emperor and Cobb Mountain events, as shown in Figure 15. Only the normal interval at 127 to 132 mbsf is unidentified with no obvious or reasonable correlation to the GPTS. Visual inspection of this interval showed that it contained exceptionally well-developed drilling biscuits with a high ratio of churned-up matrix material to in-

tact sediment. Further work on discrete samples should help in determining if this is a true normal polarity interval, an artifact of the drilling process, or a result of incomplete demagnetization of a high coercivity overprint.

Using the magneto-chronology of Cande and Kent (1992), we see that the correlations to their time scale expressed in Figures 15 and 16 are consistent with the biostratigraphy described in the "Biostratigraphy" section (this chapter) and the published ranges of the microfossils described from Site 911. On the basis of the shipboard planktonic foraminifer biostratigraphy, the Pliocene/Pleistocene boundary in Hole 911A is constrained to between Cores 151-909A-22X and -37X, which is consistent with the position estimated at 240 mbsf on the basis of shipboard magnetostratigraphy and the GPTS of Cande and Kent (1992). The magnetostratigraphic correlation proposed in Figure 16 is also consistent with the microfossils described at Site 911 and their established ranges (Sato and Takayama, 1992). In particular, the last-appearance datum (LAD) of the large form of *Gephyrocapsa*, which Sato and Takayama (1992) placed within the Cobb Mountain Event, falls very near the inclination anomaly we have tentatively identified as the Cobb Mountain Event.

Sedimentation Rates

Sedimentation rates at Site 911 ranged from 170 m/m.y. in the Pliocene and pre-Jaramillo, and were reduced to about 100 m/m.y. during the last million years (see Table 4).

Conclusions

The Site 911 sedimentary paleomagnetic record exhibited surprisingly meaningful correlations to the GPTS, despite the presence of ferromagnetic iron sulfides in the cored sediments. This suggests either short time delays between DRM and CRM acquisition or, more probably, the efficiency of a 30-mT AF demagnetization in removing the major part of spurious remagnetizations, with the notable exception of highly coercive concretionary layers in Hole 911A bottom sediments.

Temporal constraints are thus indicated with the available data set, and suggest very high Pliocene and Pleistocene sedimentation rates, similar to those of other sedimentary sequences recovered from the Yermak Plateau.

INORGANIC GEOCHEMISTRY

Interstitial Water

Table 5 and Figure 17 show the composition of interstitial water samples at Site 911. Sodium is slightly less abundant than in seawater (486 mmol/L) and shows little variation except for slightly lower values around 30 and 380 mbsf. The generally depleted sodium concentration is due to dilution by interlayer water given up by clay minerals during early diagenesis. Potassium falls from seawater levels at the sediment water interface to less than half the seawater value at the bottom of Hole 911A. Once again, fixation during early clay diagenesis is absorbing potassium.

Magnesium shows a curved decrease from near the seawater level (54.7 mmol/L) to about 30 mmol/L by 150 mbsf, then remains constant at that level in the remainder of the hole. There is no indication that magnesium is diffusing to greater depths, and magnesium is probably in equilibrium with the adsorption potential of the clay minerals in these sediments. Calcium, on the other hand, shows an interesting profile, decreasing rapidly from near the seawater value (10.7 mmol/L) to about 3 mmol/L at around 75 mbsf, then increasing steadily to 8 mmol/L at the bottom of Hole 911A. Calcium apparently is being supplied to the upper parts of the sediment column by diffusion from below. In addition, early dissolution of biogenic carbonates and/or diffusion from seawater appears to be supplying calcium near the surface.

The records of alkalinity and pH do not indicate a diffusive gradient for carbonate species. Alkalinity peaks near the surface at more than five times the seawater value (~2.3 meq/L) at 35 mbsf, then remains relatively steady at about 10 meq/L to the bottom of the hole. Chloride concentrations are nearly constant at 530 to 540 mmol/L, slightly below the seawater value of 566 mmol/L. Like sodium, chlo-

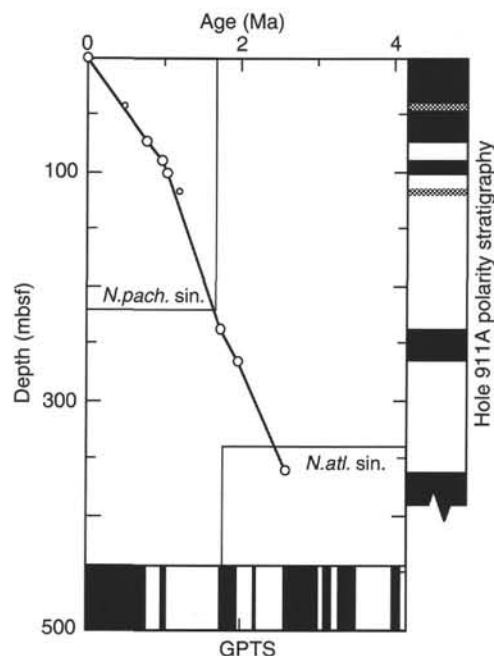


Figure 16. Age-depth model based on the magnetostratigraphy of sediments at Hole 911A. The white rectangles indicate the age and depth ranges of *Neogloboquadrina pachyderma* sin. and *Neogloboquadrina atlantica* sin. in Hole 911A (see "Biostratigraphy" section, this chapter). The black and white column along the bottom of the graph is the GPTS of Cande and Kent (1992), and the column along the right side of the graph is the polarity stratigraphy from Hole 911A (Fig. 15).

Table 4. Magnetozone boundaries and apparent sedimentation rates in Holes 911A and 911B.

Depth (mbsf)	Age (Ma)	Sed. rate (m/m.y.)	Chron
Hole 911A			
0	0		
72	0.78	(92 m/m.y.)	C1n
90	0.984	(88 m/m.y.)	
101	1.049	(169 m/m.y.)	C1r.1n
236	1.757	(191 m/m.y.)	
268	1.983	(142 m/m.y.)	C2n
360	2.6	(149 m/m.y.)	
			C2An.1n
Hole 911B			
0	0		
67	0.78	(86 m/m.y.)	C1n
81	0.984	(69 m/m.y.)	
96	1.049	(231 m/m.y.)	C1r.1n

Note: Sedimentation rates are calculated by linear interpolation between two successive ages.

Table 5. Composition of interstitial waters in Hole 911A.

Core, section	Depth (mbsf)	Na (mmol/L)	K (mmol/L)	Mg (mmol/L)	Ca (mmol/L)	Cl (mmol/L)	SO ₄ (mmol/L)	SiO ₂ (μmol/L)	NH ₄ (μmol/L)	pH	Alkalinity (meq/L)
151-911A-											
1H-5	7.45	444.06	9.87	41.33	7.30	535	11.8	155	509	7.60	9.596
4H-5	35.95	385.72	8.80	34.13	3.19	539	1.3	288	2155	7.84	17.140
7H-4	62.95	399.14	7.62	31.34	2.96	534	0.5	326	3521	7.63	9.800
10H-1	85.60	411.30	7.29	29.83	3.11	533	0.5	389	4457	7.98	10.512
13H-6	120.35	421.58	7.65	29.26	3.33	528	0.3	283	5912	7.97	11.004
16X-4	145.85	415.06	6.95	27.99	3.62	528	0.4	514	6230	7.65	11.777
19X-4	174.55	423.09	7.11	28.02	3.86	524	0.9	418	6675	7.66	10.288
22X-4	203.19	433.00	6.68	28.21	3.95	533	0.7	389	7272	7.63	10.141
25X-4	229.30	436.60	6.46	27.96	4.55	542	0.4	308	7941	7.73	10.168
28X-3	259.90	438.81	5.89	28.05	5.02	536	0.4	400	7704	7.74	9.555
31X-4	290.20	436.57	5.64	29.02	5.39	542	0.1	422	6675	7.49	8.339
34X-3	316.20	430.75	5.98	29.11	5.57	540	0.3	308	6230	7.78	8.277
37X-4	348.82	637.91	8.97	43.82	8.18	533	1.1	617	5945	7.60	9.618
40X-5	377.45	389.17	5.01	29.07	6.27	542	0.5	353	6247	7.71	9.844
43X-2	402.24	403.91	5.10	29.46	6.70	554	0.9	519	6572	7.49	10.502
46X-3	432.82	412.78	5.45	29.58	7.25	539	0.5	227	6146	7.85	8.666
49X-4	463.40	414.04	4.86	29.67	7.97	544	0.9	346	6537	7.71	8.085
52X-5	492.74	426.29	5.61	29.16	8.13	538	1.0	362	5386	7.76	8.071

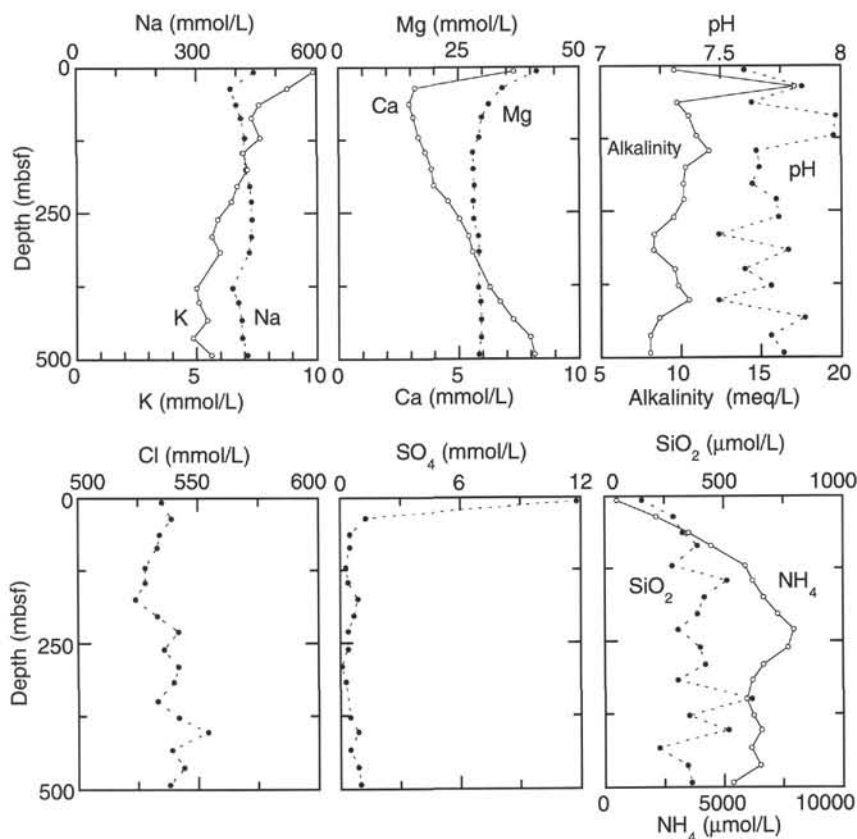


Figure 17. Interstitial water compositions at Site 911.

ride is diluted by interlayer waters exuded by clay minerals during early diagenesis.

Sulfate drops from almost 12 mmol/L (less than half the seawater value) to essentially zero within the first 60 mbsf in Hole 911A. Bacterial sulfate reduction is actively consuming sulfate, which is diffusing in from the overlying seawater. Ammonia is very abundant in the deeper parts of Hole 911A and relatively constant below about 250 mbsf. Ammonia decreases to near zero at the sediment water interface as a result of diffusion to the seafloor, where it is oxidized. The sulfate profile shows that interstitial waters are anoxic very close to the sediment water interface and that the inward diffusion of oxygen does not affect subsurface ammonia levels.

Sediment Geochemistry

Table 6 gives the abundances of major elements in Hole 911A expressed as weight percent of the oxides. Silica and alumina (Fig. 18) show little variation down the core. Silica is, however, relatively high, averaging around 60 wt%. Magnesium (Fig. 18) shows a very slight decline with increasing depth, and calcium is virtually constant except for two intervals (51.1 and 278.3 mbsf) where calcium content is elevated, probably by the accumulation of calcium carbonate.

Potassium (Fig. 18) shows a slightly variable distribution with a decreasing trend with depth. Sodium (Fig. 18) is remarkably constant down the hole. Neither alkali element shows any anomaly in its dis-

Table 6. Major element composition of sediments in Hole 911A.

Core, section	Depth (mbsf)	SiO ₂ (wt%)	TiO ₂ (wt%)	Al ₂ O ₃ (wt%)	Fe ₂ O ₃ (wt%)	MnO (wt%)	MgO (wt%)	CaO (wt%)	Na ₂ O (wt%)	K ₂ O (wt%)	P ₂ O ₅ (wt%)	Total (wt%)
151-911A-												
1H-6	7.77	58.60	0.97	16.57	7.80	0.11	3.27	2.11	1.96	3.46	0.19	95.04
2H-3	13.11	58.03	0.96	16.43	7.38	0.13	3.20	2.02	2.00	3.58	0.19	93.91
3H-3	23.06	59.52	1.01	17.19	6.85	0.05	3.16	1.98	1.94	3.26	0.19	95.15
4H-3	32.00	60.71	0.91	16.72	7.68	0.07	3.10	1.86	2.24	3.54	0.17	97.00
5H-3	41.64	60.18	0.91	15.48	6.58	0.05	3.05	2.26	1.95	3.12	0.18	93.76
6H-3	51.14	57.85	0.84	14.47	5.82	0.05	2.96	3.76	1.79	3.03	0.22	90.78
7H-3	60.63	59.53	0.94	16.64	7.43	0.16	2.99	1.91	2.03	3.43	0.21	95.27
8H-3	68.83	62.28	0.94	15.82	6.90	0.05	3.18	2.11	1.94	3.27	0.19	96.68
9H-4	79.02	60.88	0.93	16.90	6.82	0.05	3.01	2.00	2.15	3.33	0.17	96.22
10H-3	87.94	59.79	0.98	16.53	8.06	0.09	3.40	2.08	2.14	3.59	0.17	96.84
11H-3	97.34	60.25	0.97	16.51	7.78	0.05	3.33	1.94	2.08	3.48	0.16	96.55
12H-3	105.54	60.43	0.96	17.27	7.06	0.06	3.12	2.10	1.97	3.38	0.16	96.52
13H-3	115.06	60.21	0.97	16.64	6.64	0.06	3.12	2.18	2.00	3.25	0.20	95.27
14H-3	124.54	59.18	0.91	15.83	6.69	0.05	3.31	2.17	2.10	3.21	0.21	93.65
15H-3	134.03	59.52	1.00	17.42	7.50	0.05	3.04	1.90	2.03	3.53	0.15	96.13
16X-3	143.62	58.84	0.93	16.13	6.97	0.05	2.91	2.01	1.83	3.05	0.25	92.98
17X-3	152.92	61.36	0.92	16.98	6.50	0.05	2.82	1.85	2.27	3.12	0.18	96.04
18X-3	162.64	59.35	0.99	17.11	7.49	0.05	3.11	2.04	1.86	3.30	0.20	95.52
19X-3	172.28	60.64	0.96	16.62	7.13	0.07	3.05	2.00	1.93	3.24	0.27	95.91
20X-3	181.90	59.97	0.95	17.04	7.39	0.05	3.14	2.03	1.99	3.46	0.17	96.20
21X-3	191.54	60.58	0.97	16.80	6.74	0.05	3.27	2.13	2.01	3.34	0.18	96.09
22X-3	201.05	60.43	0.93	15.97	7.20	0.09	2.70	1.98	1.73	2.87	0.27	94.18
23X-3	210.71	59.64	0.94	16.58	7.61	0.07	3.11	2.06	1.97	3.37	0.19	95.53
24X-3	219.34	59.35	0.95	16.92	7.56	0.07	2.99	2.08	1.89	3.37	0.20	95.36
25X-3	230.04	60.29	0.97	17.36	7.32	0.08	3.13	1.99	2.12	3.57	0.21	97.03
26X-3	239.73	61.26	0.88	14.69	5.66	0.05	2.89	2.06	1.96	2.98	0.21	92.65
27X-3	249.38	58.63	0.92	16.84	8.73	0.08	2.95	1.90	1.99	3.32	0.39	95.75
28X-1	256.13	58.45	0.98	17.37	7.86	0.08	3.14	1.87	1.99	3.60	0.34	95.69
29X-3	268.25	60.12	0.98	17.26	7.17	0.04	2.87	1.86	1.91	3.51	0.16	95.88
30X-3	278.34	60.73	0.86	14.53	5.87	0.07	2.44	2.28	1.76	2.59	0.24	91.37
31X-3	287.94	59.52	0.84	15.78	7.23	0.05	2.92	1.92	1.98	2.90	0.19	93.34
33X-3	307.24	59.57	0.91	16.68	7.52	0.07	2.86	2.00	1.97	3.10	0.23	94.91
34X-3	316.94	60.87	0.94	16.69	6.40	0.04	2.79	1.88	1.89	3.13	0.18	94.80
35X-3	326.54	62.02	0.89	15.90	6.39	0.05	2.76	1.83	1.91	2.83	0.19	94.76
36X-3	336.20	62.02	0.96	16.19	7.23	0.05	2.96	1.80	2.02	3.26	0.15	96.65
37X-3	345.00	61.39	0.99	16.36	7.58	0.06	3.01	1.92	1.93	3.14	0.18	96.56
38X-3	354.95	59.99	0.97	17.14	7.11	0.05	2.95	1.90	1.89	3.33	0.17	95.49
39X-3	364.93	61.64	0.86	15.07	6.28	0.08	2.42	1.92	1.91	2.67	0.47	93.33
40X-3	374.49	62.68	0.85	14.06	6.45	0.07	2.46	1.77	1.82	2.45	0.24	92.85
41X-3	384.00	59.77	1.00	17.12	7.84	0.06	2.94	1.98	1.94	3.12	0.17	95.93
42X-3	392.71	60.92	0.98	16.86	6.95	0.04	2.73	1.82	2.00	3.04	0.15	95.49
43X-3	402.95	61.39	0.99	17.15	6.85	0.04	2.71	1.80	2.05	3.06	0.14	96.17
44X-3	412.94	61.35	0.91	15.34	6.91	0.04	2.70	1.92	1.90	2.81	0.26	94.15
45X-3	422.39	58.63	0.98	17.48	7.77	0.05	2.81	1.78	1.89	2.97	0.18	94.54
46X-3	432.07	60.27	0.96	16.24	6.85	0.04	2.68	1.83	1.89	2.95	0.21	93.92
47X-3	441.84	58.76	0.96	17.42	7.00	0.05	2.91	1.92	2.11	3.19	0.17	94.47
48X-3	451.01	61.08	0.92	15.32	6.61	0.04	2.67	1.85	1.87	2.74	0.24	93.33
49X-3	461.14	58.61	1.03	17.84	7.73	0.06	2.81	1.92	1.95	3.04	0.18	95.17
50X-3	470.83	60.28	0.96	16.36	7.01	0.04	2.72	1.83	1.97	2.98	0.19	94.34
51X-3	480.44	58.86	1.01	18.16	7.93	0.05	2.80	1.85	1.88	2.91	0.18	95.64
52X-3	489.18	58.67	1.01	17.65	7.75	0.05	2.95	1.98	2.00	3.21	0.18	95.44
53X-3	499.07	58.86	1.00	17.75	7.83	0.05	2.81	1.92	1.80	3.07	0.24	95.33

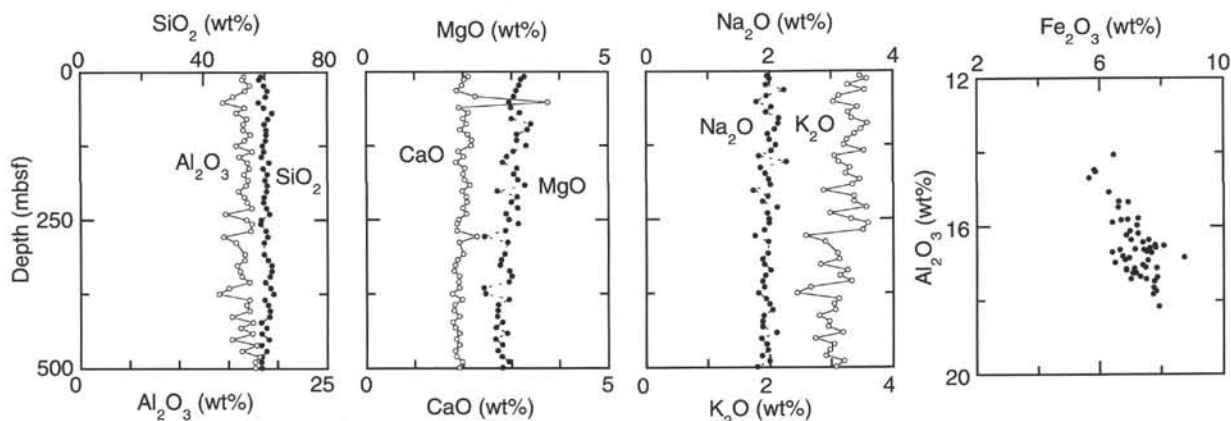


Figure 18. Sediment compositions at Site 911.

tribution, and the sediment chemistry in Hole 911A is noticeably invariant.

The only inter-element variation of any consequence is the covariance of iron and aluminum shown in Figure 18. The source of this variation is presumably variations in the abundance of an iron-bearing aluminosilicate mineral, probably glauconite.

Discussion

It is worth noting that the degradation of organic matter in the sediments at Site 911 is, for the most part, "fermentative," that is, proceeding without oxygen. The consumption of oxygen and sulfate is complete very near the surface, and the production of ammonia (Fig.

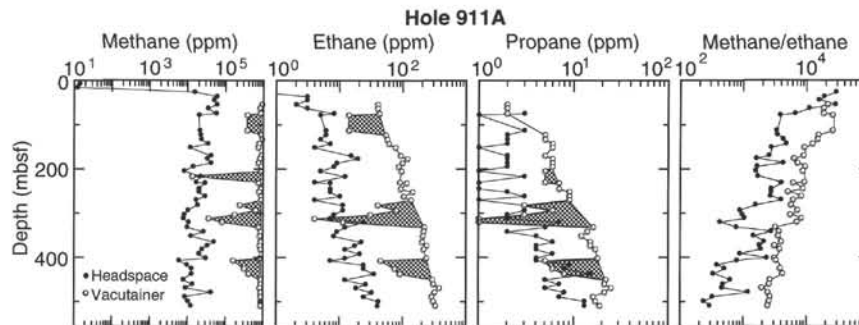


Figure 19. Records of headspace and vacutainer methane (C_1), ethane (C_2), and propane (C_3) concentrations and C_1/C_2 ratios in sediments from Hole 911A.

17) and methane (see “Organic Geochemistry” section, this chapter) is distributed throughout the column below the level where sulfate goes to zero. Neither oxygen nor sulfate penetrate to depth at this site.

The absence of a diffusive gradient for magnesium while calcium maintains its flux upward is unexplained. In addition, the rapid increase of calcium near the top of the column suggests that the sink for calcium may be within the sediments. The possibilities remain that the chemistry of the first core taken at the site is disturbed by the coring process and that the anomalous behavior of calcium in the first core sampled is an artifact.

ORGANIC GEOCHEMISTRY

The shipboard organic geochemistry program at Site 911 consisted of analyses of volatile hydrocarbons and determinations of inorganic carbon, total nitrogen, total carbon, and total sulfur (for methods, see “Explanatory Notes” chapter, this volume).

Volatile Hydrocarbons

As part of the shipboard safety and pollution monitoring program, concentrations of methane (C_1), ethane (C_2), and propane (C_3) gases were monitored every core using standard ODP headspace-sampling technique. Whenever gas voids occurred, also vacutainer samples were taken from these voids.

Except for the uppermost about 25 mbsf, concentrations of headspace methane are high throughout the sedimentary section, ranging from 6000 to 60,000 ppm (Fig. 19, Table 7). No distinct long-term change is obvious. The methane record at Site 911 is similar to that at Site 910. First minor amounts (about 3 ppm) of ethane and propane were determined below about 50 mbsf. Below this depth, ethane and propane consistently increase downhole, reaching maximum concentrations of 40 ppm and 13 ppm, respectively, at the bottom of the hole (Fig. 19).

The vacutainer concentrations show general trends similar to the headspace values; however, the vacutainer concentrations are systematically higher. Furthermore, distinct minima in gas concentrations were obvious at 80–110, 210–230, 280–330, and 400–440 mbsf (Fig. 19). Similar minima were also recorded at Site 910 in depths of 200–250 and 400–450 mbsf. These distinct variations in gas concentrations may suggest distinct variations in primary gas production and/or lithologic parameters such as porosity, grain size, etc. A comparison of the gas data with other lithologic as well as geochemical parameters should help to distinguish among different mechanisms causing the variations in gas content.

For safety considerations, the C_1/C_2 ratio is generally used to get quick information about the origin of the hydrocarbons (i.e., to distinguish between biogenic gas and gas migrated from a deeper source of thermogenic hydrocarbons). Very high C_1/C_2 ratios indicate a gas

(C_1) formation by microbiological processes. On the other hand, the occurrence of major amounts of C_2 (to C_3) in shallow depths is associated with thermogenic hydrocarbon generation. In general, the C_1/C_2 ratios consistently decrease with burial depth because of the increasing influence of early diagenetic generation of hydrocarbons.

At Site 911, the headspace C_1/C_2 ratios show the “normal” general decrease with depth, from values of $>10,000$ in shallow depths to values of 300 at 500 mbsf (Fig. 19). The same trend also is recorded in the vacutainer data, but with an offset toward higher values (see Stein et al., this volume). The high C_1/C_2 ratios suggest in-situ microbial production of methane from marine organic carbon, which is present in major amounts in the entire sedimentary sequence (see below). At Hole 911A, the methanogenesis has begun at depths shallower than 25 mbsf, as clearly indicated by the sharp increase in methane concentrations and the contemporaneous sharp cessation of sulfate reduction (see “Inorganic Geochemistry” section, this chapter).

Carbon, Nitrogen, and Sulfur Concentrations

The results of determinations of inorganic carbon, carbonate, total carbon, total nitrogen, and total sulfur are summarized in Table 8 and presented in Figures 20, 21, and 22.

Most of the carbonate values of the sedimentary sequence of Hole 911A vary between 1% and 6% (Fig. 20). Only between 210 and 240 mbsf and in the upper 50 m, several single peaks of carbonate contents as high as 10% to 25% occur (Fig. 20, Table 8). Some of the carbonate maxima at Hole 911A coincide with maxima of inorganic calcite as determined by smear slides (see “Lithostratigraphy” section, this chapter), indicating a nonbiogenic source of significant proportions of the carbonate.

The total organic carbon (TOC) contents vary between 0.5% and 1.5% (Fig. 20). The higher values of 0.7% to 1.5% (mean values of about 1.2%) occur in the upper Pliocene interval between 350 and 500 mbsf, whereas the upper 240 m (Quaternary) are characterized by lower values mostly varying between 0.5% and 1.3% (mean value of 0.9%). The transitional zone with upward decreasing mean TOC values falls into the time interval between about 2.6 and 1.9 Ma. A three-point moving-average record plotted vs. age suggests distinct short-term rhythmic (“Milankovitch-type”) changes in organic carbon deposition (see below) (Fig. 21). Because the shipboard record is based on a sampling density of 15 to 30 k.y. (which is the mean sampling interval according to mean sedimentation rates), the higher-frequency bands of the Milankovitch-type cyclicity, which appear to be reflected in the logging records (see “Downhole Measurements” section, this chapter), cannot be resolved with the present data set.

The total nitrogen contents range from 0.05% to 0.17% (Table 8). In general, the total sulfur values vary between 0.0% and 0.6% throughout the entire section (Fig. 20). Single peaks of very high values of about 2% and 5% occasionally occur (Table 8), probably reflecting sulfide-rich layers (see “Lithostratigraphy” section, this chapter).

Table 7. Results of headspace (HS) and vacutainer (VAC) gas analysis from Hole 911A.

Core, section, interval top (cm)	Depth (mbsf)	C ₁ -HS	C ₂ -HS	C ₃ -HS	C ₁ /C ₂ -HS	C ₁ -VAC	C ₂ -VAC	C ₃ -VAC	C ₁ /C ₂ -VAC
151-911A-									
1H-6, 0	8	14	0	0					
2H-6, 0	17	12	0	0					
3H-6, 0	27	15150	0	0	30300				
4H-6, 0	36	58525	3	0	19508				
5H-5, 0	44	49139	3	0	16380				
6H-6, 0	55	58525	2	0	29263	906041	40	2	22651
7H-5, 0	63	34538	3	0	11513	797391	40	2	19935
8H-6, 0	74	55453	8	3	6932	833374	42	2	19842
9H-3, 0	78	19701	5	1	3940	377197	14	0	26943
13H-2, 0	113	20652	6	3	3442	377197	14	0	26943
14H-2, 0	122	21316	6	2	3553	877132	54	5	16243
15H-2, 0	132	22273	5	2	4455	894017	57	5	15685
16X-2, 0	141	34322	7	2	4903	771746	59	6	13080
17X-2, 0	151	11630	4	1	2908	740021	77	6	9611
18X-7, 67	169	39668	15	2	2645	876138	93	5	9421
19X-5, 0	176	32069	19	2	1688	787172	118	6	6671
20X-5, 0	184	40331	9	2	4481	739008	97	6	7619
21X-5, 0	194	13767	8	2	1721	860013	85	6	10118
22X-5, 0	204	8116	5	1	1623	864659	95	5	9102
23X-6, 0	215	21253	12	3	1771				
24X-8, 0	227	16197	4	1	4049	874873	89	5	9830
25X-3, 0	229	28707	7	1	4101	730340	114	7	6406
26X-5, 0	242	19945	7	1	2849	837152	92	7	9099
27X-3, 0	249	19901	7	2	2843	766165	144	9	5321
28X-4, 0	260	27868	10	3	2787	880432	102	9	8632
29X-3, 0	268	16197	4	1	4049	873084	135	9	6467
30X-4, 0	279	17998	11	3	1636	241118	40	3	6028
31X-5, 0	290	10028	11	3	912	608672	79	6	7705
32X-5, 0	300	8038	8	2	1005	172887	30	3	5763
33X-4, 0	308	7600	7	2	1086	34783	4	1	8696
34X-4, 0	318	10688	24	7	445	81096	11	1	7372
35X-5, 0	329	9612	12	5	801	741299	219	16	3385
36X-5, 0	339	26131	9	2	2903	840424	215	14	3909
37X-5, 0	349	11918	8	4	1490	782104	206	12	3797
38X-7, 0	361	48384	22	6	2199	852403	202	15	4220
39X-7, 0	370	31643	17	4	1861	800806	241	15	3323
40X-6, 0	378	23777	12	4	1981	851243	213	17	3996
41X-6, 0	388	19376	21	6	923				
42X-6, 0	398	29399	12	4	2450	795572	241	18	3301
43X-2, 112	402	5780	7	4	826	154949	44	5	3522
44X-3, 0	412	9495	24	9	396				
45X-3, 0	422	12542	24	8	523	304567	74	6	4116
46X-4, 0	433	12280	35	15	351	402267	90	8	4470
47X-6, 0	446	7778	12	5	648	821042	293	22	2802
48X-6, 0	455	12831	26	7	494	829668	305	21	2720
49X-5, 0	464	8760	18	5	487	781638	375	25	2084
50X-5, 0	473	39765	32	8	1243	821502	322	21	2551
51X-6, 0	484	8199	24	7	342	819903	290	16	2827
52X-6, 0	494	10011	41	13	244	825412	303	17	2724
53X-6, 0	504	12167	40	13	304	843204	330	19	2555

Note: Methane (C₁), ethane (C₂), and propane (C₃) concentrations are given in parts per million (ppm).

Composition of Organic Matter

According to the C/N ratios that have been used to characterize the type of organic matter (see "Organic Geochemistry" section, "Site 907" chapter, this volume; Stein, 1991a), the sedimentary record of Hole 911A can be divided into two intervals. The lower interval between 360 and 500 mbsf is characterized by relatively constant low C/N ratios between 6 and 10, indicating a clear dominance of the marine material (Figs. 20 and 22; Table 8). The upper 350 mbsf (late Pliocene to Quaternary in age), on the other hand, show high-amplitude variations in C/N ratios between 5 and 18, which suggest distinct changes in the composition of the organic matter. The peaks with high C/N ratios of >10 probably reflect the presence of major amounts of terrigenous material. Unfortunately, only a few hydrogen index values could be determined because of technical problems with the Rock-Eval instrument. These values are all low (35 to 110 mgHC/gC) and indicate a high proportion of terrigenous material in the sediments of Site 911. Thus, at the moment, the classification of the composition of the organic matter and its change through time is only based on C/N ratios and has to be proved by further shore-based organic geochemical investigations.

Based on the present data, the changes in organic carbon contents probably reflect changes in both surface-water productivity and terrigenous organic carbon supply. The long-term decrease in (according to the low C/N marine ratios) organic carbon accumulation starting at about 2.6 Ma (380 mbsf) may indicate a major decrease in surface-water productivity, probably caused by the first occurrence of major extended sea-ice coverage in the Yermak Plateau area. This drop in productivity because of extended ice conditions is also supported by the contemporaneous increase in amounts of dropstones in the Site 911 sediments (see "Lithostratigraphy" section, this chapter). Based on average values of organic carbon, sedimentation rate, and dry-bulk density (see "Physical Properties" section, this chapter), mass accumulation rates of organic carbon have been calculated for the time intervals 2.6 to 3.2 Ma and 0 to 0.8 Ma, resulting in 0.32 gC/cm²/k.y. and 0.09 gC/cm²/k.y., respectively (for calculation procedure of accumulation rates, see "Organic Geochemistry" section, "Site 907" chapter, this volume). That means the average accumulation rate of (marine) organic carbon on the Yermak Plateau, before the major expansion of Northern Hemisphere glaciation at 2.6 Ma, was by a factor of 3–4 higher than the middle to late Quaternary rate. These relative differences in marine organic carbon accumulation

Table 8. Summary of geochemical analyses of sediments in Hole 911A.

Core, section, interval top (cm)	Depth (mbsf)	TC (%)	IC (%)	TOC (%)	CaCO ₃ (%)	TN (%)	TS (%)	C/N	C/S
151-911A-									
IH-1, 61	0.61	0.93	0.19	0.74	1.6	0.09	0.19	8.2	3.9
IH-1, 92	0.92	1.06	0.71	0.35	5.9	0.07	0.13	5.0	2.7
IH-2, 48	1.98	1.98	0.64	1.34	5.3	0.12	0.25	11.2	5.4
IH-2, 60	2.10	1.45	0.90	0.55	7.5	0.08	0.13	6.9	4.2
IH-2, 103	2.53	0.78	0.29	0.49	2.4	0.08	0.10	6.1	4.9
IH-3, 42	3.42	0.93	0.28	0.65	2.3	0.10	0.00	6.5	
IH-4, 18	4.68	1.67	0.24	1.43	2.0	0.11	0.10	13.0	14.3
IH-4, 48	4.98	0.79	0.28	0.51	2.3	0.08	0.06	6.4	8.5
IH-5, 48	6.48	1.21	0.36	0.85	3.0	0.11	0.00	7.7	
IH-5, 109	7.09	4.34	0.98	1.40	24.5	0.09	0.06	15.6	23.3
IH-6, 60	8.10	1.02	0.19	0.83	1.6	0.10	0.06	8.3	13.8
2H-1, 75	10.25	1.28	0.33	0.95	2.7	0.10	0.08	9.5	11.9
2H-2, 63	11.63	1.03	0.14	0.89	1.2	0.12	0.18	7.4	4.9
2H-3, 26	12.76	0.88	0.34	0.54	2.8	0.10	0.10	5.4	5.4
2H-4, 16	14.16	0.88	0.43	0.45	3.6	0.11	0.11	4.1	4.1
2H-5, 30	15.80	1.13	0.24	0.89	2.0	0.12	0.10	7.4	8.9
2H-6, 43	17.43	1.39	0.43	0.96	3.6	0.13	0.16	7.4	6.0
3H-1, 24	19.24	0.83	0.39	0.44	3.2	0.10	0.00	4.4	
3H-3, 24	22.24	1.71	0.60	1.11	5.0	0.06	0.17	18.5	6.5
3H-5, 24	25.24	1.24	0.24	1.00	2.0	0.12	0.16	8.3	6.2
3H-7, 24	28.24	1.28	0.39	0.89	3.2	0.09	0.09	9.9	9.9
4H-1, 42	28.92	0.79	0.09	0.70	0.7	0.10	1.71	7.0	0.4
4H-3, 42	31.92	0.87	0.27	0.60	2.2	0.10	0.28	6.0	2.1
4H-5, 42	34.92	1.24	0.38	0.86	3.2	0.12	0.36	7.1	2.4
5H-1, 32	38.32	1.43	0.35	1.08	2.9	0.11	0.43	9.8	2.5
5H-3, 32	41.32	2.07	0.34	0.93	2.8	0.10	0.48	9.3	1.9
5H-3, 43	41.43	2.09	1.12	0.97	9.3	0.09	0.33	11.0	2.9
5H-5, 33	44.33	1.30	0.37	0.93	3.1	0.10	0.34	9.3	2.7
6H-1, 49	47.99	0.97	0.26	0.71	2.2	0.09	0.08	7.9	8.9
6H-1, 133	48.83	2.34	1.18	1.16	3.1	0.10	0.22	11.6	5.3
6H-3, 49	50.99	1.47	0.81	0.66	6.7	0.08	0.14	8.2	4.7
6H-5, 49	53.99	1.29	0.47	0.82	3.9	0.10	0.36	8.2	2.3
6H-7, 49	56.99	1.20	0.44	0.76	3.7	0.09	0.37	8.4	2.0
7H-1, 41	57.41	1.00	0.42	0.58	3.5	0.08	0.10	7.2	5.8
7H-1, 136	58.36	1.58	0.40	1.18	3.3	0.12	5.48	9.8	0.2
7H-3, 40	60.40	1.01	0.19	0.82	1.6	0.11	0.12	7.4	6.8
7H-5, 40	63.40	1.01	0.01	1.00	0.1	0.11	0.12	9.1	8.3
8H-1, 27	65.47	1.26	0.34	0.92	2.8	0.12	0.18	7.6	5.1
8H-3, 27	68.47	1.35	0.30	1.05	2.5	0.08	0.06	13.1	17.5
8H-5, 27	71.47	1.18	0.56	0.62	4.7	0.10	0.08	6.2	7.7
8H-7, 25	74.45	1.78	0.26	1.52	2.2	0.11	0.07	13.8	21.7
9H-1, 24	74.94	0.94	0.19	0.75	1.6	0.09	0.07	8.3	11.0
9H-3, 23	77.03	1.12	0.24	0.88	2.0	0.11	0.06	8.0	14.0
9H-5, 21	80.01	0.88	0.45	0.83	3.7	0.10	0.16	8.3	5.2
10H-1, 76	84.96	0.83	0.21	0.62	1.7	0.08	0.14	7.7	4.4
10H-3, 76	87.96	1.00	0.28	0.72	2.3	0.10	0.34	7.2	2.1
10H-5, 75	90.95	0.76	0.19	0.57	1.6	0.09	0.09	6.3	6.3
11H-1, 56	94.26	1.51	0.33	1.18	2.7	0.12	0.19	9.8	6.2
11H-3, 56	97.26	1.16	0.29	0.87	2.4	0.11	0.12	7.9	7.2
11H-5, 58	100.28	1.24	0.24	1.00	2.0	0.11	0.08	9.1	12.5
12H-1, 28	102.18	1.13	0.27	0.86	2.2	0.10	0.07	8.6	12.0
12H-3, 58	105.48	1.48	0.25	1.23	2.1	0.14	0.08	8.8	15.4
12H-5, 90	108.80	1.13	0.24	0.89	2.0	0.11	0.07	8.1	13.0
13H-1, 26	111.66	1.07	0.24	0.83	2.0	0.11	0.12	7.5	6.9
13H-3, 26	114.66	1.66	0.32	1.34	2.7	0.10	0.23	13.4	5.8
13H-5, 26	117.66	1.51	0.27	1.24	2.2	0.13	0.10	9.5	12.4
14H-1, 37	121.27	0.91	0.17	0.74	1.4	0.09	0.08	6.7	3.8
14H-5, 24	127.10	1.17	0.17	1.00	1.4	0.09	0.26	11.1	3.8
15H-1, 19	130.59	0.75	0.18	0.57	1.5	0.10	0.11	5.7	5.2
15H-3, 34	133.74	1.19	0.25	0.94	2.1	0.13	0.09	7.2	10.0
15H-5, 25	136.65	1.27	0.26	1.01	2.2	0.12	0.10	8.4	10.1
16X-1, 26	146.16	1.24	0.13	1.11	1.1	0.11	0.07	9.2	15.8
16X-2, 110	142.50	1.25	0.31	0.94	2.6	0.11	0.09	8.5	10.0
16X-5, 26	146.16	1.14	0.28	0.86	2.2	0.12	0.08	7.1	11.0
17X-1, 111	150.51	1.46	0.26	1.20	2.2	0.12	0.08	10.0	15.0
17X-3, 111	153.51	1.71	0.58	1.13	4.8	0.12	0.18	9.4	6.3
18X-1, 110	160.10	1.67	0.48	1.19	4.0	0.12	0.12	9.9	9.9
18X-3, 23	162.23	0.90	0.18	0.72	1.5	0.06	0.10	12.0	7.2
18X-5, 26	164.86	0.75	0.24	0.51	2.0	0.11	0.08	4.6	6.4
19X-1, 59	169.19	1.26	0.25	1.01	2.1	0.12	0.00	8.4	
19X-3, 28	171.88	0.92	0.10	0.82	0.8	0.12	0.00	6.8	
19X-5, 27	174.87	1.29	0.15	1.14	1.2	0.14	0.14	8.1	
20X-1, 33	178.63	1.08	0.08	1.00	0.7	0.14	2.35	7.1	0.4
20X-3, 33	181.63	1.09	0.15	0.94	1.2	0.11	0.60	8.5	1.5
20X-5, 33	184.63	1.35	0.26	1.09	2.2	0.09	0.21	12.1	5.2
21X-1, 32	188.22	1.53	0.27	1.26	2.2	0.14	0.22	9.0	5.7
21X-3, 39	191.29	0.78	0.18	0.60	1.5	0.11	0.09	5.4	6.6
21X-5, 23	194.13	1.29	0.30	0.99	2.5	0.10	0.08	9.9	12.0
22X-1, 19	197.69	1.58	0.31	1.27	2.6	0.14	0.06	9.1	21.1
22X-3, 25	200.68	1.22	0.36	0.86	3.0	0.12	0.20	7.1	4.3
22X-5, 114	204.38	1.12	0.25	0.87	2.1	0.11	1.25	7.9	0.7
23X-1, 15	207.35	2.09	1.23	0.86	10.2	0.09	0.59	9.5	1.4
23X-3, 48	210.68	1.01	0.21	0.80	1.7	0.12	0.07	6.6	11.0
23X-5, 88	214.08	1.03	0.13	0.90	1.1	0.13	0.11	6.9	8.2
24X-1, 98	217.78	1.47	0.43	1.04	3.6	0.12	0.06	8.7	17.3
24X-3, 77	219.47	1.58	0.39	1.19	3.2	0.13	0.00	9.1	
24X-5, 89	222.00	1.23	0.24	0.99	2.0	0.11	0.00	9.0	
25X-1, 24	226.64	1.00	0.36	0.64	3.0	0.09	0.00	7.1	
25X-3, 24	229.64	1.60	0.78	0.82	6.5	0.08	0.34	10.0	2.4
26X-1, 83	236.93	0.64	0.24	0.40	2.0	0.09	0.06	4.4	6.6
26X-3, 16	239.26	3.11	2.11	1.00	17.6	0.08	1.79	12.5	0.6
26X-5, 19	242.29	1.07	0.31	0.76	2.6	0.06	0.62	12.0	1.2
27X-1, 29	246.09	1.11	0.15	0.96	1.2	0.14	0.11	6.8	8.7
27X-3, 18	248.98	1.31	0.38	0.93	3.2	0.10	0.07	9.3	13.0
27X-5, 64	251.12	1.35	0.36	0.99	3.0	0.14	0.08	7.1	12.0
28X-1, 34	255.84	1.07	0.29	0.78	2.4	0.00	0.00	6.5	
28X-3, 34	258.84	0.65	0.12	0.53	1.0	0.09	0.05	5.9	10.0
28X-5, 35	261.85	0.97	0.23	0.74	1.9	0.11	0.00	6.7	
28X-7, 13	264.63	1.04	0.24	0.80	2.0	0.09	0.00	8.9	
29X-1, 20	265.30	1.98	0.25	1.73	2.1	0.11	0.04	15.7	43.2
29X-3, 19	267.82	1.66	0.37	1.29	3.1	0.12	0.00	10.7	

Table 8 (continued).

Core, section, interval top (cm)	Depth (mbsf)	TC (%)	IC (%)	TOC (%)	CaCO ₃ (%)	TN (%)	TS (%)	C/N	C/S
29X-5, 22	270.85	1.25	0.15	1.10	1.2	0.12	0.00	9.2	
30X-1, 32	275.02	1.26	0.30	0.96	2.5	0.09	0.00	10.0	
30X-3, 26	277.96	1.39	0.77	0.62	6.4	0.06	0.06	10.0	10.0
30X-5, 28	280.88	1.70	0.60	1.10	5.0	0.07	0.00	15.7	
31X-1, 24	284.54	1.50	0.32	1.18	2.7	0.10	0.00	11.8	
31X-3, 23	287.53	1.65	0.38	1.27	3.2	0.09	0.05	14.1	25.4
31X-5, 24	290.54	1.13	0.19	0.94	1.6	0.07	0.00	13.0	
31X-7, 23	293.53	1.42	0.16	1.26	1.3	0.16	0.15	7.9	8.4
32X-1, 28	294.28	0.97	0.22	0.75	1.8	0.13	0.44	5.7	1.7
32X-3, 28	297.28	1.15	0.26	0.89	2.2	0.13	0.20	6.8	4.4
32X-5, 28	300.28	0.93	0.24	0.69	2.0	0.14	0.14	4.9	4.9
33X-1, 17	303.77	0.88	0.07	0.81	0.6	0.12	0.07	6.7	11.0
33X-3, 14	306.74	1.15	0.16	0.99	1.3	0.12	0.19	8.2	5.2
33X-4, 13	308.23	1.20	0.28	0.92	2.3	0.11	0.10	8.3	9.2
34X-1, 16	313.46	1.57	0.28	1.29	2.3	0.13	0.06	9.9	21.5
34X-3, 20	316.50	1.64	0.37	1.27	3.1	0.11	0.27	11.5	4.7
34X-5, 18	319.30	1.40	0.43	0.97	3.6	0.12	0.11	8.1	8.8
35X-1, 44	323.34	1.26	0.32	0.94	2.7	0.09	0.93	10.0	1.0
35X-3, 18	326.08	1.35	0.23	1.12	1.9	0.12	0.14	9.3	8.0
35X-5, 22	329.12	1.05	0.34	0.71	2.8	0.08	0.16	8.9	4.4
36X-1, 26	332.86	1.27	0.32	0.95	2.7	0.10	0.19	9.5	5.0
36X-3, 72	336.28	0.87	0.05	0.82	0.4	0.12	0.46	6.8	1.8
36X-5, 47	338.96	0.69	0.03	0.66	0.2	0.11	0.08	6.0	8.2
37X-1, 26	342.46	1.17	0.16	1.01	1.3	0.09	0.09	11.2	11.2
37X-3, 99	346.01	1.45	0.41	1.04	3.4	0.12	0.08	8.7	13.0
37X-5, 83	348.55	1.18	0.42	0.76	3.5	0.11	0.14	6.9	5.4
38X-1, 72	352.62	1.18	0.26	0.92	2.2	0.12	0.18	7.6	5.1
38X-3, 18	354.49	1.48	0.35	1.13	2.9	0.13	0.19	8.7	5.9
38X-5, 63	357.87	1.90	0.34	1.56	2.8	0.11	0.21	14.2	7.4
38X-6, 78	359.22	1.14	0.18	0.96	1.5	0.12	0.40	8.0	2.4
39X-1, 49	361.89	1.50	0.31	1.19	2.6	0.13	0.10	9.1	11.9
39X-3, 15	364.44	1.12	0.26	0.86	2.2	0.08	0.35	11.0	2.4
39X-5, 108	368.20	1.40	0.35	1.05	2.9	0.13	0.10	8.1	10.5
40X-1, 121	372.11	1.19	0.17	1.02	1.4	0.12	0.09	8.5	11.3
40X-3, 83	374.68	1.33	0.26	1.07	2.2	0.13	0.05	8.2	21.4
40X-5, 62	377.25	1.27	0.27	1.00	2.2	0.12	0.05	8.3	20.0
41X-1, 24	380.64	1.60	0.40	1.20	3.3	0.12	0.09	10.0	13.3
41X-3, 18	383.58	1.41	0.68	0.73	5.7	0.12	0.07	6.1	10.4
41X-5, 24	386.64	1.24	0.17	1.07	1.4	0.14	0.30	7.6	3.6
41X-6, 0	387.90	1.59	0.18	1.41	1.5	0.15	0.39	9.4	3.6
42X-1, 78	390.78	1.27	0.28	0.99	2.3	0.11	0.13	9.0	7.6
42X-3, 79	392.88	1.47	0.23	1.24	1.9	0.13	2.61	9.5	0.5
42X-5, 85	395.31	1.62	0.17	1.45	1.4	0.17	0.47	8.5	3.1
42X-7, 76	397.79	1.70	0.38	1.32	3.2	0.17	0.47	7.8	2.8
43X-1, 21	399.81	1.63	0.61	1.02	5.1	0.15	0.15	6.8	6.8
43X-3, 17	402.48	1.31	0.18	1.13	1.5	0.14	0.41	8.1	2.8
43X-5, 46	405.14	1.52	0.11	1.41	0.9	0.13	0.58	10.8	2.4
44X-1, 13	409.43	1.37	0.23	1.14	1.9	0.15	0.31	7.6	3.7
44X-2, 15	410.95	1.53	0.02	1.51	0.2	0.14	0.43	10.8	3.5
44X-3, 22	412.52	1.56	0.30	1.26	2.5	0.13	0.40	9.7	3.2
45X-1, 20	419.10	1.45	0.18	1.27	1.5	0.13	0.20	9.8	6.3
45X-3, 17	421.94	1.46	0.20	1.26	1.7	0.15	0.22	8.4	5.7
45X-5, 18	424.60	0.99	0.22	0.77	1.8	0.13	0.07	5.9	11.0
45X-7, 25	427.52	1.36	0.22	1.14	1.8	0.14	0.25	8.1	4.6
46X-1, 21	428.81	1.42	0.38	1.04	3.2	0.12	0.12	8.7	8.7
46X-3, 26	431.82	1.29	0.17	1.12	1.4	0.12	0.25	9.3	4.5
46X-5, 24	434.66	1.65	0.30	1.35	2.5	0.14	0.00	9.6	
47X-1, 20	438.40	1.47	0.27	1.20	2.2	0.14	0.05	8.6	24.0
47X-3, 21	441.41	1.35	0.30	1.05	2.5	0.11	0.00	9.5	
47X-5, 21	444.07	1.15	0.24	0.91	2.0	0.13	0.07	7.0	13.0
47X-7, 37	446.68	1.85	0.30	1.55	2.5	0.14	0.12	11.1	12.9
48X-1, 17	447.97	1.44	0.16	1.28	1.3	0.14	0.27	9.1	4.7
48X-3, 20	450.57	1.36	0.15	1.21	1.2	0.12	0.41	10.1	3.0
48X-5, 26	453.54	1.18	0.13	1.05	1.1	0.12	0.66	8.8	1.6
49X-1, 27	457.77	1.54	0.34	1.20	2.8	0.13	0.15	9.2	8.0
49X-3, 77	461.27	0.92	0.24	0.68	2.0	0.10	0.06	6.8	11.0
49X-5, 81	464.31	1.34	0.21	1.13	1.7	0.15	0.31	7.5	3.6
50X-1, 73	467.93	1.45	0.19	1.26	1.6	0.12	0.24	10.5	5.2
50X-3, 76	470.96	1.18	0.19	0.99	1.6	0.13	0.59	7.6	1.7
50X-5, 73	473.93	1.24	0.15	1.09	1.2	0.13	0.73	8.4	1.5
51X-1, 21	477.01	1.53	0.26	1.27	2.2	0.13	0.10	9.8	12.7
51X-3, 49	480.29	1.73	0.38	1.35	3.2	0.15	0.00	9.0	
51X-5, 42	483.22	1.67	0.34	1.33	2.8	0.14	0.04	9.5	33.2
52X-1, 26	486.76	1.12	0.35	0.77	2.9	0.13	0.09	5.9	8.5
52X-3, 69	489.44	1.30	0.37	0.93	3.1	0.12	0.00	7.7	
52X-5, 58	492.26	1.18	0.30	0.88	2.5	0.12	0.21	7.3	4.2
53X-1, 27	496.47	1.22	0.10	1.12	0.8	0.14	0.00	8.0	
53X-3, 109	499.53	1.48	0.10	1.38	0.8	0.17	0.07	8.1	19.7
53X-5, 27	501.45	0.96	0.08	0.88	0.7	0.11	0.04	8.0	22.0

Notes: IC = inorganic carbon; CaCO₃ = carbonate; TC = total carbon; TOC = total organic carbon; TN = total nitrogen, TS = total sulfur; C/N = total organic carbon/total nitrogen ratios; C/S = total organic carbon/total sulfur ratios.

(and surface-water productivity) might become even more drastic when the terrigenous organic carbon fraction, which is certainly higher in the Quaternary interval (see above), can be determined more accurately and subtracted from the total organic carbon values.

Based on these first shipboard results, which suggest distinct long-term and short-term ("Milankovitch-type") variations in marine and terrigenous organic carbon fluxes, the sedimentary record of Site 911 gives an excellent opportunity for a detailed organic-geochemical study of the history of surface-water productivity and climatic change during the last 3 m.y.

PHYSICAL PROPERTIES

Introduction

The shipboard physical properties program at Site 911 included nondestructive measurements of bulk density, bulk magnetic susceptibility, compressional-wave velocity, and total natural gamma activity on whole sections of core using the multi-sensor track (MST), as well as discrete measurements of thermal conductivity, compressional-wave velocity, shear strength, and index properties. The downhole

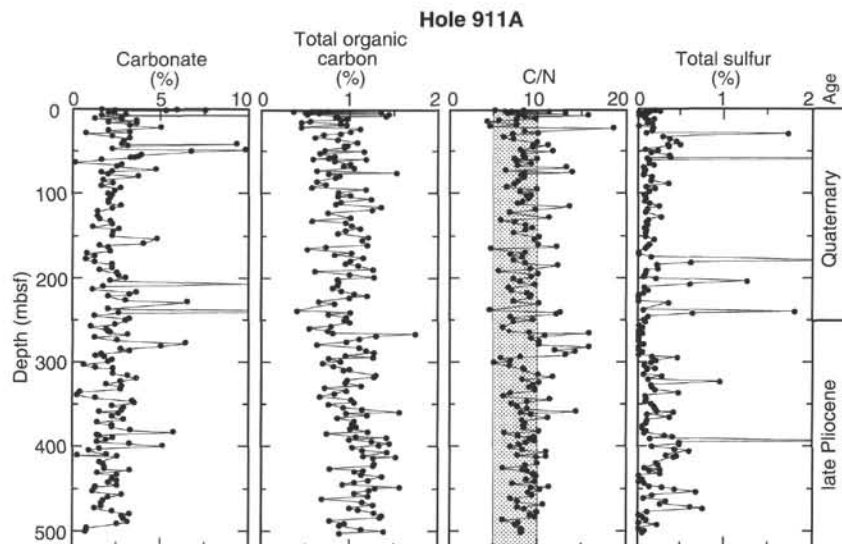


Figure 20. Carbonate contents, total organic carbon contents, organic carbon/total nitrogen (C/N) ratios, and total sulfur contents in sediments from Hole 911A. Shaded range in the C/N record marks range of dominantly marine organic matter; C/N ratios >10 may suggest significant amounts of terrigenous organic matter.

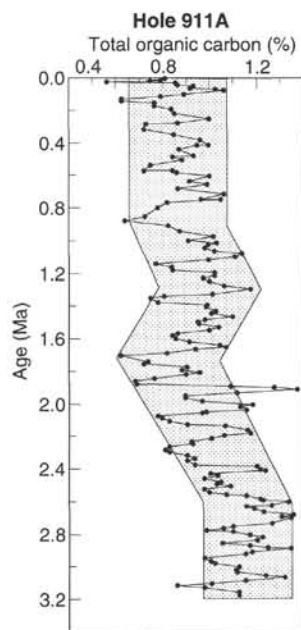


Figure 21. Smoothed record of total organic carbon contents in Hole 911A using three-point moving-average calculation, plotted vs. age. A long-term decrease in organic carbon contents between 2.6 and 1.9 Ma, and distinct short-term (cyclic) variations are obvious. The age scale is based on paleomagnetic datums (see “Paleomagnetism” section, this chapter).

temperature measurements are also reported here. Methodology is discussed in the “Explanatory Notes” chapter (this volume).

Three holes were drilled at Site 911; however, physical properties measurements were performed only in Holes 911A and 911B. In Hole 911A, 35 cores were sampled to a maximum depth of 505.8 mbsf using both APC (0–140 mbsf) and XCB (140–505.8 mbsf) drilling methods. In Hole 911B, 15 cores were retrieved to a depth of 112.1 mbsf using APC techniques exclusively. Both holes exhibited evidence of disruption caused by gas. The disruption varied in extent

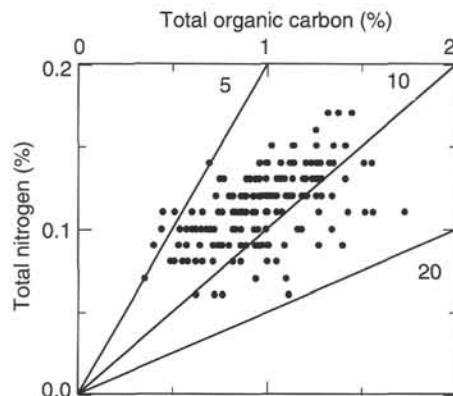


Figure 22. Total organic carbon vs. total nitrogen diagram for Hole 911A. Lines of C/N ratios of 5, 10, and 20 are indicated.

downhole from nearly intact/slightly disturbed sediment to totally broken apart. Severe biscuiting was observed in Hole 911A below 375 mbsf. The amount of useful information was thus limited, and in some cases (e.g., MST compressional-wave velocity), measurements were virtually impossible. Therefore, areas of least disturbance were selected for measurement.

Whole-core Measurements

Multi-sensor Track

Figures 23 through 25 show filtered fast Fourier transform versions of whole-core measurements performed at Site 911, together with the recovery for each hole. Whole-round velocities became extremely erratic below depths of 10–20 mbsf, probably because of the effects of gas expansion, and therefore were discontinued. Because of time constraints, measurements of natural gamma activity were not performed at Hole 911C.

The GRAPE density record for Hole 911A (Fig. 23) shows an overall trend of increasing values with depth, from ~1.6 g/cm³ at the surface to ~2 g/cm³ at ~500 mbsf. Numerous GRAPE-density fluctuations on scales of 1–20 m also are superimposed on this trend. These are best seen in the records for Holes 911B and 911C (Figs. 24 and

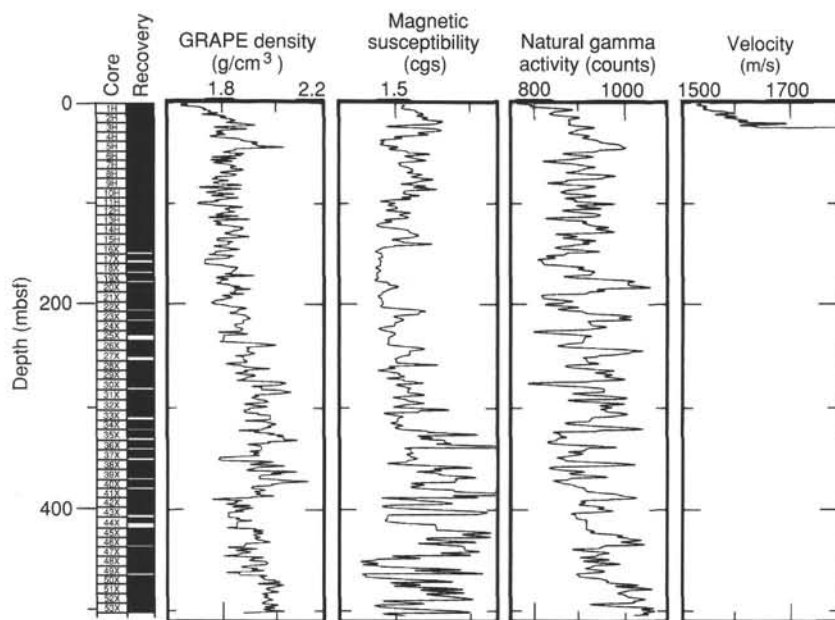


Figure 23. Multi-sensor track results from Hole 911A (0–503 mbsf). Data are filtered using a fast Fourier transform routine.

25), which are plotted on an expanded scale. This agrees with observations of sharp minor variations in sediment texture (see “Lithostratigraphy” section, this chapter). The records of magnetic susceptibility and natural gamma activity also show an overall trend of increasing values with depth, with significant short-term fluctuations. The susceptibility values increase markedly below ~320 mbsf, coincident with observations of iron sulfide concretions in the cores. X-ray diffraction analysis of these concretions indicated the presence of the ferromagnetic minerals greigite and pyrrhotite, together with paramagnetic vivianite (see “Paleomagnetism” section, this chapter). The intervals containing the iron sulfides are clearly visible in the Formation MicroScanner (FMS) images (see “Downhole Measurements” section, this chapter).

As at Site 910, there is some correspondence between the multi-sensor track records and sediment lithology. Lithologic Subunit IA (0–380.4 mbsf) is recognized on the basis of increased dropstone abundance (see “Lithostratigraphy” section, this chapter), and coincides with an abrupt but temporary shift to higher GRAPE densities above this depth.

The high-frequency fluctuations in GRAPE density, magnetic susceptibility, and natural gamma activity provide the basis for high-resolution stratigraphic correlations among the upper parts of the three holes drilled at Site 911. Figure 26 illustrates the use of magnetic susceptibility for correlation of the upper 33 m of Holes 911A, 911B, and 911C. The three records were matched using an inverse correlation method (Martinson et al., 1982). Figure 27 shows the matching function resulting from the “stretching” of the depth scale of Hole 911B so that susceptibility features correlative with Hole 911A are aligned. The four discontinuities in the matching function coincide with core breaks and underline the necessity of constructing composite depth sections for high-resolution stratigraphic studies of ODP core material. Unfortunately, between-hole correlations become difficult below ~40 mbsf at Site 911, probably because of the disruption of the stratigraphy by gas expansion. Recognition of short correlative intervals between holes indicated depth offsets of up to 8 m, which also were recognized in the natural remanent magnetization record (see “Paleomagnetism” section, this chapter).

Thermal Conductivity

Thermal conductivity measurements were performed throughout Hole 911A to a depth of 503.3 mbsf. Only 10 discrete measurements

were performed in Hole 911B to 18.55 mbsf because of disruption due to gas. The data are shown in Figure 28, and summarized in Table 9.

The record of thermal conductivity in Hole 911A reveals a general weak downhole increase from a 0.75 mbsf value of 1.13 W/m·K to 1.44 W/m·K at 503.3 mbsf. A maximum conductivity of 2.21 W/m·K occurs at 378.95 mbsf. A linear fit to the data is unsuitable (correlation coefficient = 0.302), and considerable scatter is apparent (indicated by the wide standard deviation 0.23 W/m·K around the depth-mean conductivity 1.27 W/m·K). The data mirror, to an extent, the downhole variation in porosity and water content (Fig. 28) and, therefore, may indicate thin zones of higher density and compaction. In some zones the inverse relationship of conductivity to water content is quite pronounced (e.g., around 400 mbsf). However, note that just below the seafloor conductivity varies only slightly across the steep density gradients.

Bottom-hole Temperature Measurements

In-situ temperatures were determined at the seafloor and at three depths in Hole 911A by the Adara Temperature Tool, and the equilibrium temperature was calculated (see “Explanatory Notes” chapter, this volume). The results of these calculations are as follows: seafloor, -0.277°C ; 37.0 mbsf, 2.560°C ; 65.2 mbsf, 4.374°C ; and 93.7 mbsf, 6.078°C . The geothermal gradient was estimated by linear regression at $67.8^{\circ}\text{C}/\text{km}$ (Fig. 29). Taking the value for the mean thermal conductivity (1.27 W/m·K), the heat flow is estimated at $86 \text{ mW}/\text{m}^2$.

Split-core Measurements

Compressional-wave Velocity

Measurements of compressional-wave velocity were performed at various depths using the Digital Sound Velocimeter and the Hamilton Apparatus. Severe problems were encountered because of gas, which confined measurements to the upper 21 mbsf. Even where cores appeared intact, internal micro-cracks often prevented the successful collection of velocity data. The downhole logs provide a better downhole coverage of compressional-wave velocities (see “Downhole Measurements” section, this chapter). Table 10 summarizes the velocity data collected at this site.

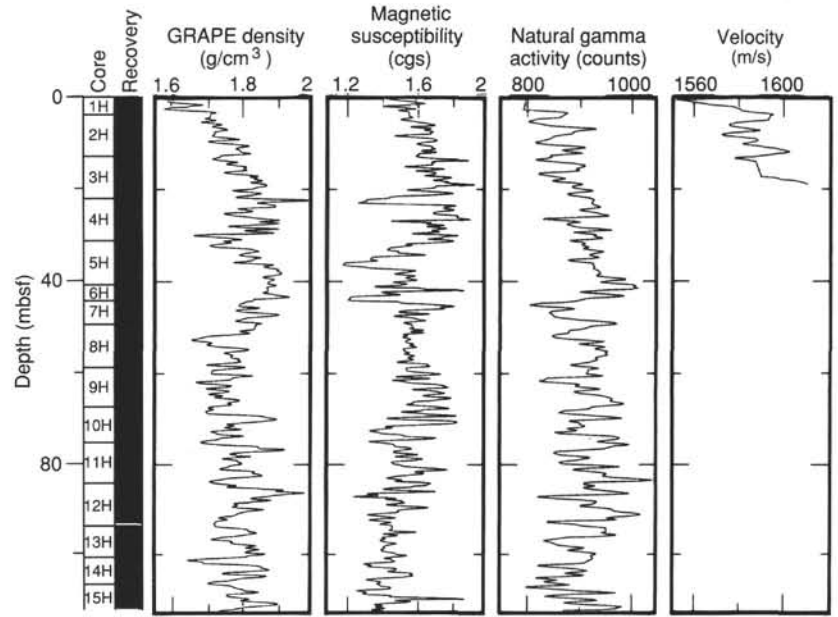


Figure 24. Multi-sensor track results from Hole 911B (0–112.1 mbsf). Data are filtered using a fast Fourier transform routine.

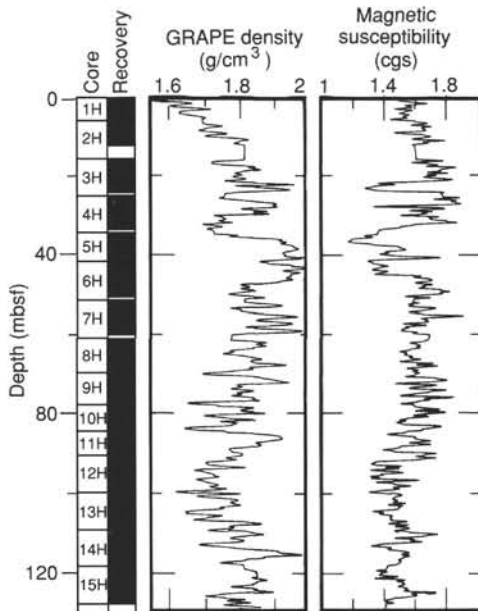


Figure 25. GRAPE bulk density and magnetic susceptibility whole-core measurements from Hole 911C (0–127.9 mbsf). Data are filtered using a fast Fourier transform routine.

Both sets of measurements depict gentle fluctuations in acoustic velocity over intervals of ~5 m within a general downhole increase (Fig. 30). Wave velocities range between 1420 and 1560 m/s. There is a poor cross-hole correlation, and only below 16 mbsf do the trends appear to be of the same magnitude and direction. This may be a function of distortions of the sedimentary fabric caused by gas, which would invariably be different in each core. The relation of acoustic velocity to sediment bulk density (usually a positive covariation) is also poor.

Shear Strength

Shear strength was determined to 396.49 mbsf in Hole 911A using both the vane shear device and the hand-held penetrometer. Mea-

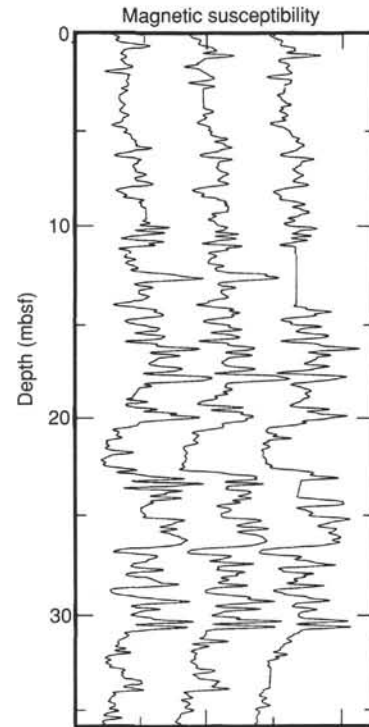


Figure 26. Results of inverse correlation of the magnetic susceptibility records for the interval 0–36 mbsf from (left to right) Holes 911A, 911B, and 911C. Records from Holes 911B and 911C are offset by an arbitrary amount.

surements were performed in Hole 911B to 108.4 mbsf using only the vane. The data are summarized in Table 11.

The downhole record for Hole 911A depicts an approximately linear increase in sediment strength with depth, from a mud-line value ~10 kPa to 221 kPa at 397.8 mbsf (221 kPa is the upper limit of the penetrometer range of measurement; Fig. 31A). The maximum recorded vane strength is 220 kPa (at 264.2 mbsf). Both sets of data record an increase in variability of shear strength with depth (i.e., a

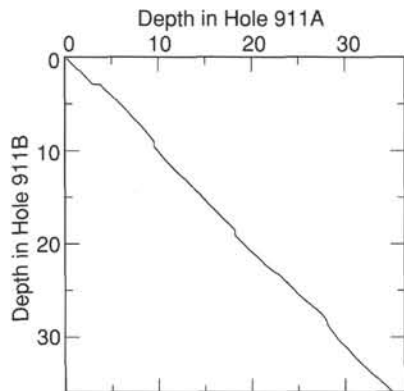


Figure 27. Matching function of the depths of correlative magnetic susceptibility features in Holes 911A and 911B.

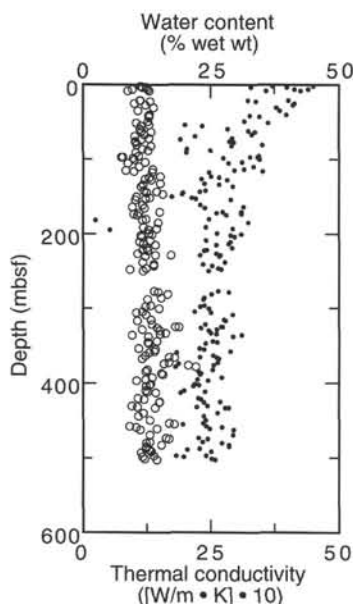


Figure 28. Downhole record of water content (closed circles) and thermal conductivity (open circles) for Hole 911A.

broadening range) perhaps indicative of a greater sediment heterogeneity. The penetrometer data generally exhibit a greater scatter than do the vane measurements, which is a function of both operator error and centimeter-scale patchiness in strength. A considerable part of the observed strength gain in these sediments therefore can be explained through physical-mechanical compaction.

The upper 50 m of the section is characterized by a peak in sediment strength at 43 mbsf. This is recorded by both instruments, and a maximum strength of 131 kPa is estimated by the penetrometer. This horizon coincides with peaks in bulk density recorded by the discrete laboratory measurements and by the GRAPE. This layer is relatively thin (from 44 to 50 mbsf). Below this depth sediment strength quickly drops to around 40 kPa. This trend is more clearly seen in Hole 911B (Fig. 31B), although a large discrepancy is seen between the magnitudes of the peak strength in each hole. Hole 911B also reveals the presence of several shear strength peaks in the upper layers, including a smaller increase in strength at about 20 mbsf, which also correlates well with the density data.

Index Properties

Selected downhole profiles of bulk density and water content (% wet wt) are displayed in Figure 32. Index properties measured at Site

911 are summarized in Table 12. Downhole trends in measured index properties reflect a gradual compactive de-watering, as illustrated by the increase in bulk density downward. A comparatively water-rich, low-density upper layer grades slowly into a thick bed, more uniform in its properties below about 400 mbsf. Bulk density ranges between 1.69 and 2.14 g/cm³ through this transition, corresponding to a moisture content (% wet wt) reduction from 45% to 24%. As with other sites of this leg, greater variability is observed in the upper sediment layers, particularly between 50 and 130 mbsf in this hole. Deeper muds (below ~200 mbsf) appear generally less heterogeneous in their properties.

Superimposed on the mean trends are several localized gradients. The upper 80 m of sediment is dominated by layers of relatively uniform bulk density interspaced with layers of sharp positive gradients. These features are also apparent in the MST GRAPE data (Figs. 23 and 24), although a detailed quantitative match is not apparent. A detailed plot of this zone is shown in Figure 33. Four layers are easily distinguished down to 45 mbsf, below which density fluctuations are small and closely spaced around a mean value of 1.93 g/cm³ (± 0.06 g/cm³). The variations are reminiscent of changes in sediment properties at Site 910, although at Site 911 they appear slightly deeper in the sediment (at 45 mbsf rather than at 20 mbsf at Site 910).

The peak in bulk density at 44 mbsf is particularly interesting because it coincides with a peak in shear strength (see Fig. 31). This layer corresponds to a deep brown clay, enriched in dropstones, sand, and silt grains (% quartz >50; see "Lithostratigraphy" section, this chapter). The depth distribution of dropstones down to 50 mbsf, in fact, traces approximately the same gradient as the bulk-density profile (increasing from 2 to 6 stones per core, recovery ~100%). An increase in the percentage of inorganic clay-sized calcite also is reported at the horizon in peak strength. A smaller covariation of strength and bulk density is apparent at 22–28 mbsf; however, the change in color of these shallower sediments is not so marked, and dropstone content is much less (only 2 per core).

Sediment properties also change markedly from 380 to 420 mbsf. Bulk density falls to below 2.0 g/cm³. Water content increases, although not dramatically, and thermal conductivity decreases (as it tracks the water content; see Fig. 28). This layer was recorded on the MST GRAPE (Fig. 23) and is also clearly evident in the downhole logs. However, there is little evidence to account for its existence. No dropstones and very few microfossils are present throughout the interval. Textural variability is not particularly pronounced, although the sand content increases from about 2% to 18% from 400 mbsf through 440 mbsf. This might contribute to an increase in bulk density between 400 and 420 mbsf, but can have no relation to the marked decrease in bulk density immediately above this. The comparatively small change in water content against bulk density, and marked swelling of the borehole wall (detected at the top of the layer by the logging tool) strongly suggest a change in lithologic composition for this layer. The observed physical property changes may indicate thickly bedded clay-rich/sand-rich layering, where the inflection in bulk density is a transition zone between the two types of beds.

Geotechnical Units

Five geotechnical units are proposed at this site based upon a synthesis of physical properties data. Geotechnical Unit G-I is defined by the interval with variable density and frequent dropstone occurrences from 0 to 50 mbsf. Geotechnical Unit G-II (50–150 mbsf) is characterized by wide variation in sediment properties. No downhole gradients in index properties are evident in this unit. Geotechnical Unit G-III consists of the increasing compaction gradient to 380 mbsf. The base of Unit III corresponds to the boundary between lithologic Sub-units IA and IB (see "Lithostratigraphy" section, this chapter). Geotechnical Unit G-IV relates specifically to the low density interval 380–420 mbsf, and geotechnical Unit G-V continues from 420 mbsf to the base of the hole at 505.8 mbsf. The index properties data reveal geotechnical Unit G-V to be predominantly uniform with depth, with

Table 9. Thermal conductivity measurements from Holes 911A and 911B.

Core, section, interval top (cm)							Core, section, interval top (cm)						
Depth (mbsf)	M	P #	TC _{corr} (W/m-K)	Std dev (W/m-K)	Drift (°C/min)		Depth (mbsf)	M	P #	TC _{corr} (W/m-K)	Std dev (W/m-K)	Drift (°C/min)	
151-911A-							24X-6, 54	F	339	1.27	0.00137	-0.023	
1H-2, 75	F	332	1.13	0.00280	0.023		25X-1, 60	F	332	1.07	0.00329	0.001	
1H-3, 66	F	325	1.24	0.00303	0.036		25X-2, 60	F	325	1.41	0.00251	-0.028	
1H-5, 75	F	338	0.97	0.00226	-0.010		25X-2, 80	F	339	1.72	0.00197	0.018	
1H-6, 75	F	339	0.88	0.00642	-0.032		25X-3, 60	F	338	1.22	0.00252	0.002	
2H-2, 75	F	332	1.14	0.00256	0.028		26X-2, 75	F	332	1.17	0.00132	0.005	
2H-3, 75	F	325	1.17	0.00127	-0.004		26X-4, 75	F	338	1.39	0.00178	0.010	
2H-5, 75	F	338	1.27	0.00293	0.020		26X-5, 75	F	339	1.38	0.00197	0.012	
2H-6, 75	F	339	1.30	0.00290	-0.004		27X-1, 90	F	332	1.24	0.00261	0.007	
3H-2, 75	F	332	1.13	0.00251	0.015		27X-2, 90	F	325	0.92	0.00244	0.012	
3H-2, 75	F	332	1.12	0.00251	0.011		27X-3, 90	F	338	1.18	0.00221	0.010	
3H-3, 75	F	325	1.32	0.00373	0.010		27X-5, 90	F	338	1.08	0.00243	0.008	
3H-5, 75	F	338	1.01	0.00505	-0.016		30X-3, 75	F	338	1.47	0.00363	0.004	
3H-6, 75	F	339	1.23	0.00289	0.024		30X-5, 75	F	17	1.66	0.00301	0.020	
4H-2, 75	F	332	1.39	0.00212	0.028		31X-2, 75	F	332	1.53	0.00117	0.017	
4H-5, 75	F	338	1.08	0.00319	0.015		31X-3, 75	F	338	1.27	0.00340	0.013	
5H-2, 75	F	332	1.31	0.00273	0.027		32X-2, 75	F	332	1.33	0.00245	0.030	
5H-3, 75	F	325	1.29	0.00223	0.030		32X-3, 75	F	338	1.23	0.00301	0.037	
5H-4, 75	F	338	1.30	0.00334	0.020		32X-5, 75	F	17	1.49	0.00421	0.034	
6H-2, 75	F	332	1.28	0.00226	-0.001		33X-1, 75	F	352	1.17	0.00220	0.009	
6H-3, 75	F	325	1.05	0.00201	-0.009		33X-2, 75	F	338	1.05	0.00222	0.012	
6H-5, 75	F	338	1.30	0.00219	0.028		33X-4, 75	F	17	1.24	0.00228	0.029	
6H-6, 75	F	339	1.14	0.00216	0.019		34X-2, 75	F	332	1.34	0.00297	0.035	
7H-2, 75	F	332	1.12	0.00381	0.028		34X-3, 75	F	338	1.07	0.00235	0.023	
7H-4, 75	F	338	1.15	0.00293	0.010		34X-6, 75	F	17	1.35	0.00290	0.039	
7H-5, 75	F	339	1.34	0.00238	0.011		35X-2, 75	F	332	1.81	0.00344	0.030	
8H-2, 75	F	332	1.21	0.00387	0.020		35X-2, 75	F	332	1.88	0.00354	0.035	
8H-3, 97	F	325	1.02	0.00177	0.021		35X-3, 75	F	338	1.46	0.00232	0.038	
8H-5, 75	F	338	1.30	0.00357	0.026		35X-4, 75	F	339	1.16	0.00448	0.034	
8H-6, 75	F	339	1.15	0.00381	0.027		35X-5, 75	F	17	1.50	0.00117	0.035	
9H-2, 65	F	332	1.03	0.00270	0.028		36X-1, 75	F	332	1.61	0.00305	0.011	
9H-3, 65	F	325	1.04	0.00433	0.032		36X-2, 75	F	338	1.50	0.00188	0.022	
9H-5, 75	F	338	1.06	0.00295	0.034		36X-3, 75	F	339	0.96	0.00493	0.004	
9H-6, 75	F	339	1.34	0.00263	0.038		36X-4, 75	F	350	1.28	0.00181	0.026	
10H-2, 75	F	332	1.17	0.00276	0.016		37X-2, 75	F	332	1.44	0.00306	0.024	
10H-3, 90	F	325	1.28	0.00322	0.030		37X-3, 75	F	338	1.27	0.00297	0.013	
10H-5, 75	F	338	1.04	0.00239	0.029		37X-4, 75	F	339	1.29	0.00399	0.024	
11H-2, 60	F	332	1.09	0.00110	0.014		38X-2, 75	F	332	1.09	0.00262	-0.004	
11H-3, 60	F	325	0.75	0.00675	-0.020		38X-3, 75	F	338	1.41	0.00115	0.027	
11H-3, 60	F	325	0.78	0.00539	0.007		38X-5, 75	F	339	1.40	0.00312	0.034	
11H-4, 60	F	338	0.98	0.00236	0.012		38X-6, 75	F	350	1.30	0.00309	0.038	
11H-5, 60	F	339	1.01	0.00124	0.001		39X-2, 60	F	332	1.22	0.00138	0.031	
12H-2, 50	F	332	1.22	0.00229	0.032		39X-3, 70	F	338	1.68	0.00404	0.031	
12H-3, 50	F	325	0.88	0.00134	0.010		39X-4, 60	F	339	1.79	0.00224	0.036	
12H-6, 50	F	339	1.10	0.00264	0.017		39X-5, 40	F	350	1.16	0.00250	0.014	
13H-2, 60	F	332	1.37	0.00296	0.004		40X-2, 55	F	332	1.68	0.00226	0.021	
13H-3, 60	F	325	0.84	0.00380	0.037		40X-3, 55	F	338	1.58	0.00262	0.011	
13H-4, 60	F	338	1.00	0.00380	0.005		40X-4, 55	F	339	2.06	0.00328	0.026	
13H-5, 60	F	339	1.35	0.00259	0.009		40X-6, 55	F	350	2.21	0.00407	0.037	
14H-2, 90	F	332	1.51	0.00281	0.004		41X-2, 75	F	332	1.26	0.00220	0.016	
14H-3, 90	F	325	1.30	0.00703	0.021		41X-3, 75	F	338	1.23	0.00231	0.012	
14H-4, 90	F	338	1.22	0.00245	0.001		41X-5, 75	F	339	1.53	0.00261	0.017	
14H-6, 90	F	339	1.34	0.00245	0.008		41X-6, 75	F	350	1.56	0.00266	-0.007	
15H-2, 40	F	332	1.51	0.00263	0.009		42X-3, 60	F	339	1.36	0.00286	0.018	
15H-3, 40	F	325	1.18	0.00218	-0.018		42X-5, 80	F	338	1.23	0.00252	0.001	
15H-5, 40	F	338	1.14	0.00237	0.036		42X-6, 70	F	339	1.05	0.00305	0.032	
16X-2, 90	F	332	1.20	0.00313	0.010		43X-2, 50	F	332	1.33	0.00177	0.036	
16X-3, 90	F	325	1.44	0.00185	0.026		43X-3, 50	F	338	1.31	0.00148	0.035	
16X-4, 90	F	338	1.25	0.00186	0.000		43X-4, 50	F	339	1.24	0.00331	0.032	
16X-5, 90	F	339	1.56	0.00190	0.021		44X-1, 75	F	332	1.23	0.00274	0.036	
17X-1, 75	F	332	1.05	0.00354	0.026		44X-2, 80	F	338	1.27	0.00142	0.024	
17X-2, 75	F	325	1.31	0.00215	0.039		44X-3, 80	F	339	1.43	0.00262	0.004	
17X-3, 75	F	338	1.23	0.00287	0.017		45X-2, 50	F	332	1.08	0.00176	0.011	
17X-4, 75	F	339	1.03	0.00194	0.022		45X-3, 50	F	338	1.20	0.00208	0.035	
18X-2, 70	F	332	1.17	0.00189	0.027		45X-5, 55	F	339	1.50	0.00220	0.028	
18X-4, 70	F	338	0.97	0.00118	-0.006		45X-6, 50	F	350	1.49	0.00353	0.030	
18X-5, 70	F	339	1.21	0.00344	0.035		46X-2, 75	F	332	0.96	0.00224	0.001	
19X-2, 70	F	332	1.50	0.00235	0.017		46X-3, 75	F	338	1.07	0.00327	0.029	
19X-2, 70	F	332	1.50	0.00235	0.017		46X-4, 75	F	339	1.41	0.00288	0.031	
19X-3, 70	F	325	1.10	0.00405	-0.028		46X-4, 75	F	339	1.41	0.00288	0.031	
19X-4, 75	F	338	1.00	0.00744	0.020		47X-2, 75	F	332	1.19	0.00378	0.014	
19X-5, 75	F	339	1.07	0.00440	0.029		47X-3, 60	F	338	0.82	0.00428	0.043	
20X-2, 75	F	332	1.24	0.00242	0.021		47X-5, 75	F	339	1.09	0.00222	0.026	
20X-3, 75	F	325	1.17	0.00419	0.035		48X-2, 75	F	332	1.31	0.00241	0.019	
20X-5, 75	F	339	1.47	0.00144	0.036		48X-5, 75	F	339	1.68	0.00365	0.039	
21X-3, 70	F	325	1.19	0.00448	-0.028		48X-6, 75	F	350	1.78	0.00357	0.025	
21X-4, 82	F	338	1.45	0.00249	0.009		49X-1, 75	F	332	0.91	0.00359	-0.008	
21X-5, 79	F	339	1.29	0.00338	0.021		49X-2, 75	F	338	1.04	0.00193	-0.003	
22X-2, 75	F	332	1.30	0.00223	0.036		49X-3, 75	F	339	1.45	0.00184	0.027	
22X-3, 75	F	325	1.35	0.00112	0.020		49X-4, 75	F	350	1.12	0.00340	0.012	
22X-4, 66	F	338	1.14	0.00290	0.028		50X-2, 75	F	332	1.31	0.00301	0.014	
22X-5, 75	F	339	1.16	0.00499	0.032		50X-5, 75	F	339	1.62	0.00375	0.020	
23X-2, 55	F	332	1.32	0.00344	0.011		50X-6, 75	F	350	1.68	0.00263	0.013	
23X-3, 55	F	325	1.11	0.00203	0.000		51X-2, 75	F	332	1.31	0.00226	0.006	
23X-5, 55	F	338	1.18	0.00230	-0.005		51X-3, 75	F	338	1.24	0.00281	0.027	
23X-6, 55	F	339	1.41	0.00421	-0.016		51X-5, 75	F	339	1.53	0.00302	0.034	
24X-3, 54	F	332	1.25	0.00240	0.009		51X-6, 75	F	350	1.24	0.00537	-0.025	
24X-5, 54	F	338	1.17	0.00332	0.019		52X-2, 75	F	332	1.23	0.00219	0.011	

Table 9 (continued).

Core, section, interval top (cm)	Depth (mbsf)	M	P #	TC _{corr} (W/m-K)	Std dev (W/m-K)	Drift (°C/min)
52X-3, 75	489.5	F	338	1.30	0.00237	0.025
52X-5, 75	492.43	F	339	1.34	0.00264	0.020
52X-6, 75	493.59	F	350	1.14	0.00288	0.012
53X-2, 75	497.69	F	332	1.38	0.00155	0.013
53X-2, 75	497.69	F	332	1.38	0.00155	0.013
53X-3, 75	499.19	F	338	1.17	0.00295	0.032
53X-5, 75	501.93	F	339	1.21	0.00172	0.009
53X-6, 75	503.3	F	350	1.44	0.00261	-0.010
151-911B-						
1H-1, 40	0.4	F	332	1.03	0.00214	0.014
1H-1, 70	0.7	F	338	1.01	0.00256	-0.015
1H-2, 40	1.9	F	339	1.06	0.00235	0.001
1H-2, 70	2.2	F	350	1.08	0.00347	-0.018
2H-2, 75	6.05	F	332	1.01	0.00262	-0.008
2H-3, 75	7.55	F	338	1.09	0.00245	-0.005
2H-4, 75	9.05	F	350	1.22	0.00875	0.014
2H-5, 75	10.55	F	339	1.22	0.00224	0.039
3H-2, 75	15.55	F	332	1.14	0.00432	0.024
3H-4, 75	18.55	F	339	1.75	0.00310	0.039

Notes: M = method used, either F = full-space or H = half-space; P # = probe number used for test; TC_{corr} = thermal conductivity corrected for drift; Std dev = standard deviation of the measurement.

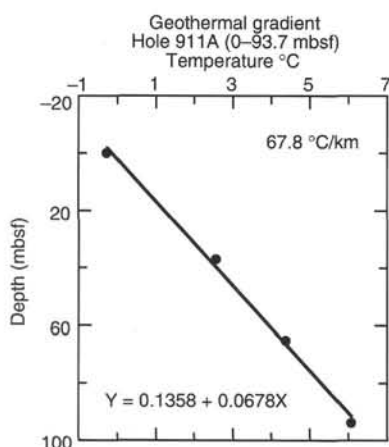


Figure 29. Downhole geothermal gradient in Hole 911A (0-93.7 mbsf) measured by the Adara tool.

a mean bulk density of 2.08 g/cm³ (±0.04 g/cm³). However, the GRAPE data depict a linear increase in bulk density to the base of the hole, and the wireline data show a gradual decrease in bulk density to ~450 mbsf, and then a sharp decrease to 470 mbsf (see “Downhole Measurements” section, this chapter).

DOWNHOLE MEASUREMENTS

Logging Operations

Three Schlumberger tool strings were run at Hole 911A: the quad combination, the Formation MicroScanner, and the geochemical logging tool. The wireline heave compensator (WHC) was used to counter the mild ship heave (0.1-0.2 m of motion). In anticipation of poor hole conditions the conical sidewall entry sub (CSES) was rigged up and the base of the drill pipe set at 117 mbsf. A summary description of the logging tool strings used during Leg 151 is presented in the “Explanatory Notes” chapter (this volume). A summary of the logging operations at Hole 911A is given in Table 13.

The quad combination tool string comprising sonic (SDT), induction (DIT), lithodensity (HLDT) and natural gamma-ray (NGT) tools was run first. Total penetration in Hole 911A was 505.8 mbsf; how-

Table 10. Compressional-wave velocity measurements from Holes 911A and 911B.

Core, section, interval (cm)	Depth (mbsf)	Tool	Velocity Perp (m/s)
151-911A-			
1H-1, 97-104	0.97	dsv	1493
1H-3, 89-96	3.89	dsv	1498
1H-4, 53-60	5.03	dsv	1526
1H-5, 38-45	6.38	dsv	1531
1H-6, 55-62	8.05	dsv	1507
2H-1, 70-77	10.20	dsv	1511
2H-2, 58-65	11.58	dsv	1499
2H-3, 20-27	12.70	dsv	1548
2H-3, 106-113	13.56	dsv	1527
2H-4, 75-82	14.75	dsv	1517
2H-5, 28-35	15.78	dsv	1512
2H-6, 39-46	17.39	dsv	1557
3H-1, 50-57	19.50	dsv	1557
151-911B-			
2H-1, 59-66	4.39	dsv	1526
2H-2, 54-61	5.84	dsv	1514
2H-3, 46-53	7.26	dsv	1494
2H-4, 46-53	8.76	dsv	1531
2H-5, 56-63	10.36	dsv	1548
2H-6, 65-72	11.95	dsv	1503
2H-7, 34-41	13.14	dsv	1503
3H-1, 50-57	13.80	dsv	1486
3H-2, 50-57	15.30	dsv	1560
3H-3, 50-57	16.80	dsv	1527
3H-4, 50-57	18.30	dsv	1564
3H-5, 83-90	20.13	dsv	1564
3H-6, 33-40	21.13	dsv	1425

Note: Tool = device used for measurement, either dsv = digital sound velocimeter or ham = Hamilton Frame. Perp = perpendicular, Par = parallel.

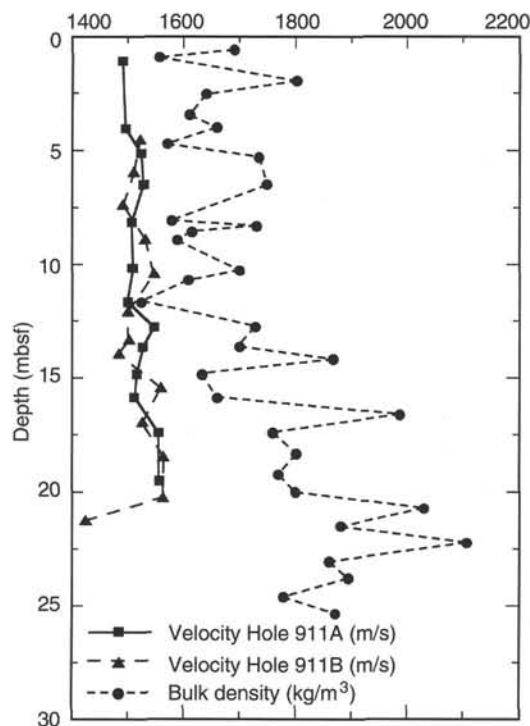


Figure 30. Comparison of velocity from Holes 911A and 911B with bulk density from Hole 911A.

ever, hole fill or possibly a bridge prevented the tool string from getting below 476 mbsf. Data were recorded at a logging speed of 900 ft/hr from this depth to 148 mbsf. A second upgoing log was then recorded at 900 ft/hr from 247 mbsf to the mud line. The HLDT was run in high-resolution mode recording data at 1.2-in. increments. The second tool string run in the hole was the Formation MicroScanner

Table 11. Strength measurements from Holes 911A and 911B.

Core, section, interval (cm)	Depth (mbsf)	Vane SN (kPa)	Res (kPa)	Pen (kPa)	Core, section, interval (cm)	Depth (mbsf)	Vane SN (kPa)	Res (kPa)	Pen (kPa)
151-911A-					17X-2, 110-111	152.00	4	56	21
1H-2, 100-101	2.50	1	10	5	17X-3, 110-111	153.50	4	87	37
1H-3, 95-96	3.95	1	8	5	17X-4, 25-26	154.15	4	88	25
1H-4, 56-57	5.06	1	10	6	17X-4, 110-111	155.00	4	108	84
1H-5, 52-53	6.52	1	10	4	18X-1, 105-106	160.05	4	109	33
1H-6, 58-59	8.08	1	12	8	18X-2, 53-54	161.03	4	125	26
2H-1, 73-74	10.23	1	12	6	18X-2, 109-110	161.59	4	145	25
2H-2, 62-63	11.62	1	14	6	18X-3, 96-97	162.96	4	119	25
2H-3, 24-25	12.74	1	15	8	18X-4, 112-113	164.36	4	133	25
2H-3, 109-110	13.59	1	16	7	19X-1, 100-101	169.60	4	77	35
2H-4, 79-80	14.79	1	17	9	19X-2, 25-26	170.35	4	76	38
2H-5, 51-52	16.01	1	15	7	19X-2, 112-113	171.22	4	72	30
2H-6, 50-51	17.50	1	20	9	19X-3, 121-122	172.81	4	68	26
3H-1, 55-56	19.55	1	18	8	19X-4, 100-101	174.10	4	87	28
3H-1, 119-120	20.19	1	25	12	19X-5, 110-111	175.70	4	96	28
3H-2, 30-31	20.80	1	33	16	20X-1, 100-101	179.30	4	156	35
3H-2, 115-116	21.65	1	16	7	20X-1, 110-111	179.40	4	113	35
3H-3, 92-93	22.92	1	29	13	20X-2, 105-106	180.85	4	102	34
3H-4, 102-103	24.52	1	31	14	20X-3, 109-110	182.39	4	131	26
3H-5, 102-103	26.02	1	36	15	20X-4, 110-111	183.90	4	146	47
3H-6, 82-83	27.32	1	40	19	20X-5, 120-121	185.50	4	122	116
4H-1, 109-110	29.59	1	25	9	21X-1, 120-121	189.10	4	67	29
4H-2, 55-56	30.55	1	20	10	21X-2, 108-109	190.48	4	73	25
4H-2, 109-110	31.09	1	38	14	21X-5, 107-108	194.97	4	70	24
4H-3, 109-110	32.59	1	28	13	22X-1, 120-121	198.70	4	70	19
4H-4, 123-124	34.23	1	28	13	22X-1, 125-126	198.75	4	73	18
4H-5, 110-111	35.60	1	37	17	22X-2, 145-146	201.68			74
4H-6, 113-114	37.13	1	40	18	23X-1, 115-116	208.35	4	71	23
5H-1, 109-110	39.09	1	45	24	23X-4, 100-101	212.70	4	110	27
5H-1, 113-114	39.13	1	57		23X-6, 67-68	215.37	4	167	54
5H-1, 117-118	39.17	3	55	23	24X-1, 100-101	217.80	4	167	0
5H-2, 108-109	40.58	3	56	26	24X-4, 70-71	220.90	4	65	19
5H-3, 25-26	41.25	3	52	25	24X-5, 88-89	221.99	4	65	27
5H-3, 50-51	41.50	3	51	24	25X-1, 100-101	227.40	4	87	29
5H-3, 90-91	41.90	3	91	33	25X-3, 100-101	230.40	4	77	18
5H-3, 109-110	42.09	3	90	30	26X-2, 100-101	238.60	4	119	35
5H-3, 129-130	42.29	3	144	85	26X-4, 100-101	241.60	4	109	33
5H-4, 109-110	43.59	3	151	75	26X-6, 60-61	244.20	4	207	0
6H-1, 7-8	47.57	3	103	44	27X-1, 105-106	246.85	4	144	55
6H-1, 15-16	47.65	3	34	16	27X-3, 105-106	249.85	4	111	25
6H-1, 109-110	48.59	3	39	18	27X-5, 100-101	251.48	4	141	47
6H-2, 114-115	50.14	3	45	21	28X-1, 106-107	256.56	4	164	0
6H-3, 109-110	51.59	3	48	22	28X-2, 120-121	258.20	4	87	31
6H-4, 110-111	53.10	3	40	17	28X-4, 120-121	261.20	4	131	40
6H-5, 110-111	54.60	3	33	18	28X-6, 105-106	264.05	4	162	33
6H-6, 110-111	56.10	3	32	14	28X-6, 120-121	264.20	4	220	
7H-1, 129-130	58.29	3	49	21	29X-1, 70-71	265.80	4	196	153
7H-2, 98-99	59.48	3	39	17	29X-2, 102-103	267.15	4	98	30
7H-2, 108-109	59.58	3	41	13	29X-3, 118-119	268.81	4	73	32
7H-3, 112-113	61.12	3	40	16	29X-4, 117-118	270.30	4	89	33
7H-4, 108-109	62.58	3	57	25	29X-5, 121-122	271.84	4	137	109
7H-5, 110-111	64.10	3	52	23	30X-1, 134-135	276.04	4	150	105
8H-1, 47-48	65.67	3	50	22	30X-2, 120-121	277.40	4	170	149
8H-1, 95-96	66.15	3	81	38	30X-3, 120-121	278.90			88
8H-1, 119-120	66.39	3	24	10	30X-4, 120-121	280.40			111
8H-2, 93-94	67.63	3	54	24	30X-5, 120-121	281.80			136
8H-3, 118-119	69.38	3	41	18	31X-1, 145-146	285.75			129
8H-4, 118-119	70.88	3	58	23	31X-2, 110-111	286.90	4	161	147
8H-5, 80-81	72.00	3			31X-3, 110-111	288.40			132
8H-6, 90-91	73.60	3	42	18	31X-4, 110-111	289.90			129
8H-6, 100-101	73.70	3	44	17	31X-5, 110-111	291.40			119
9H-1, 37-38	75.07	3	54	24	31X-6, 110-111	292.90			160
9H-2, 108-109	76.38	3	54	28	31X-7, 25-26	293.55			181
9H-3, 108-109	77.88	3	48	24	32X-1, 110-111	295.10			221
9H-4, 140-141	79.70	3	62	27	32X-2, 110-111	296.60			132
9H-5, 109-110	80.89	3	58	22	32X-3, 110-111	298.10			152
9H-6, 90-91	82.20	3	69	25	32X-4, 110-111	299.60			129
10H-5, 108-109	91.28	3	58	21	32X-5, 110-111	301.10			158
11H-3, 81-82	97.51	3	76	31	33X-1, 100-101	304.60			180
12H-1, 83-84	102.73	3	67	28	33X-2, 100-101	306.10			92
12H-1, 90-91	102.80	4	84	32	33X-3, 100-101	307.60			113
12H-3, 88-89	105.78	4	83	29	33X-4, 100-101	309.10			144
12H-6, 90-91	110.30	4	36	13	34X-1, 100-101	314.30			162
13H-1, 99-100	112.39	4	107	65	34X-2, 100-101	315.80			140
13H-3, 81-82	115.21	4	107	60	34X-3, 100-101	317.30			142
13H-5, 95-96	118.35	4	66	31	34X-4, 100-101	318.80			145
13H-7, 22-23	120.62	4	62	23	34X-5, 100-101	320.12			167
14H-3, 90-91	124.80	4	96	334	34X-6, 90-91	321.52			190
14H-6, 96-97	128.11	4	58	17	35X-1, 120-121	324.10			203
15H-2, 30-31	132.20				35X-2, 120-121	325.60			124
15H-3, 52-53	133.92	4	104	26	35X-3, 120-121	327.10			180
15H-4, 20-21	135.10				35X-4, 120-121	328.60			188
15H-6, 32-33	138.22	4	102	40	35X-5, 120-121	330.10			163
16X-1, 109-110	140.99	4	55	19	36X-1, 80-81	333.40			205
16X-2, 109-110	142.49	4	79	27	36X-2, 80-81	334.88			120
16X-3, 110-111	144.00	4	88	37	36X-3, 80-81	336.36			147
16X-4, 110-111	145.50	4	84	32	36X-4, 80-81	337.86			141
16X-5, 110-111	147.00	4	67	30	36X-5, 40-41	338.89			146
17X-1, 110-111	150.50	4	50	22	37X-1, 70-71	342.90			133

Table 11 (continued).

Core, section, interval (cm)	Depth (mbsf)	Vane SN	Res (kPa)	Pen (kPa)
37X-2, 70-71	344.30			120
37X-3, 70-71	345.72			101
37X-4, 70-71	347.06			124
37X-5, 60-61	348.32			173
37X-6, 50-51	349.42			124
38X-1, 50-51	352.40			216
38X-2, 75-76	353.56			123
38X-3, 75-76	355.06			168
38X-4, 75-76	356.56			101
38X-5, 60-61	357.84			117
38X-6, 65-66	359.09			148
38X-7, 75-76	360.51			161
38X-8, 35-36	361.58			161
39X-1, 80-81	362.20			197
39X-2, 80-81	363.65			145
39X-3, 80-81	365.09			160
39X-4, 80-81	366.49			195
39X-5, 80-81	367.92			206
39X-6, 30-31	368.84			202
40X-1, 130-131	372.20			170
40X-2, 80-81	373.20			190
40X-3, 80-81	374.65			205
40X-4, 80-81	376.15			198
40X-5, 80-81	377.43			217
40X-6, 80-81	378.35			203
41X-1, 80-81	381.20			221
41X-2, 80-81	382.70			221
41X-3, 80-81	384.20			221
41X-4, 80-81	385.70			221
41X-5, 80-81	387.20			209
41X-6, 80-81	388.70			217
42X-1, 80-81	390.80			221
42X-2, 80-81	391.82			221
42X-3, 80-81	392.89			221
42X-4, 80-81	394.39			221
42X-5, 80-81	395.26			221
42X-6, 80-81	396.49			221
42X-7, 80-81	397.83			221
151-911B-				
3H-1, 92-93	14.22	1	16	9
3H-3, 105-106	17.35	1	15	7
3H-4, 100-101	18.80	1	22	11
3H-6, 104-105	21.84	1	39	15
4H-1, 100-101	23.80	1	18	7
4H-2, 109-110	25.39	1	28	13
4H-3, 109-110	26.89	1	21	11
4H-4, 109-110	28.39	1	23	9
4H-5, 105-106	29.85	1	22	9
4H-6, 115-116	31.45	1	30	17
5H-1, 116-117	33.46	1	29	13
5H-2, 109-110	34.89	1	36	16
5H-3, 109-110	36.39	1	24	10
5H-4, 109-110	37.89	1	35	15
5H-5, 113-114	39.43	1	39	20
5H-6, 115-116	40.95	1	43	22
6H-1, 130-131	43.10	1	28	20
7H-1, 96-97	45.76	3	51	28
7H-2, 90-91	47.20	3	47	24
7H-3, 103-104	48.83	3	40	21
8H-1, 104-105	50.84	3	27	17
8H-3, 112-113	53.92	3	32	15
8H-4, 59-60	54.89	3	27	15
8H-5, 96-97	56.76	3	30	15
9H-1, 75-76	60.05	3	24	15
9H-2, 122-123	62.02	3	22	13
9H-3, 109-110	63.39	3	18	11
9H-4, 123-124	65.03	3	31	19
9H-5, 99-100	66.29	3	27	14
9H-5, 112-113	66.42	3	30	17
10H-1, 136-137	69.36	3	33	17
10H-2, 136-137	70.86	3	37	18
10H-3, 122-123	72.22	3	24	12
10H-4, 120-121	73.70	3	29	15
11H-1, 118-119	76.88	3	47	15
11H-2, 119-120	78.39	3	59	20
11H-4, 122-123	81.42	3	66	27
12H-3, 100-101	88.70	3	82	19
13H-1, 44-45	94.64	3	71	25
13H-3, 56-57	97.76	3	60	15
13H-4, 92-93	99.62	3	58	16
14H-3, 126-127	105.26	3	78	17
15H-1, 140-141	107.03	3	83	27
15H-1, 3-124	108.40	3	87	30

Notes: SN = numbered spring used to make the measurement. Vane = undrained shear strength; Res = residual shear strength; Pen = unconfined shear strength as measured by the penetrometer.

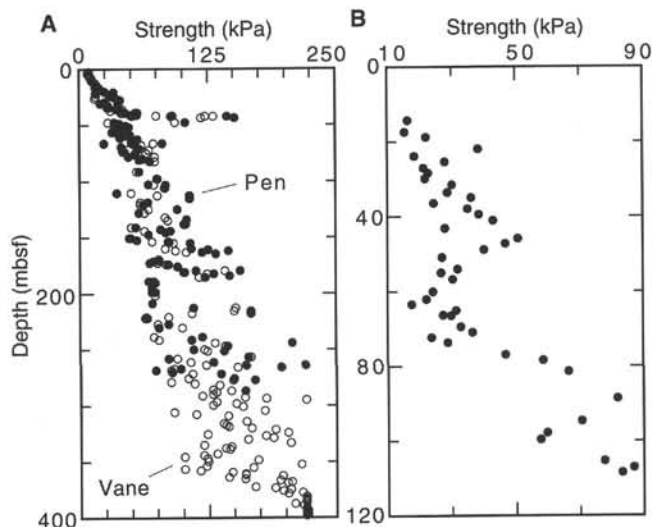


Figure 31. Strength measurements; vane plotted with filled squares, penetrometer with open squares. A. Hole 911A. B. Hole 911B.

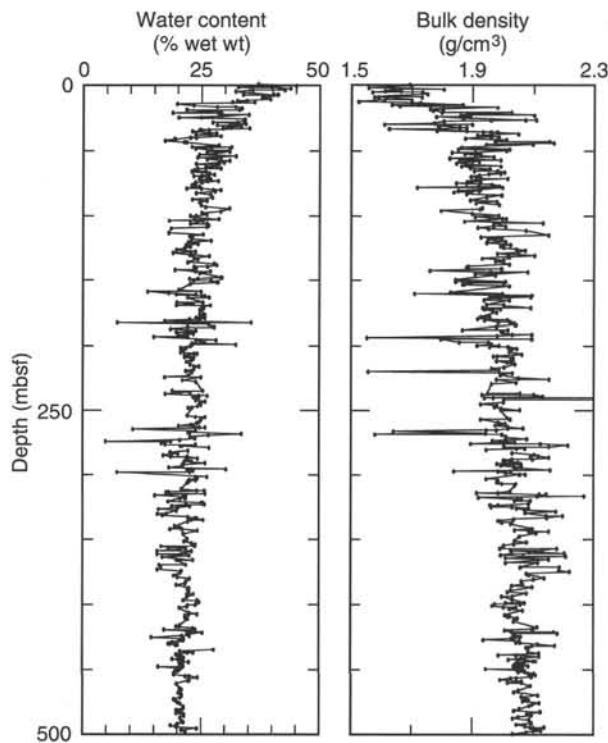


Figure 32. Water content and bulk density (Method B) variation with depth in Hole 911A.

(FMS) in combination with an NGT tool. The tool string reached 343 mbsf, where a bridge prevented further downward progress. An upgoing log was recorded at 1100 ft/hr from this depth to the end of pipe. The tool was pulled back in to pipe, which was then run down-hole through the bridge at 343 mbsf. The tool was deployed a second time, and an upgoing log was recorded at a speed of 1600 ft/hr over the interval 448-107 mbsf. The geochemical tool string, consisting of an NGT, aluminum activation clay tool (AACT), and the gamma-ray spectrometry tool (GST), was run last in Hole 911A. Data were recorded from 445 mbsf to the mud line at a speed of 550 ft/hr.

Table 12. Index properties of samples from Holes 911A and 911B.

Core, section, interval (cm)	Depth (mbsf)	WC-d (%)	WC-w (%)	WBD ^a (g/cm ³)	WBD ^b (g/cm ³)	GD ^a (g/cm ³)	GD ^b (g/cm ³)	DBD ^a (g/cm ³)	DBD ^b (g/cm ³)	Por ^a (%)	Por ^b (%)	VR ^a	VR ^b
151-911A-													
IH-1, 58-60	0.58	59.14	37.16	1.69	1.68	2.70	2.76	1.06	1.05	61.40	60.87	1.59	1.56
IH-1, 88-90	0.88	82.28	45.14	1.56	1.57	2.78	2.73	0.86	0.86	68.64	69.05	2.19	2.23
IH-2, 44-46	1.94	49.04	32.90	1.81	1.76	2.70	2.88	1.21	1.18	57.94	56.36	1.38	1.29
IH-2, 100-102	2.5	66.53	39.95	1.64	1.64	2.73	2.74	0.99	0.98	64.03	63.91	1.78	1.77
IH-3, 39-41	3.39	78.76	44.06	1.61	1.60	2.86	2.95	0.90	0.89	69.36	68.70	2.26	2.20
IH-3, 93-95	3.93	70.86	41.47	1.66	1.63	2.80	2.98	0.97	0.95	67.30	65.93	2.06	1.94
IH-4, 16-18	4.66	74.43	42.67	1.57	1.59	2.69	2.61	0.90	0.91	65.45	66.12	1.89	1.95
IH-4, 76-78	5.26	55.94	35.87	1.74	1.71	2.72	2.83	1.11	1.10	60.73	59.79	1.55	1.49
IH-5, 45-47	6.45	47.71	32.30	1.75	1.80	2.83	2.65	1.19	1.22	55.21	56.84	1.23	1.32
IH-6, 57-59	8.07	67.36	40.25	1.58	1.65	2.79	2.48	0.94	0.98	62.00	64.70	1.63	1.83
IH-6, 81-83	8.31	51.24	33.88	1.73	1.74	2.71	2.68	1.14	1.15	57.21	57.57	1.34	1.36
IH-6, 103-105	8.53	70.64	41.40	1.62	1.62	2.73	2.74	0.95	0.95	65.35	65.27	1.89	1.88
IH-6, 137-139	8.87	69.97	41.16	1.59	1.62	2.73	2.59	0.94	0.95	63.85	65.09	1.77	1.86
2H-1, 73-75	10.2	60.99	37.88	1.70	1.66	2.69	2.85	1.06	1.03	62.88	61.51	1.69	1.60
2H-1, 116-118	10.7	62.71	38.54	1.61	1.66	2.73	2.50	0.99	1.02	60.50	62.53	1.53	1.67
2H-2, 62-64	11.6	66.08	39.79	1.53	1.66	2.83	2.25	0.92	1.00	59.21	64.58	1.45	1.82
2H-3, 24-26	12.7	48.55	32.68	1.73	1.76	2.70	2.60	1.16	1.19	55.15	56.16	1.23	1.28
2H-3, 109-111	13.6	52.92	34.61	1.70	1.75	2.79	2.61	1.11	1.14	57.43	59.06	1.35	1.44
2H-4, 15-17	14.2	46.18	31.59	1.87	1.77	2.67	3.01	1.28	1.21	57.59	54.63	1.36	1.20
2H-4, 79-81	14.8	56.82	36.23	1.63	1.70	2.73	2.47	1.04	1.09	57.78	60.17	1.37	1.51
2H-5, 29-31	15.8	25.04	20.03	1.66	2.35	3.49	1.97	1.33	1.88	32.47	46.01	0.48	0.85
2H-5, 112-114	16.6	30.52	23.38	1.99	1.94	2.67	2.78	1.52	1.49	45.30	44.27	0.83	0.79
2H-6, 41-43	17.4	39.55	28.34	1.76	1.85	2.70	2.46	1.26	1.32	48.67	51.06	0.95	1.04
2H-6, 134-136	18.3	47.86	32.37	1.80	1.76	2.69	2.83	1.22	1.19	56.90	55.70	1.32	1.26
3H-1, 25-27	19.3	50.68	33.63	1.77	1.75	2.73	2.81	1.18	1.16	58.16	57.48	1.39	1.35
3H-1, 100-102	20	49.50	33.11	1.80	1.76	2.72	2.88	1.20	1.17	58.15	56.73	1.39	1.31
3H-2, 25-27	20.8	28.13	21.95	2.03	1.98	2.67	2.80	1.58	1.54	43.45	42.30	0.77	0.73
3H-2, 100-102	21.5	41.21	29.18	1.88	1.85	2.76	2.86	1.33	1.31	53.51	52.56	1.15	1.11
3H-3, 25-27	22.3	23.55	19.06	2.10	2.01	2.60	2.80	1.70	1.63	39.14	37.36	0.64	0.60
3H-3, 100-102	23	40.27	28.71	1.86	1.83	2.69	2.77	1.33	1.31	52.09	51.39	1.09	1.06
3H-4, 25-27	23.8	41.88	29.52	1.89	1.84	2.76	2.93	1.33	1.30	54.51	53.01	1.20	1.13
3H-4, 100-102	24.5	54.15	35.13	1.78	1.72	2.71	2.96	1.15	1.12	60.99	58.91	1.56	1.43
3H-5, 25-27	25.3	41.18	29.17	1.87	1.83	2.72	2.84	1.33	1.30	53.26	52.18	1.14	1.09
3H-5, 100-102	26	25.55	20.35	2.07	2.01	2.67	2.81	1.65	1.60	41.18	39.96	0.70	0.67
3H-5, 108-110	26.1	33.31	24.99	1.96	1.93	2.73	2.82	1.47	1.45	47.85	46.98	0.92	0.89
3H-6, 25-27	26.8	25.32	20.21	2.11	2.05	2.74	2.88	1.68	1.63	41.59	40.33	0.71	0.68
3H-6, 100-102	27.5	52.39	34.38	1.81	1.76	2.81	3.01	1.19	1.15	60.61	58.97	1.54	1.44
4H-1, 40-42	28.9	51.88	34.16	1.77	1.77	2.82	2.85	1.17	1.16	59.08	58.84	1.44	1.43
4H-1, 120-122	29.7	48.59	32.70	1.61	1.76	2.71	2.23	1.08	1.19	51.35	56.20	1.06	1.28
4H-2, 40-42	30.4	37.89	27.48	1.90	1.89	2.78	2.81	1.38	1.37	50.94	50.67	1.04	1.03
4H-2, 120-122	31.2	52.76	34.54	1.79	1.11	1.16	2.95	1.17	0.73	60.28	37.33	1.52	0.60
4H-3, 40-42	31.9	45.07	31.07	1.86	1.81	2.77	2.93	1.28	1.25	56.31	54.94	1.29	1.22
4H-3, 120-122	32.7	39.77	28.45	1.88	1.85	2.73	2.82	1.35	1.32	52.23	51.40	1.09	1.06
4H-4, 40-42	33.4	50.24	33.44	1.79	1.74	2.69	2.88	1.19	1.16	58.49	56.91	1.41	1.32
4H-4, 50-52	33.5	46.08	31.54	1.63	1.79	2.73	2.23	1.11	1.22	50.03	55.06	1.00	1.23
4H-4, 120-122	34.2	42.03	29.59	1.88	1.84	2.77	2.90	1.33	1.30	54.34	53.18	1.19	1.14
4H-5, 40-42	34.9	54.35	35.21	1.78	1.74	2.80	2.98	1.16	1.13	61.26	59.71	1.58	1.48
4H-5, 120-122	35.7	32.69	24.64	1.96	1.93	2.71	2.80	1.48	1.45	47.13	46.38	0.89	0.87
4H-5, 127-129	35.8	33.47	25.08	1.98	1.92	2.71	2.89	1.49	1.44	48.54	46.98	0.94	0.89
4H-6, 40-42	36.4	36.41	26.69	1.94	1.89	2.72	2.86	1.42	1.38	50.40	49.14	1.02	0.97
4H-6, 120-122	37.2	30.10	23.14	2.05	1.99	2.77	2.93	1.58	1.53	46.29	44.87	0.86	0.81
5H-1, 30-32	38.3	39.36	28.24	1.92	1.87	2.78	2.92	1.38	1.34	52.82	51.62	1.12	1.07
5H-1, 110-112	39.1	31.14	23.75	1.99	1.96	2.73	2.81	1.52	1.49	46.06	45.30	0.85	0.83
5H-2, 30-32	39.8	36.29	26.62	1.96	1.91	2.78	2.93	1.44	1.40	50.94	49.61	1.04	0.98
5H-2, 110-112	40.6	41.48	29.32	1.88	1.84	2.73	2.87	1.33	1.30	53.72	52.49	1.16	1.10
5H-3, 30-32	41.3	31.50	23.95	1.98	1.94	2.70	2.81	1.51	1.48	46.30	45.35	0.86	0.83
5H-3, 110-112	42.1	29.64	22.87	2.01	1.96	2.70	2.82	1.55	1.51	44.94	43.81	0.82	0.78
5H-4, 30-32	42.8	24.36	19.59	1.98	2.05	2.71	2.55	1.59	1.65	37.74	39.14	0.61	0.64
5H-4, 110-112	43.6	24.07	19.40	2.16	2.07	2.75	2.94	1.74	1.67	40.81	39.25	0.69	0.65
5H-5, 30-32	44.3	21.11	17.43	2.17	2.11	2.71	2.83	1.79	1.74	36.85	35.83	0.58	0.56
5H-5, 110-112	45.1	27.11	21.33	1.94	2.02	2.74	2.57	1.53	1.59	40.45	42.05	0.68	0.73
5H-6, 30-32	45.8	28.33	22.08	2.10	2.01	2.75	2.99	1.64	1.56	45.27	43.20	0.83	0.76
6H-1, 50-52	48	40.70	28.93	1.87	1.83	2.70	2.80	1.33	1.30	52.65	51.74	1.11	1.07
6H-1, 113-115	48.6	29.78	22.95	2.02	1.97	2.71	2.85	1.56	1.52	45.26	44.02	0.83	0.79
6H-2, 50-52	49.5	45.71	31.37	1.85	1.79	2.72	2.94	1.27	1.23	56.74	54.81	1.31	1.21
6H-2, 113-115	50.1	31.35	23.87	2.01	1.96	2.74	2.88	1.53	1.49	46.85	45.62	0.88	0.84
6H-3, 50-52	51	37.60	27.32	1.91	1.87	2.70	2.83	1.39	1.36	50.90	49.79	1.04	0.99
6H-3, 113-115	51.6	45.04	31.05	1.83	1.79	2.69	2.85	1.26	1.23	55.56	54.18	1.25	1.18
6H-4, 50-52	52.5	35.48	26.19	1.93	1.89	2.71	2.80	1.42	1.40	49.21	48.38	0.97	0.94
6H-4, 113-115	53.1	44.90	30.98	1.88	1.78	2.67	2.99	1.29	1.23	56.68	53.90	1.31	1.17
6H-5, 50-52	54	38.92	28.02	1.91	1.87	2.76	2.88	1.38	1.35	52.22	51.16	1.09	1.05
6H-5, 113-115	54.6	32.78	24.69	1.97	1.92	2.68	2.82	1.48	1.44	47.46	46.19	0.90	0.86
6H-6, 50-52	55.5	2.48	2.42	1.49	2.58	2.68	1.50	1.45	2.52	3.51	6.10	0.04	0.06
6H-6, 113-115	56.1	48.00	32.43	1.83	1.77	2.72	2.92	1.23	1.20	57.80	56.03	1.37	1.27
6H-7, 50-52	57	31.79	24.12	1.99	1.95	2.73	2.85	1.51	1.48	46.92	45.83	0.88	0.85
7H-1, 40-42	57.4	41.52	29.34	1.86	1.83	2.72	2.81	1.31	1.29	53.21	52.41	1.14	1.10
7H-1, 107-109	58.1	5.64	5.34	1.75	2.50	2.72	1.83	1.66	2.37	9.13	13.02	0.10	0.15
7H-2, 40-42	58.9	35.63	26.27	1.92	1.90	2.74	2.80	1.42	1.40	49.31	48.75	0.97	0.95

Notes: WC-d = water content (% dry sample weight); WC-w = water content (% wet sample weight); WBD = wet-bulk density; GD = grain density; DBD = dry-bulk density; Por = porosity; VR = void ratio.

^aValue calculated using Method B.

^bValue calculated using Method C.

As a guide to the reader, the first page of this table is reproduced here. The entire table is given in the CD-ROM (back pocket).

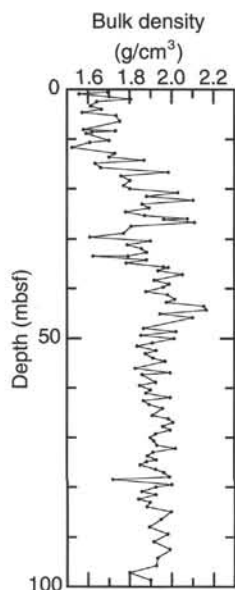


Figure 33. Bulk density (Method B) variation in the upper layers of Hole 911A.

Log Quality

The main logs from Hole 911A are shown in Figures 34 and 35. The logs are generally of good quality, although within pipe the sonic, induction, and density data are invalid and the natural gamma-ray data are highly attenuated. As Hole 911A is quite wide and rugose in parts, shown by the hole caliper in Figure 35, the density and FMS logs have suffered somewhat in quality. The white area in the center of the figure shows the diameter of a gauge hole drilled with the XCB coring bit, and the shaded areas show how much wider the hole is than originally drilled. Flat sections in the log mark where the caliper on the HLDT density tool extended to its maximum and where the eccentric tool could drift away from the borehole wall. These sections are also areas where the density data are of poor quality because borehole fluids partly occupied the measurement path. The resistivity data are also affected by the large borehole diameter but to a much less severe degree.

Hole width also affected the natural gamma-ray activity log by artificially raising the count rate where the hole is narrow and lowering it where the hole is wide. This type of artifact is most obvious at 350

and 375 mbsf (Fig. 36) where the narrow borehole diameter causes large peaks in the gamma-ray log. The log on the right-hand side of Figure 36 has undergone preliminary correction for borehole size using an exponential correction factor. Standard shore-based processing will more fully correct the NGT logs for these environmental factors.

For the most part, the velocity data from the logs are of very good quality. Some cycle skipping and other noise is present in the raw log data, but shipboard processing of the traveltimes eliminated most of these excursions. The sonic velocity presented in Figure 35 is the processed data.

Results

Lithology

The interval logged in Hole 911A (~107–476 mbsf) covers lithostratigraphic Units IA to IB (see "Lithostratigraphy" section, this chapter). This Quaternary and Pliocene lithologic sequence is dominantly an unlithified, homogeneous, dark gray silty clay. No major lithologic variations are described downhole, a feature reflected in the downhole natural gamma-ray activity log, which has cyclicity but no major trends (Fig. 34).

Subunit IB was defined by the reduced abundance of dropstones found in the cores below about 380 mbsf. A change in character is visible in several of the logs at the slightly higher level of 370 mbsf. The sonic velocity log exhibits a fairly constant velocity increase with depth in this hole, from about 1.65 km/s at 110 mbsf to about 1.9 km/s at 460 mbsf. At 370 mbsf, just above the Subunit IA/IB boundary, a decrease in sonic velocity is followed by a more sharp velocity gradient increase from about 380 mbsf to the bottom of the hole. The bulk-density measurement shows a different character in Subunit IB, although this may be caused in part by fluctuations in borehole diameter.

The log that exhibits the most distinct change from Subunit IA to IB is the thermal-neutron capture cross section from the gamma-ray spectrometry tool (GST) (Fig. 37). Whereas the elemental yields from the GST require considerable post-cruise processing and are not presented here, the capture cross section also can be used to show lithologic variation downhole. It exhibits a distinct increase at 370 mbsf, just above the boundary to lithologic Subunit IB and is fairly constant from here to the base of the hole. Although it is not possible to characterize the origin of the lithologic change, as the capture cross section is dependent on many fluid and matrix parameters, it serves to distinguish this subunit from the one above.

A subtle change in logging properties occurs roughly between 180 and 220 mbsf. Sedimentological distinctions also can be made at this level, although they were not sufficient to demarcate a subunit.

Table 13. Summary of logging operations at Hole 911A.

25 Aug. 1993	
06:00	Last core on deck; prepare hole for logging. Rig up CSES.
15:30	Rig up NGT-SDT-HLDT-DIT.
16:25	RIH with NGT-SDT-HLDT-DIT. Manage to get near TD (476.6 mbsf) without lowering pipe.
17:19	Main upgoing log at 900 ft/hr from 476 to 147.6 mbsf; HLDT run in high-resolution mode.
18:32	RIH for repeat section. Upgoing log from 247.6 to mud line at 900 ft/hr. POOH.
20:00	Rig up NGT-FMS.
21:30	RIH with NGT-FMS. Had to pump tool out of pipe.
	Tool unable to pass bridge at 344 mbsf.
22:30	Upgoing log from 343 mbsf to EOP at 1100 ft/hr.
22:48	Tool pulled back into pipe. Pipe then RIH to 434 mbsf. Problem getting tool out of pipe; had to be pumped.
26 Aug. 1993	
01:54	Upgoing log from 448.6 mbsf to EOP (pulled to 107 mbsf) at 1600 ft/hr. POOH.
04:30	Rig up NGT-AACT-GST.
05:30	RIH with NGT-AACT-GST. Reached TD at 445.6 mbsf.
06:02	Main upgoing log at 550 ft/hr from 445 mbsf to mud line.
08:41	End of upgoing log. POOH.
09:10	Rig down (2 hr). End of logging operations.

Note: Times given in Universal Time Coordinated (UTC). Drillers TD (total depth) = 505.8 mbsf; WD (water depth) = 912.4 mbsf; EOP (end of pipe) = 117 mbsf; RIH = run in hole; POOH = pull out of hole. For further details, see "Explanatory Notes" chapter (this volume).

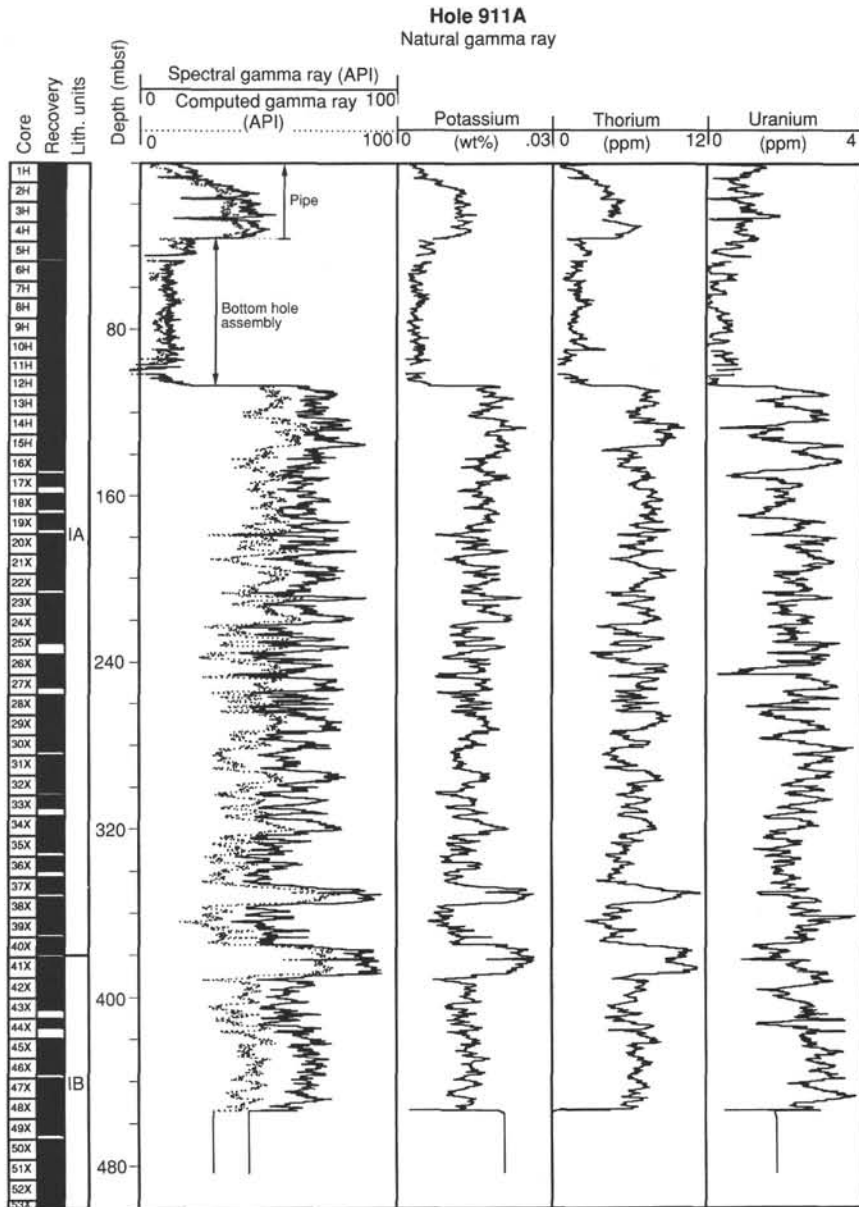


Figure 34. Data from the natural gamma-ray spectrometry tool (NGT) recorded on the quad combination tool strings.

Above the transition, variability in the natural gamma activity, resistivity (particularly the medium depth logs), and in sonic velocity is somewhat lower than deeper in the section. This distinction also appears in the seismic section; the reflectors become stronger below the transition (see “Seismic Stratigraphy” section, this chapter).

Formation MicroScanner

The two passes of the FMS have a blotchy character, with only indistinct bedding. Nevertheless, the two passes repeat individual features well. The logs have numerous light, high-resistivity patches about 5–10 cm high and about the same width (Fig. 38). Although the horizontal exaggeration in the raw logs makes them appear as strips, they are roughly circular. They may represent some type of diagenetic halo in the sediment, although no similar features were seen in the recovered cores. Some of the resistive patches may be dropstones, but the average size and the abundance are too large for all to be stones.

Apparent in the recovered cores throughout the hole are iron-sulfide nodules usually infilling burrows in bioturbated sections. These iron-sulfide nodules were observed to be commonly 0.5 to 1.5 cm across and up to 3 cm at a maximum. Because of their highly conductive nature, they appear on the FMS microresistivity images as black (conductive) spots (Fig. 38), which are consistent and repeatable between the two passes of the FMS. The figure also shows the individual resistivity traces from one of the FMS pads. The very sharp drops in resistivity are interpreted to mark the sulfide nodules. Post-cruise processing of the images (which can be found at the back of this volume on CD-ROM) should enhance the image quality.

Log Cyclicality–Paleoclimatic Significance

Several of the recorded logs exhibit a cyclic nature, most prominently the resistivity logs (Fig. 35), which in turn are least affected by the environmental problems of borehole size and rugosity. Figure 39

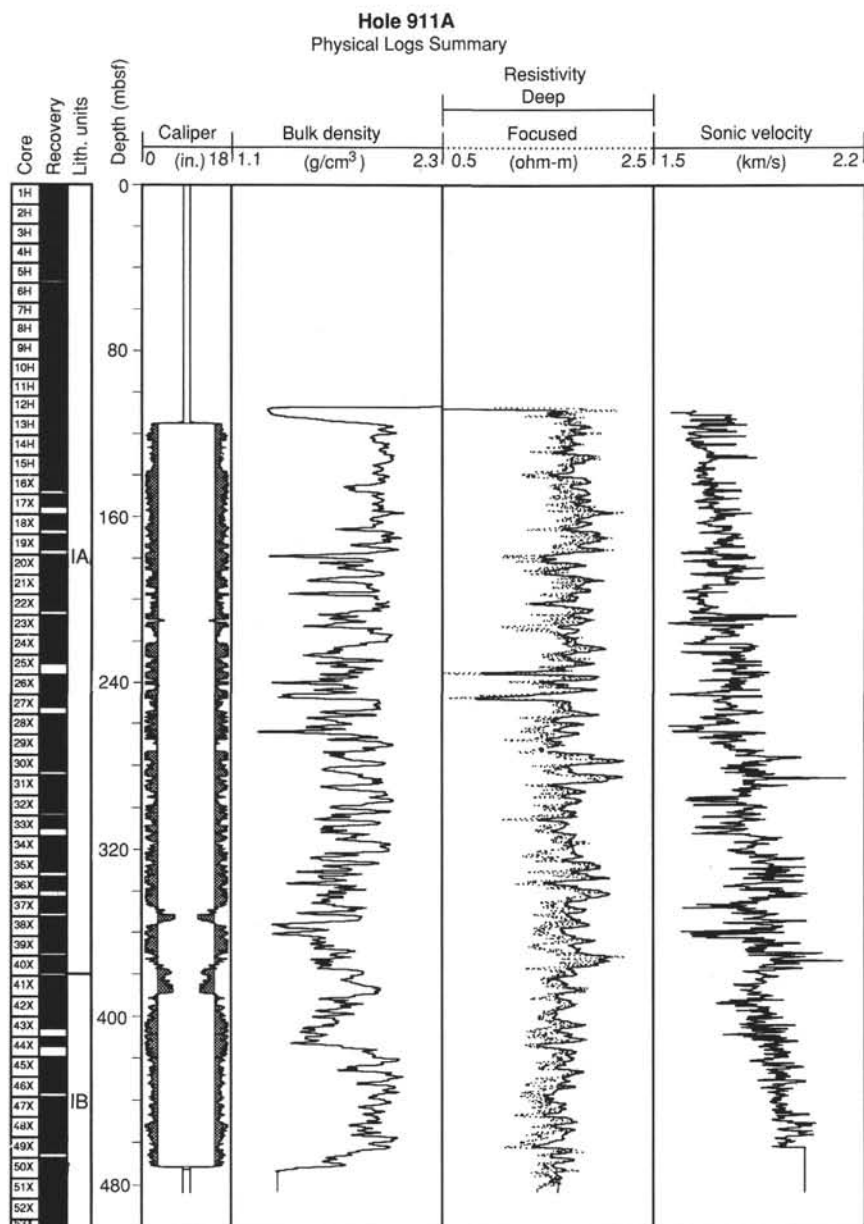


Figure 35. Caliper data from the high-temperature lithodensity tool (HLDT) shown with bulk density data from the HLDT, deep phasor induction and spherically focused resistivity from the phasor dual induction tool (DIT), and sonic velocity data from the long-spaced digital sonic tool (SDT). The central white area in the caliper log represents the XCB bit size (11 5/8 in.), and the shading represents the “washed out” portion of the hole from the bit size to actual measured diameter. The bulk density and velocity data have undergone a linear 7-point (1.05 m) moving average filter for presentation clarity.

displays a short section of the very enhanced intermediate-penetrations phasor induction log recorded over two separate passes to show the precision of the measurement (the two curves are linearly offset for clarity).

Unlike the recovered core material, downhole logs are continuous high-resolution records of the physical and chemical variability of the drilled sequence. Extracting paleoclimatic information from logs is often compromised by low accumulation rates, limiting the temporal resolution of the logs. At Site 911 as well as at the other sites drilled during Leg 151, however, the average sedimentation rates were high. At Hole 911A the sedimentation rate is as high as 193 m/m.y. as calculated from the preliminary paleomagnetic time constraints. This

gives the logs a temporal resolution of the order of 1 k.y. Although cyclicity is apparent in much of the logged section, paleomagnetic time constraints are currently only reliable in the upper portion of the hole. Figure 40 shows a spectral analysis of the deep phasor induction log over the interval 1.1–1.8 Ma (~110–240 mbsf). This preliminary spectral analysis shows encouraging results, with much spectral power in the log occurring at ~40- and ~100-k.y. bands, concurring with known Milankovitch frequencies. In this section a 40-k.y. peak is dominant in the spectrum and is probably a climatic expression of the 41-k.y. orbital obliquity cycle. It is uncertain at this stage what physical components in the formation vary with this cyclicity. Resistivity is proportional to the inverse square of porosity (Archie, 1942), and

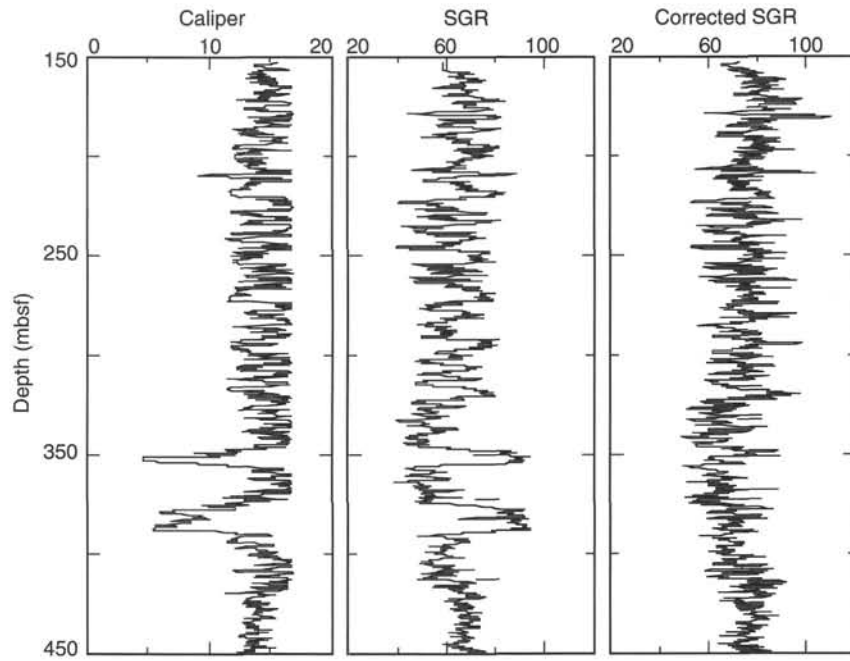


Figure 36. Comparison of the total gamma-ray (SGR) and the caliper logs over the interval 150–450 mbsf. The negative correlation indicates the influence on the SGR measurement of the borehole diameter. The gamma-ray curve on the right has been corrected for borehole size based on the algorithm from Schlumberger (1989).

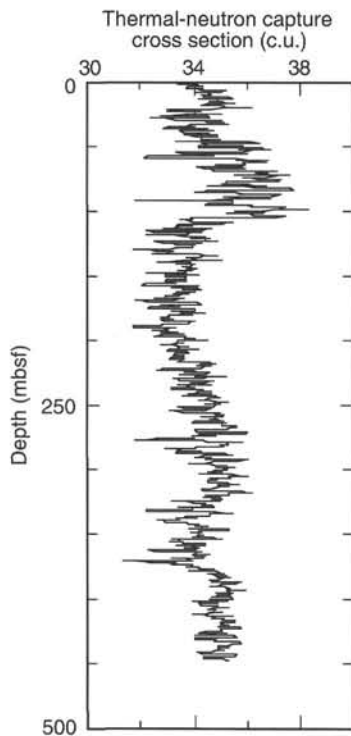


Figure 37. Thermal neutron capture cross section log from the gamma-ray spectrometry tool (GST) as a function of depth. The data have undergone a linear 5-point (0.75 m) moving average smoothing for presentation clarity.

these porosity changes may relate to grain size variations in turn driven by fluctuations in ice cover.

Porosity Estimates from Resistivity

We calculated porosity (see “Explanatory Notes” chapter, this volume) using the deep phasor induction resistivity log (IDPH) from the dual induction tool with set values for the Archie equation (1942) of $a = 1$ and $m = 2.4$. R_w is calculated based on its known relationships to temperature and salinity (Keller, 1982), temperature was taken from the internal temperature measurement of the logging tool, and interstitial salinities from core measurements (see “Inorganic Geochemistry” section, this chapter). At low temperatures such as encountered at this hole, R_w varies significantly downhole, and therefore a log of R_w was calculated as a function of depth.

The calculated porosities have only a reasonably good correlation with those determined from discrete core samples (Fig. 41).

SEISMIC STRATIGRAPHY

Introduction

A synthetic seismogram was generated from the velocity and density profiles at Site 911 to correlate reflectors in the seismic section to stratigraphic changes. The acoustic impedance profile (the product of density and velocity) and the profile of reflection coefficients (the rate of change of acoustic impedance) were determined both as a function of depth and of two-way acoustic traveltime. Convolution of the reflection coefficient profile with an assumed source acoustic wavelet resulted in a synthetic seismogram to compare with the measured seismic section.

The seismic section used for correlation is the line AWI-91127, collected by the Alfred Wegener Institute for Polar and Marine Research, Bremerhaven. Site 911 is located at shotpoint 324.

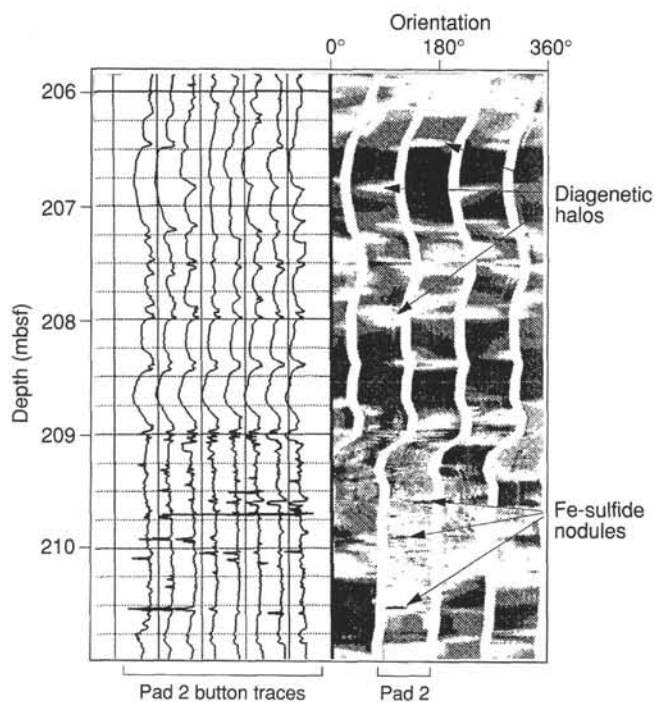


Figure 38. Data from the FMS for the interval 206–211 mbsf. On the right are the oriented microresistivity traces from the four orthogonal pads of the FMS: the lighter the color the more resistive the beds. The interpretations of diagenetic halos and Fe-sulfides are annotated. On the left, the microresistance traces from eight of the individual “buttons” on pad number 2 are shown, with resistance decreasing to the left. The Fe-sulfide nodules, which appear as small dark spots in the microresistivity images, correspond to sharp decreases in resistance on the traces from the individual buttons.

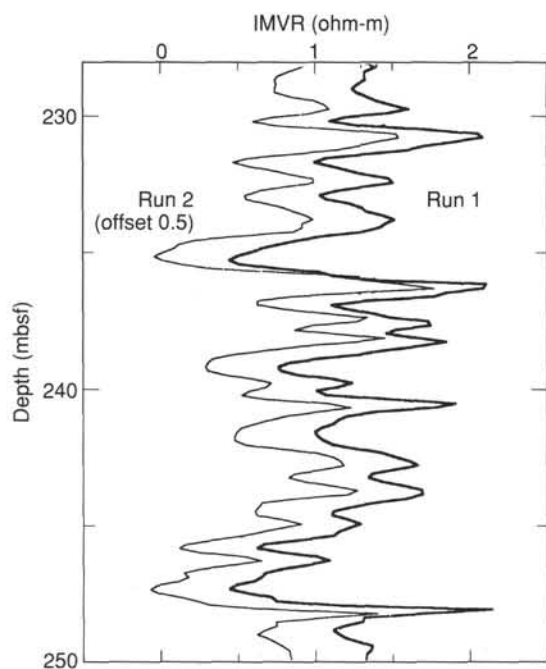


Figure 39. Comparison of the very enhanced medium phasor induction log (IMVR) from the DIT over the interval 250–228 mbsf. The logs are laterally offset and show the precision (repeatability) of the resistivity data. This interval also demonstrates the cyclic nature of the logs.

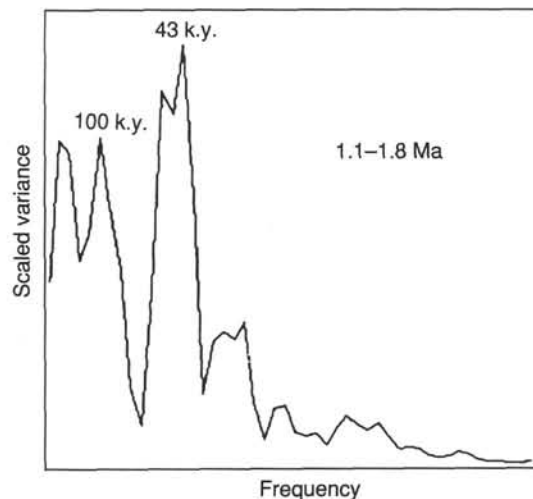


Figure 40. Results of spectral analysis of the deep phasor induction log from the DIT over the interval 110–240 mbsf, which represents an age interval of 1.1–1.8 Ma based on preliminary paleomagnetic constraints (see “Paleomagnetism” section, this chapter). The log shows strong variance at known Milankovitch periodicities. Standard power spectra analysis methods were used (Imbrie et al., 1984).

Acoustic Wavelet

We did not have a record of the acoustic wavelet from the AWI-91127 line and therefore created a wavelet based upon the strong doublet exhibited at the seafloor. The wavelet used has a 20-ms period with an e-folding attenuation of 14 ms.

Reflection Coefficients

Discrete measurements of density and compressional velocity on the recovered cores (see “Physical Properties” section, this chapter) were combined with logging data (see “Downhole Measurements” section, this chapter) to form a profile of reflection coefficients for Hole 911A. The logs provided detailed velocity data on the interval between 108 and 465 mbsf. Discrete laboratory measurements completed the density data set from 0 to 108 mbsf. Velocity measurements on recovered core were invalid below a depth of 18 mbsf. To make a complete velocity profile, a linear interpolation of velocities was made through the gap between the two data sets.

The composite velocity profile can be used to convert between mbsf and two-way traveltime in the seismic section. A quicker but still accurate conversion also can be made by the following 2nd order equation:

$$Z = 0.764(\text{TWT}) + 0.000194(\text{TWT})^2$$

where Z is mbsf, and TWT is two-way traveltime in milliseconds.

Density measurements from the logs were poor because of bad hole conditions (see “Downhole Measurements” section, this chapter) and were not used to create the density profile at Site 911. Instead, the deep phasor induction resistivity (IDPH) log was inverted to create a pseudo-density log (see “Explanatory Notes” chapter, this volume). The estimated densities from the logs were combined with measured bulk density on cores from the upper 108 m of the site.

The resulting data were interpolated to a 1-m sample spacing, and were used to generate an acoustic impedance profile for Site 911 (Fig. 42). Also shown on the figure are the lithostratigraphic subunits (see “Lithostratigraphy” section, this chapter) and the synthetic seismogram.

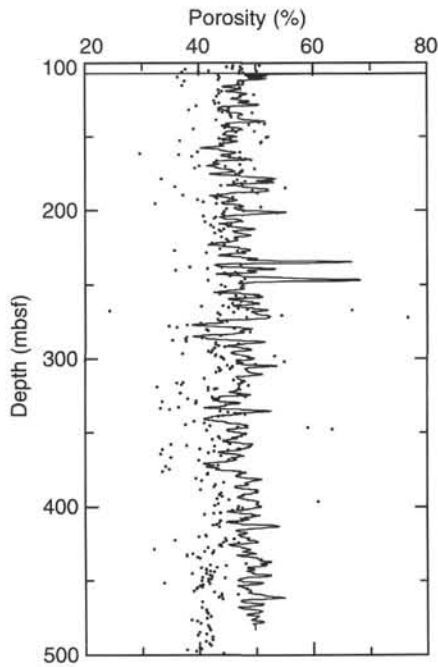


Figure 41. Porosity derived from the deep phasor induction of the DIT compared with porosity measurements on discrete core samples. The input resistivity data and the final porosity log are unsmoothed.

The Synthetic Seismogram

Figure 42 shows the synthetic seismogram resulting from the convolution of the seismic wavelet with the reflection coefficient profile, whereas Figure 43 compares the synthetic seismogram to the recorded seismic section through Site 911. The synthetic seismogram matches the recorded seismic profile reasonably well.

The synthetic seismogram and the seismic profile are both marked by large numbers of reflectors. The section is marked by strong reflections near the seafloor, followed by a section of continuous reflectors of roughly equal size (reflectors D–I), switching to a more chaotic set of reflectors below 200 mbsf (245 ms TWT; Figs. 42 and 43). This boundary, at about 1.4 Ma, also marks a subtle change in other properties measured by the logging tools (see “Downhole Measurements” section, this chapter). The Subunit IA/IB boundary at 380 mbsf is not strongly expressed in the seismic record and occurs between reflectors V and W in the synthetic seismogram.

Site 911 has sharp increases in the density and velocity profiles near the seafloor, similar to Site 910. Large variations in density are spaced roughly 20 m apart. These produce a strong doublet from the seafloor and also reflector A (Fig. 43). These are followed by a series of moderately strong reflectors (D–I) that are more prominent in the synthetic seismogram than in the actual seismic profile.

For the most part, the other reflectors in the synthetic seismogram can be correlated easily with the seismic section. One exception is reflector R, which appears much stronger in the synthetic seismogram than in the seismic line. The strength of this reflector is in part an artifact produced by a section of poor data (Fig. 44). The SDT seismic tool records a series of traveltimes between source and receivers and is a redundant data set. Figure 44 shows the average interval travel-

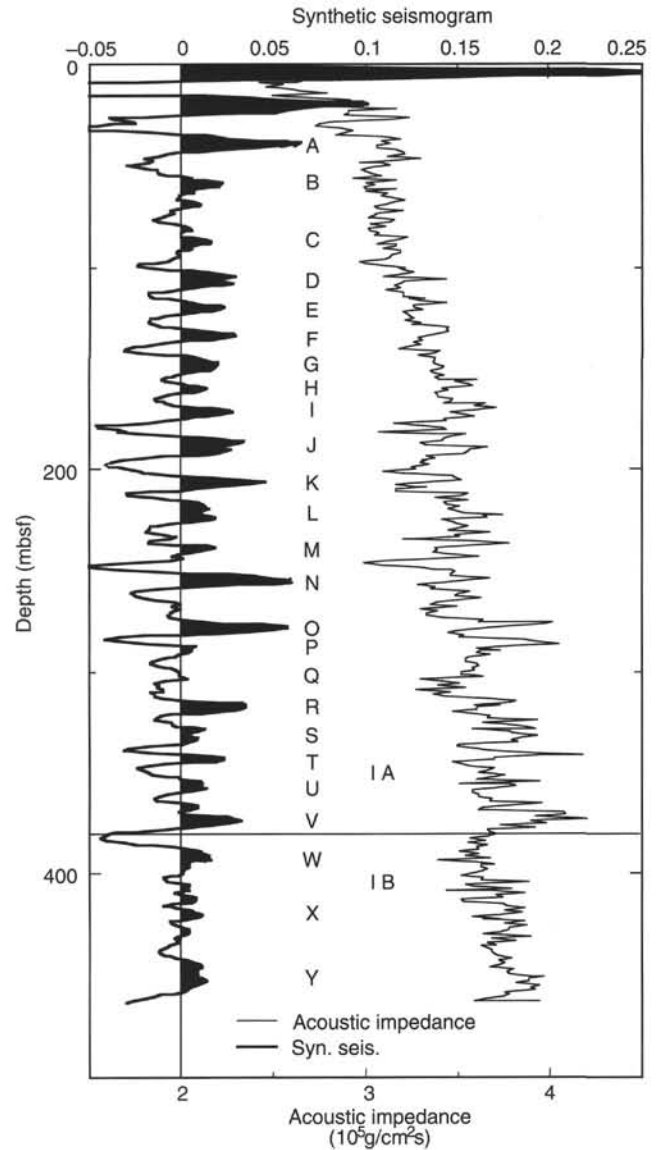


Figure 42. Acoustic impedance compared to the synthetic seismogram at Site 911. Also shown are the lithostratigraphic unit boundaries from the “Lithostratigraphy” section, this chapter. The seismogram has been converted from two-way traveltime into equivalent depth (mbsf).

time and the individual records used to calculate the average. A series of poor traveltimes was recorded in the interval 309–312 mbsf that resulted in an interval of anomalously low velocities immediately below a high-velocity interval. Because the acoustic impedance is artificially enhanced, the resultant reflector in the synthetic seismogram is much stronger than it should be.

The base of the data used to construct the synthetic seismogram occurs at 460 mbsf (0.58 s TWT). The base of the hole (506 mbsf) should be at about 0.63 s below the seafloor.

Ms 15IIR-109

NOTE: For all sites drilled, core-description forms (“barrel sheets”) and core photographs can be found in Section 6, beginning on page 465. Forms containing smear-slide data can be found in Section 7, beginning on page 849. Thin-section descriptions are given in Section 8, beginning on page 885, and sediment thin sections in Section 9, beginning on page 895. Dropstone descriptions are included in Section 10, beginning on page 903.

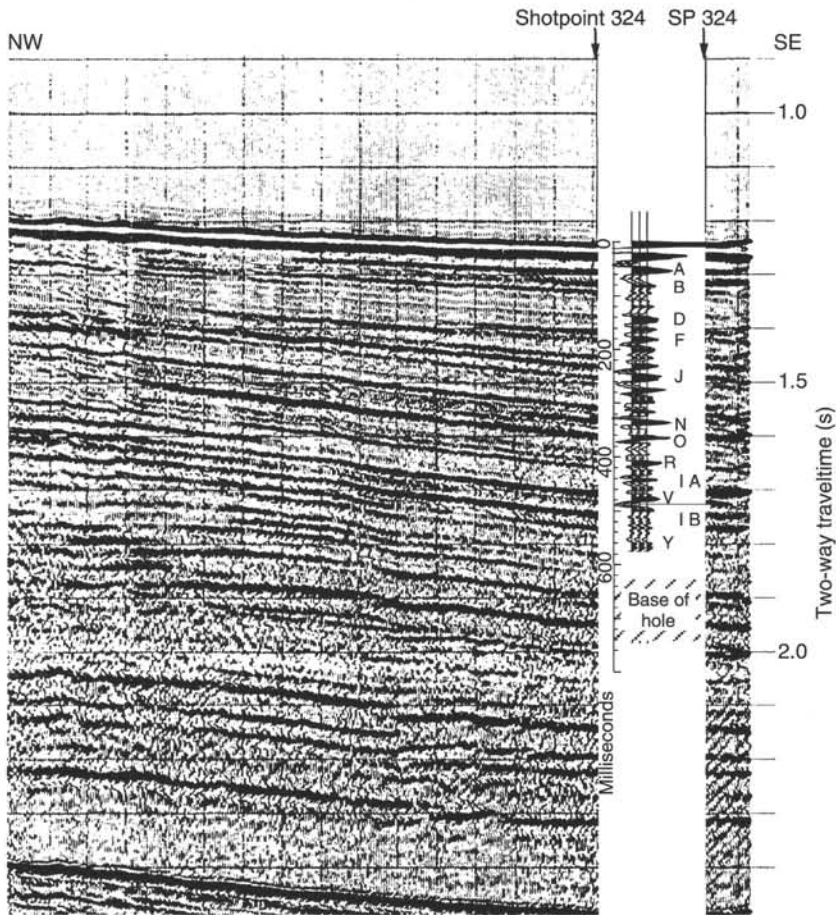


Figure 43. Comparison between synthetic seismogram from Site 911 and seismic line AWI-91127, shotpoint 324. Scale shown is in milliseconds TWT from the ocean floor. The base of reflector V marks the lithostratigraphic Subunit IA/IB transition.

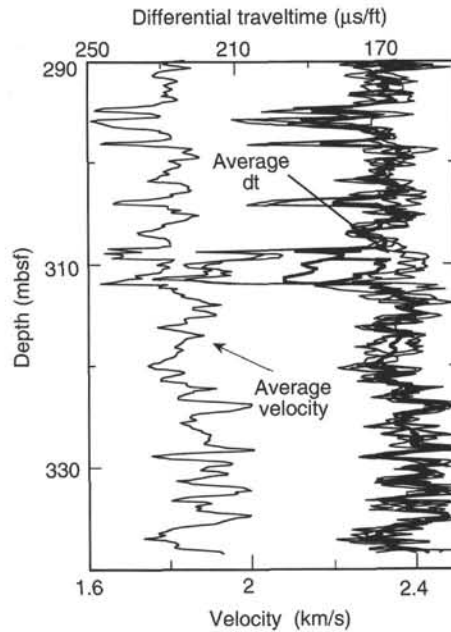


Figure 44. A comparison of the raw differential traveltimes (dt) to the resultant average interval sonic velocities for the interval between 290 and 340 mbsf. Reflector R is generated by the velocity contrast at about 312–316 mbsf. Poor velocity determinations in the preceding interval artificially strengthen this reflector in the synthetic seismogram.

SHORE-BASED LOG PROCESSING

Hole 911A

Bottom felt: 912.4 mbrf (used for depth shift to seafloor)

Total penetration: 505.8 mbsf

Total core recovered: 464.51 m (91%)

Logging Runs

Logging string 1: DIT/SDT/HLDT/NGT (upper and lower)

Logging string 2: FMS/GPIT/NGT (two passes)

Logging string 3: ACT/GST/NGT

Wireline heave compensator was used to counter ship heave resulting from the mild sea state conditions.

Drill Pipe/Bottom-hole Assembly/Casing

The following drill pipe depths are as they appear on the logs after differential depth shift (see **Depth shift** section) and depth shift to the seafloor. As such, there might be a discrepancy with the original depths given by the drillers on board. Possible reasons for depth discrepancies are ship heave, use of wireline heave compensator, and drill-string and/or wireline stretch.

DIT/HLDT/SDT/NGT: Bottom of drill pipe at 32.5 mbsf. Bottom-hole assembly at 102.5 mbsf.

FMS/GPIT/NGT: Bottom of drill pipe at 102.5 mbsf. Never reached bottom of drill pipe.

ACT/GST/NGT: Bottom of drill pipe at 32.5 mbsf. Bottom-hole assembly at 102.5 mbsf.

Processing

Depth shift: All logs have been interactively depth shifted with reference to NGT from ACT/GST/NGT run, and to the seafloor (-912.4 m). A list of the amount of differential depth shifts applied at this hole is available upon request.

Gamma-ray processing: NGT data have been processed to correct for borehole size and type of drilling fluid.

Acoustic data processing: The sonic logs have been processed to eliminate some of the noise and cycle skipping experienced during the recording.

Geochemical processing: (For detailed explanation of the processing, please refer to the "Explanatory Notes" chapter [this vol-

ume] or to the "geochem.doc" file on the enclosed CD-ROM). The elemental yields recorded by the GST tool represent the relative contribution of only some of the rock-forming elements (iron, calcium, chlorine, silica, sulfur, hydrogen, gadolinium, and titanium—the last two computed during geochemical processing) to the total spectrum. Because other rock-forming elements (such as aluminum, potassium, etc.) are present in the formation, caution is recommended in using the yields to infer lithologic changes. Instead, ratios (see "acronyms.doc" on CD-ROM) are more appropriate to determine changes in the macroscopic properties of the formation. A list of oxide factors used in geochemical processing includes the following:

SiO₂ = 2.139

CaO = 1.399

FeO* = 1.358

TiO₂ = 1.668

K₂O = 1.205

Al₂O₃ = 1.889

FeO* = computed using an oxide factor that assumes a 50:50 combination of Fe₂O₃ and FeO factors.

Quality Control

Hole diameter was recorded by the hydraulic caliper on the HLDT tool (CALI) and by the caliper on the FMS string (C1 and C2).

Invalid gamma-ray data were detected at 42, 92, and 96.5 mbsf (BHA joints, DIT/SDT/HLDT/NGT string) and at 33, 42, 52, 62, 79.5, 84, 92, and 96.5 mbsf (BHA joints, ACT/GST/NGT string).

FACT = quality control curve in geochemical processing. Accuracy of the estimates is inversely proportional to the magnitude of the curve.

Note: Details of standard shore-based processing procedures are found in the "Explanatory Notes" chapter, this volume. For further information about the logs, please contact:

Cristina Broglia

Phone: 914-365-8343

Fax: 914-365-3182

E-mail: chris@ldeo.columbia.edu

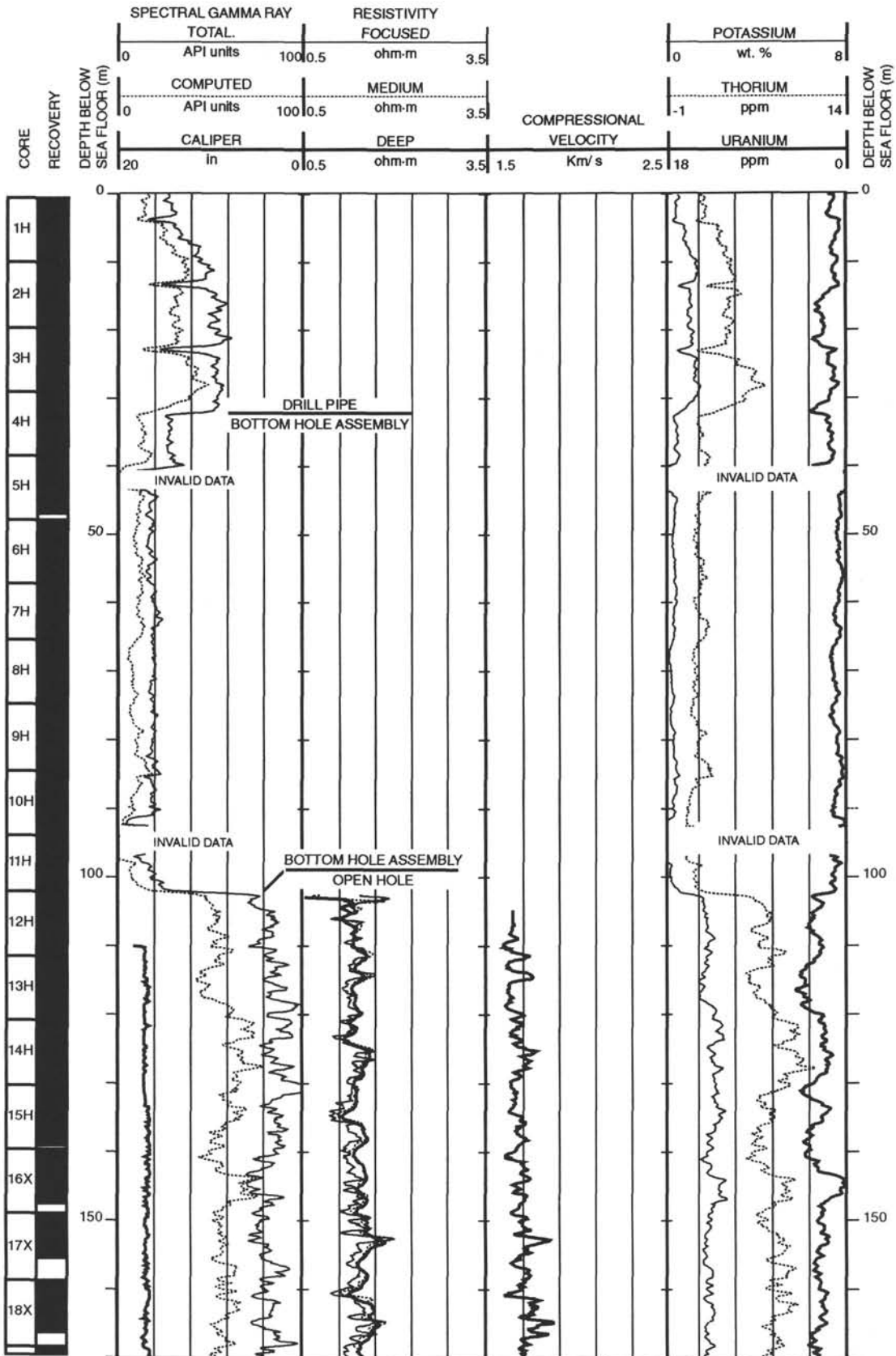
Elizabeth Pratson

Phone: 914-365-8313

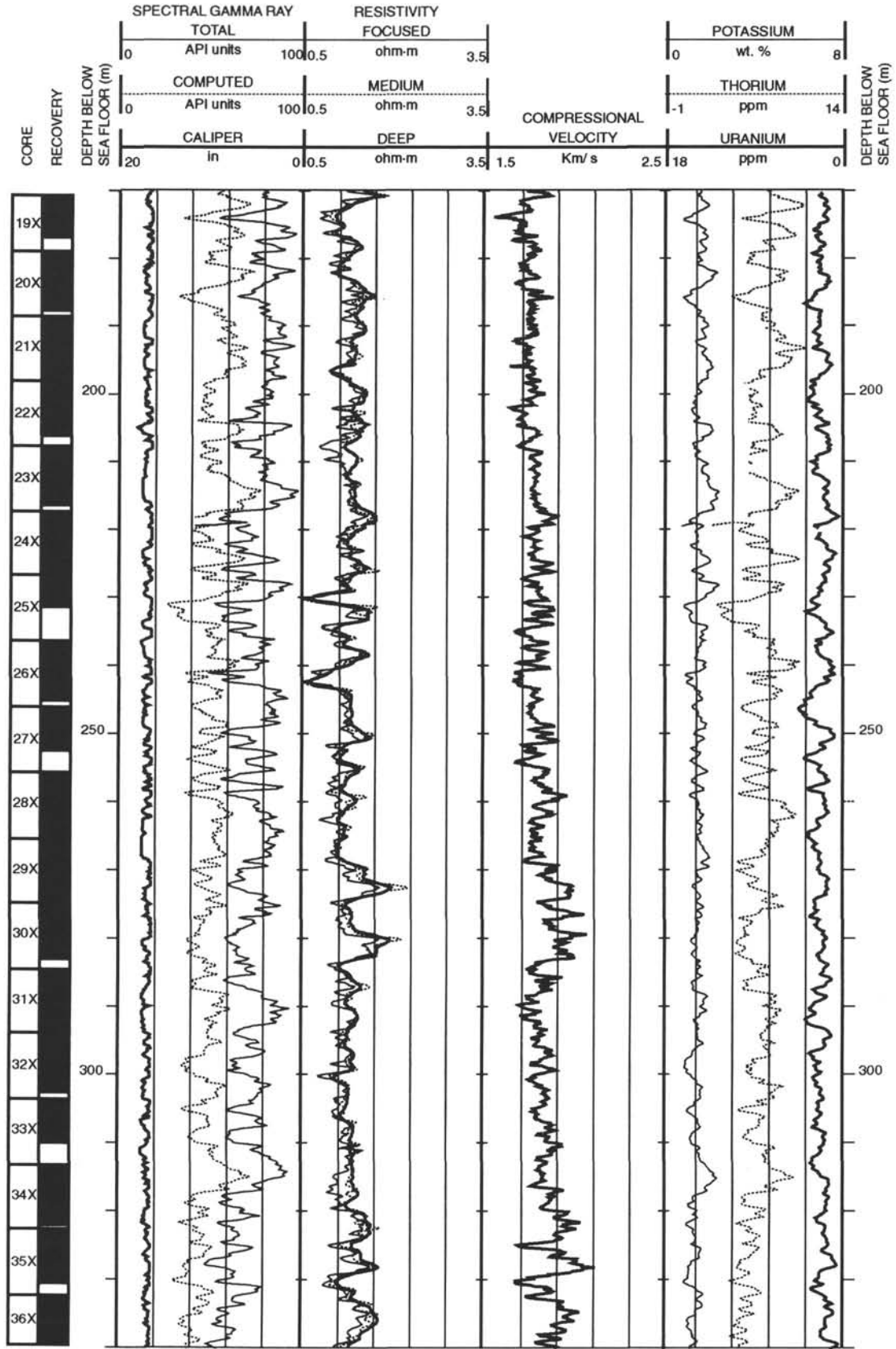
Fax: 914-365-3182

E-mail: beth@ldeo.columbia.edu

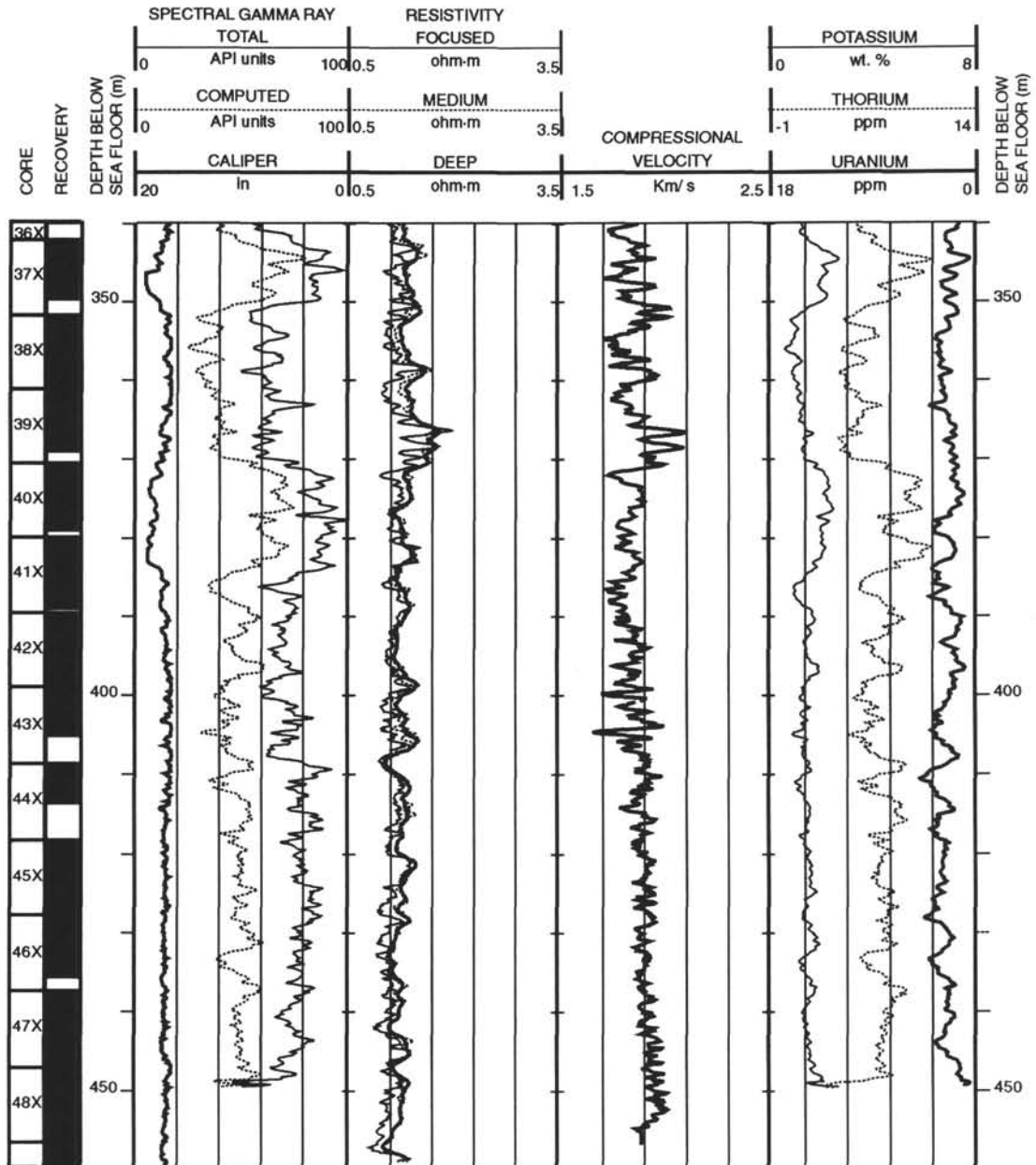
Hole 911A: Resistivity-Velocity-Natural Gamma Ray Log Summary



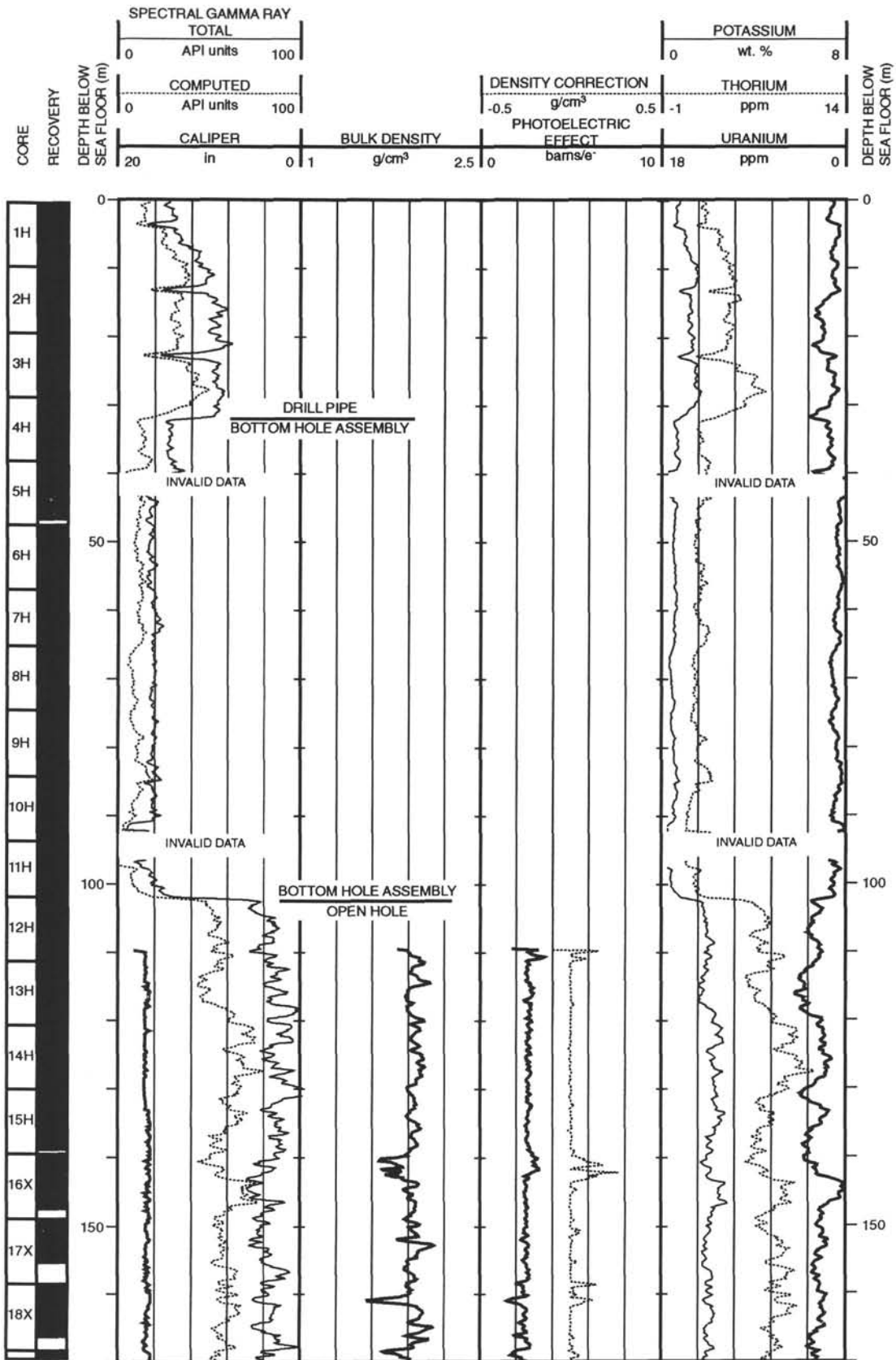
Hole 911A: Resistivity-Velocity-Natural Gamma Ray Log Summary



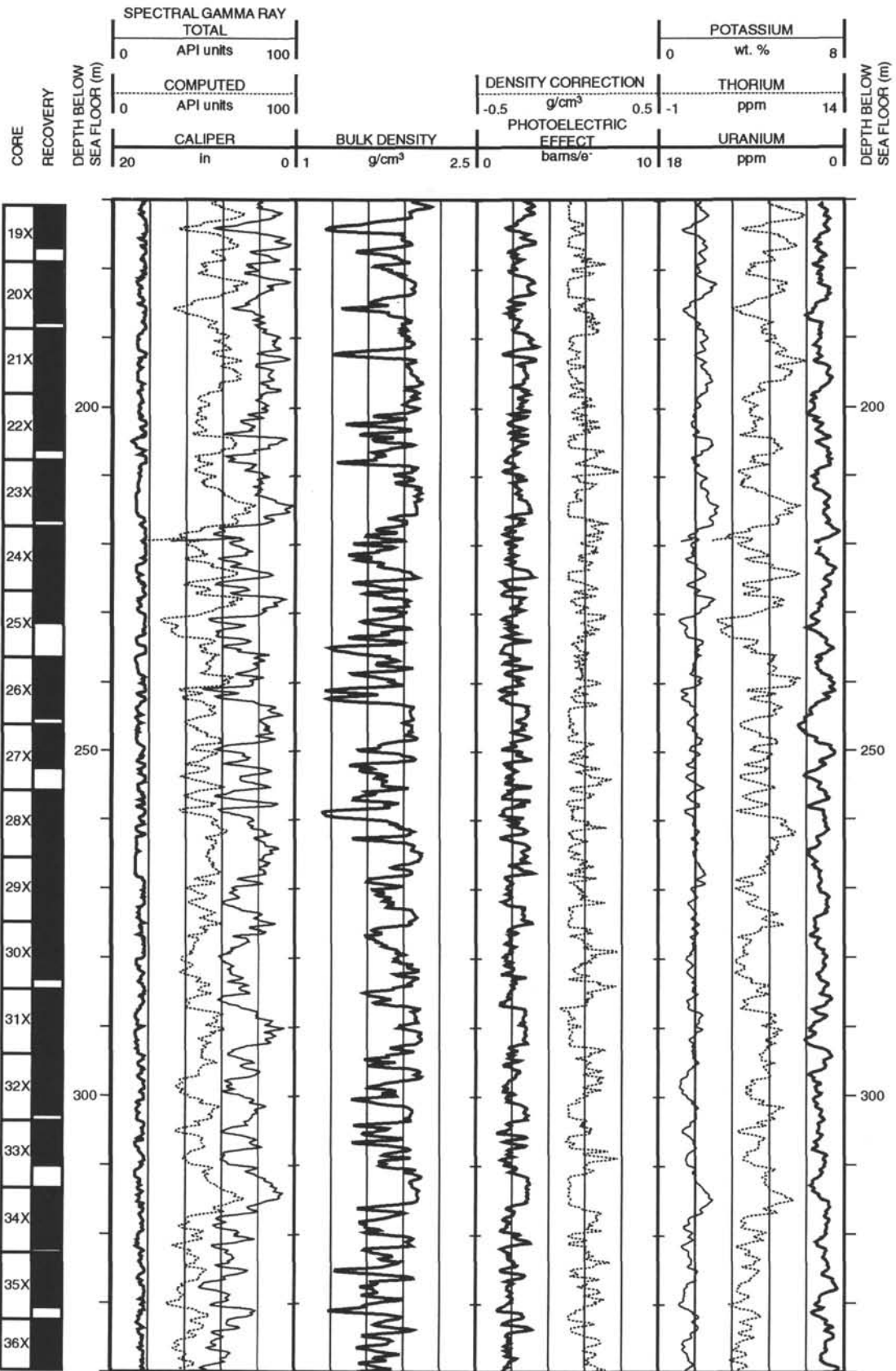
Hole 911A: Resistivity-Velocity-Natural Gamma Ray Log Summary



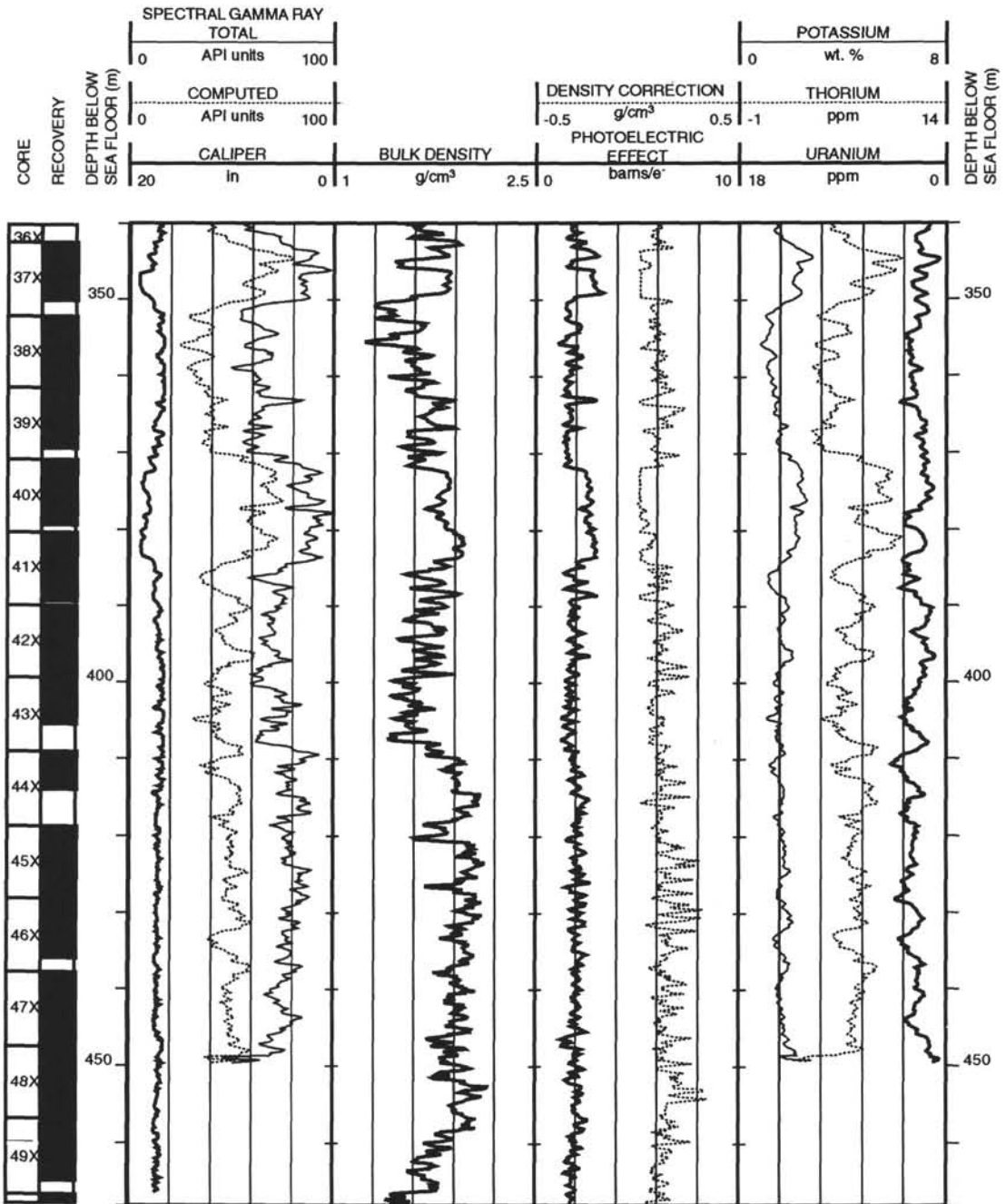
Hole 911A: Density-Natural Gamma Ray Log Summary



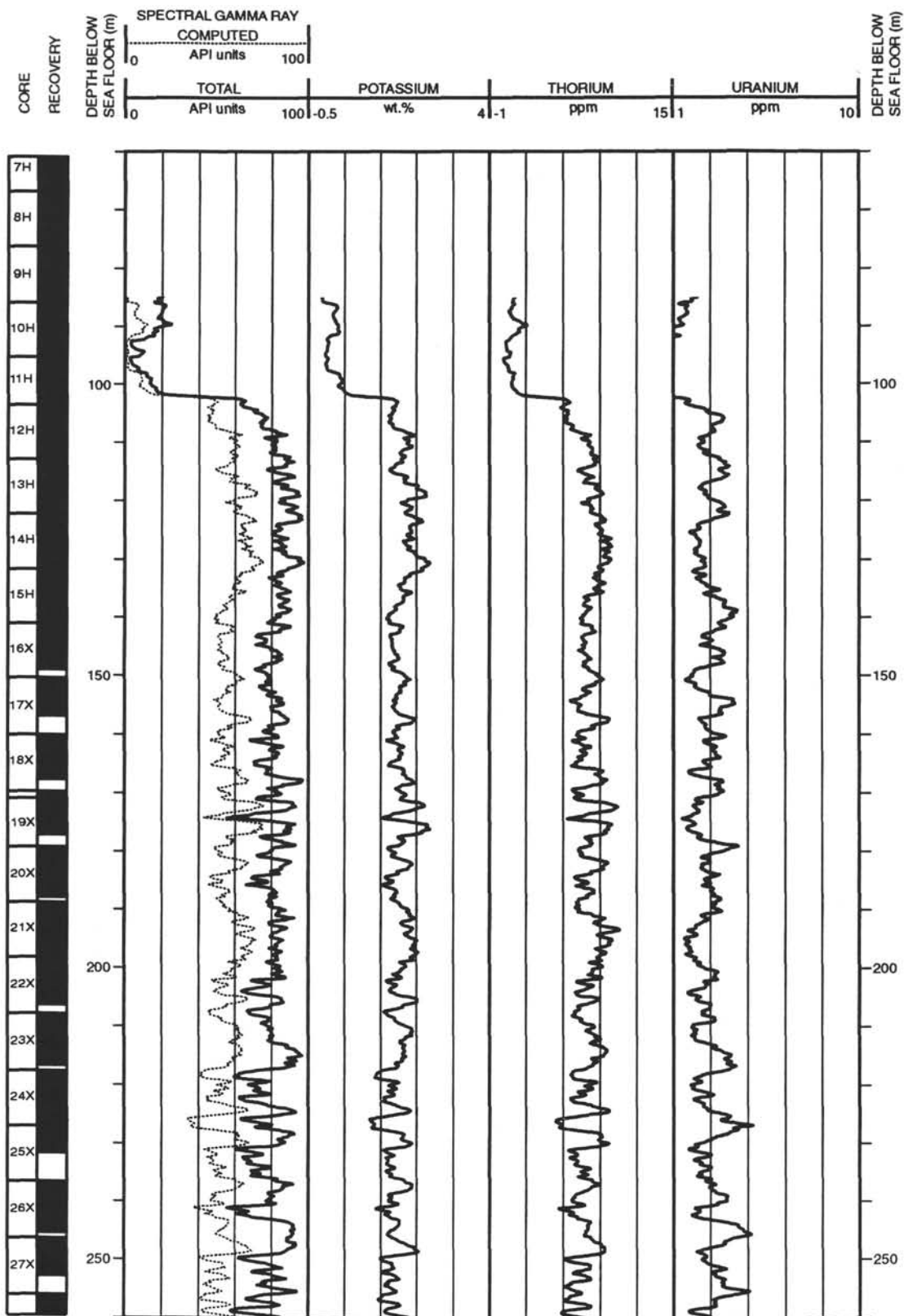
Hole 911A: Density-Natural Gamma Ray Log Summary



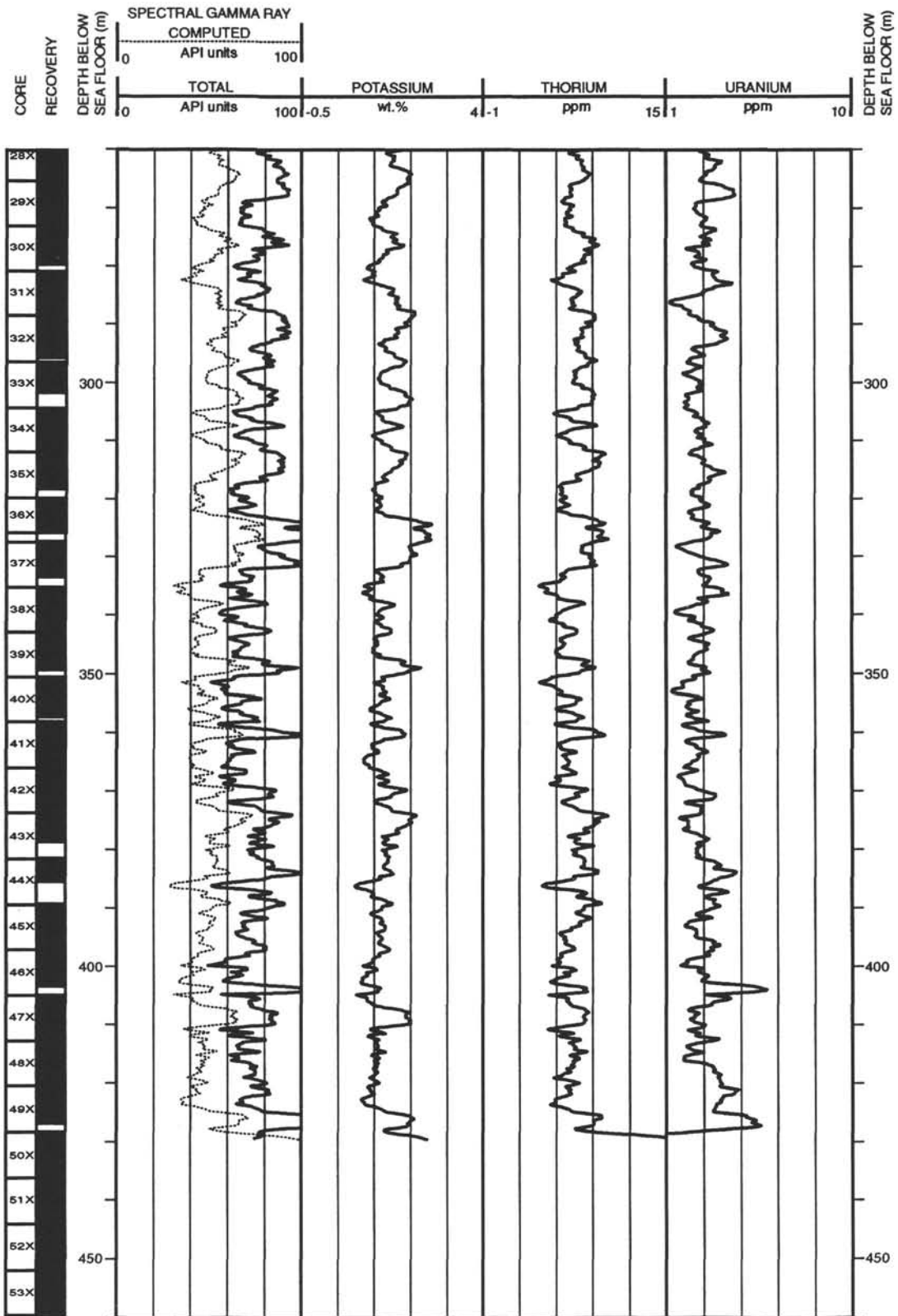
Hole 911A: Density-Natural Gamma Ray Log Summary



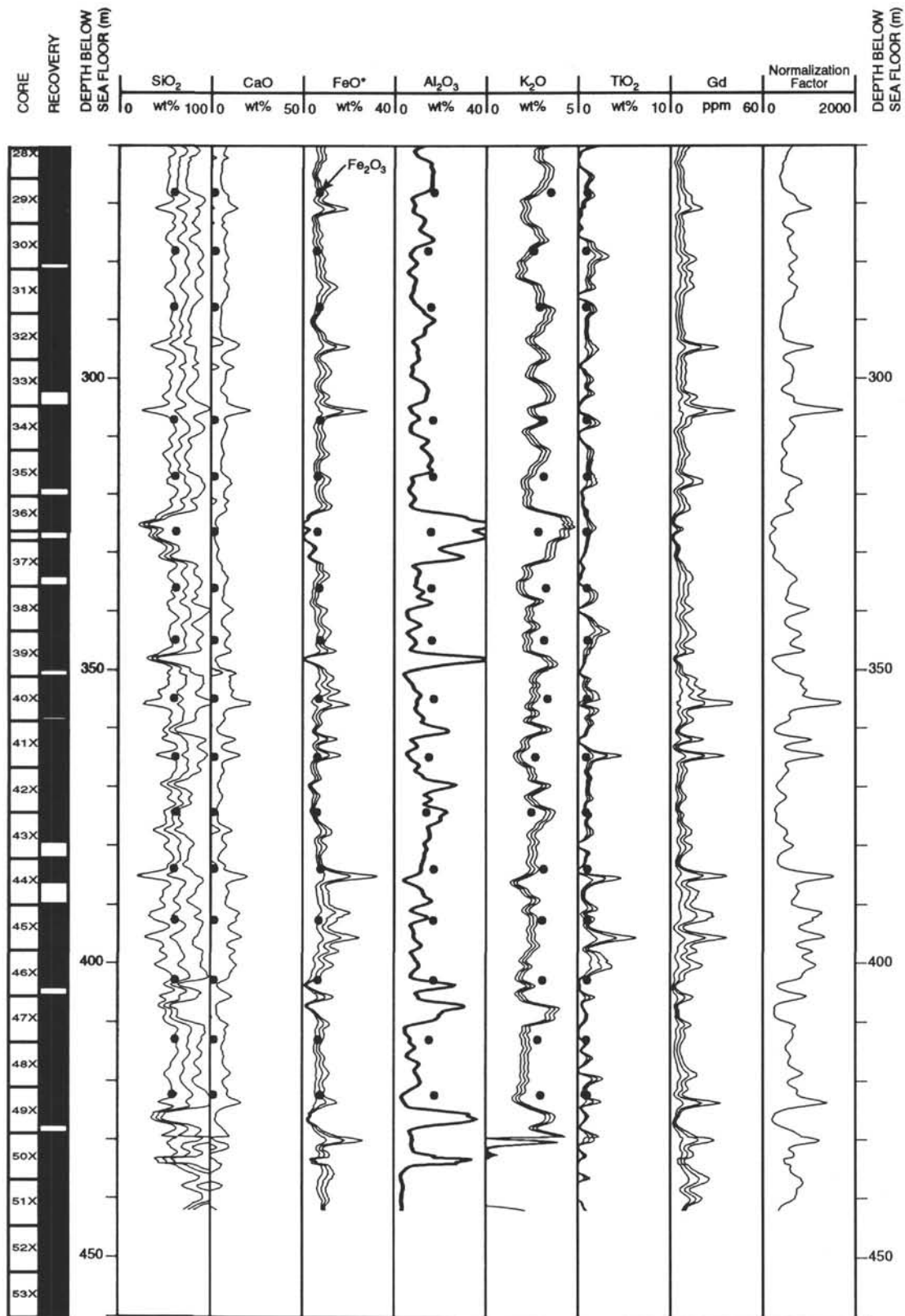
Hole 911A: Natural Gamma Ray Log Summary



Hole 911A: Natural Gamma Ray Log Summary



Hole 911A: Processed Geochemical Log Summary



Hole 911A: Processed Geochemical Log Summary

